Perturbation Growth and Prediction of Extreme Events

Dissertation
zur Erlangung des mathematisch-naturwissenschaftlichen Doktorgrades
"Doctor rerum naturalium"
der Georg-August-Universität Göttingen

vorgelegt von
Nahal Sharafi
aus Teheran

Göttingen 2017

Mitglieder des Betreuungsausschusses:

Prof. Dr. Marc Timme (Referent)
Network Dynamics
Max Planck Institute for Dynamics and Self-Organization
Prof. Dr. Rainer Kree (Referent)
Institute for Theoretical Physics
Georg-August-Universität Göttingen
Prof. Dr. Ulrich Parlitz
Biomedical Physics
Max Planck Institute for Dynamics and Self-Organization

Weitere Mitglieder der Prüfungskommision:

Prof. Dr. Fred Wolf
Theoretical Neurophysics
Max Planck Institute for Dynamics and Self-Organization
Dr. Claus Heussinger
Institute for Theoretical Physics
Georg-August-Universität Göttingen

I comfirm that I have written this thesis independently and with no other sources and aids than quoted.

Göttingen,

Contents

1 Introduction

Extreme events and critical transitions occur in a variety of natural and artificial systems. Incidents as diverse as seizures in epileptic patients [1, 2], sudden crashes in financial markets [3], abrupt changes in the climate [4, 5] and in ecosystems [6], wars and revolutions all share the property of going beyond the realm of normal expectations [7, 8].

In spite of the highly determinant role of extreme events in nature and society, they still remain a problem that science is not particularly comfortable with. Science is dominantly devoted to understanding and explaining the mean behavior of systems rather than focusing on the tails of probability distributions, or the outliers that exist beyond the distribution of their smaller siblings. In recent years, however, scientist from different fields have shown increased interest in the study of extreme events. For some examples, see [9–20].

In the heart of the quest for understanding and explaining extreme events lies the task of predicting them. Predicting extreme events, however, is far from trivial. Classical model based methods of prediction largely fail to predict extreme events. In the context of weather forecasting, for instance, existing mathematical models are capable of effectively predicting the most likely weather in the next few days. However, prediction of the unlikely extreme events that may potentially have a larger impact remains a challenge. A more successful approach than model based predictions, is precursor based predicting. Different quantities such as return times of events, finite-time estimates of variance and autocorrelations have been employed as precursors to extreme events [6, 21].

The objective of this thesis is to identify changes in the dynamical structure of a given system, prior to an extreme event and to use those changes to explain and

predict extreme events. More specifically, we will probe the geometrical structure of the tangent space, the space of all possible perturbations to a system's state, to look for fingerprints of extreme events. We show how specific changes in the directions of perturbation growth lead to extreme events and critical transitions. We will characterize covariant Lyapunov vectors [22–25], the local intrinsic directions of perturbation growth in the phase space and finite-time Lyapunov exponents [26], the local growth rate of perturbations. We are going to test the predictive power of the covariant Lyapunov vectors and hopefully by the end of this thesis, you will be convinced that the changes in the covariant Lyapunov vectors not only have the potential to be better precursors than the classical precursors of extreme events but also, they shed light on the underlying mechanisms leading to extreme events.

On December 26, year 2003 an earthquake struck Bam, a city in the southeastern Iran leaving 26271 dead and 30000 injured. The historic city of Bam turned into a pile of rubble in a matter of seconds.

The Iranian plateau is one of the most seismically active regions in the world and earthquakes are very frequent in Iran. Nonetheless, the dimensions of this tragedy stirred up discussions about earthquakes and particularly the impending high magnitude earthquake of Tehran. A big earthquake striking the giant metropolis built recklessly on a major fault will have far more devastating results than Bam's earthquake. The government even considered moving the capital to a safer place. Of course, it never happened and after some time we, the people of Tehran, forgot about it. What brought the issue back to the surface the following year was a complex systems research group in the physics department where I studied, that was working on seismic data. In an informal seminar the group claimed that, not only they could have predicted the earthquake of Bam, but also the major earth quake of Tehran is probably coming within the next 10 days. Furthermore they claimed that they are able to predict it several hours before it happens. The prediction method was based on the increase in the Markov time scale prior to an earthquake as well as another variable based on the concept of extended self-similarity of the data. The claim was that using both quantities as precursors leads to zero rate of failure [27]. Although the group refused to talk to the media, the story went viral fast and caused another panic. The occurrence of several minor earthquakes around the same time didn't help either. Many left Tehran and many spent several nights

sleeping in their cars. I remember walking around the city wondering when it all comes to an end. It didn't come to an end, it still hasn't.

In fact, it is not only my experience with earthquake prediction that was fortunately unsuccessful. The record of earthquake predictions despite all the efforts is a long line of failures. But what qualifies as an extreme event, and are some extreme events predictable?

What is an Extreme Event? Truth be told, there is no well established, generally accepted definition of extreme events. Nevertheless there are several qualities that are loosely agreed upon. Although the term "extreme" is open to interpretations, it is expected to entail elements of surprise, rarity, high impact and unpredictability. However, while high-impact is a necessary quality for an event to be considered extreme from the point of view of a journalist, a politician or an insurer, from a scientific point of view any large deviation in a series of measurements can be considered as an extreme event. The impact can be negative as in sudden market crashes, floods or hurricanes, or positive as in the transition of the earth from the harsh Pleistocene epoch (a.k.a. Ice age) to the Holocene climate that facilitated the growth of human civilization.

Statistical Analysis and Complex Systems Approach. Extreme events have been studied from a statistical point of view for several decades [28, 29]. Extreme Value Theory is a well established area of statistics that deals with the distributions of the "outliers". The original idea of Extreme Value Theory is that the maxima of independently, identically distributed, random variables fall into a three-parameter family of generalized extreme value distributions (GEV) [30]. While in reality time series can rarely be assumed statistically independent, the corollaries of Extreme Value Theory help finding the distributions of extrema of statistically dependent data. Some useful examples include the Poisson limit theory of Volkonski and Rozanov [31], Strook-Varadhan large deviation theory and the Freidlin–Wentzell minimum action principle [32–38].

Although statistical analysis can give a description of extreme events and their return times, it cannot provide information about the underlying mechanisms, nor can it help with predicting them. Extreme events typically emerge from complex dynamics of systems with a large number of coupled degrees of freedom where the

collective effects are more important than the dynamics of the individual element. Consequently, tools from statistical mechanics which traditionally deals with large degrees of freedom as well as more recent approaches of complex systems science can be applied to study extreme events. Concepts such as transients, intermittency, large deviation theory and recurrence, have also been used to describe extreme events in the context of dynamical systems [39–41]. While in catastrophe theory, as a branch of bifurcation theory [42], singularities are perceived as extreme events [43, 44], in the context of statistical physics, extreme events are associated with critical transitions [6]. The notion of self-organized criticality (SOC) [45] has also been widely used to explain extreme events. The sand pile model that led to the concept of self-organized criticality [46, 47] exhibits arbitrarily large events. The system possesses a critical state as an attractor and therefore, it can reach the critical point with no external tuning of the bifurcation parameters. Consequently, it can be used to explain extreme events that are inherent to the system and do not happen as a result of an external shock. SOC has been associated with extreme events such as earthquakes, landslides and forest fires [48–51].

Despite the fact that, statistical analysis of extreme events has been conducted fore several decades, and more recent approaches from statistical physics and complex systems science have also assisted explaining them, the path to a detailed understanding of the underlying mechanisms leading to extreme events is a long one and we are still at the beginning [12]. Nevertheless, the high impact of extreme events, makes the task of understanding, predicting and anticipating them a necessity.

Dragon King or Black Swan? Early views on the prediction of extreme events are not very optimistic. Nasim Taleb introduced the term "Black Swan" to describe high-profile, rare events [7]. The term is based on an old saying that assumed Black Swans didn't exist and is used to emphasize on unpredictability of extreme events. Black swans, although not mathematically well defined, are typically considered to be the tails of event distributions. This view that was first introduced during the formulation of self-organized criticality [49, 52] , assumes that since extreme events are the tails of the same distribution other events belong to, they are products of the same mechanisms as the smaller events and are therefore unpredictable. In this sense, a major earthquake is inherently the same as a minor one. It just so happened that it did not stop.

In spite of Taleb's pessimistic view on the prediction of extreme events, a variety of studies have shown that a wide range of extreme events are in fact predictable [6, 8, 53–55]. Dragon king theory was developed by Sornette [56] to describe extreme events that live outside the heavy tails of power laws or Gaussian distributions of the smaller events. The term "king" is used to refer to their high magnitude and "dragon" refers to the unique conditions that generate them. The Dragon Kings are statistically and mechanistically different from the smaller events of the same system. In fact, many of the extreme events that we encounter are Dragon Kings and do not belong to the event distribution that describes their smaller siblings. Examples can be observed in the distribution of financial draw-downs, city sizes, turbulent velocity fluctuations, epileptic seizures and many other complex dynamical systems [56]. The downside of the existence of Dragon Kings is that the mechanisms leading to Dragon King like extreme events are inherent to the dynamical structure of complex systems and extreme events produced this way are much more frequent than what the tail of event distributions would predict. The upside is that these events are born due to specific mechanisms that can be identified if we take a more dynamical rather than statistical view and this is what this thesis is dedicated to; finding dynamical precursors of extreme events.

Dynamical Precursors of Dragon Kings During the course of this thesis we will analyze the dynamical precursors of the Dragon Kings. Our goal is to identify the specific changes in dynamical structure that give rise to extreme events or critical transitions. A powerful tool for characterizing the structure of dynamical systems that can also be applied to high dimensions is the concept of Lyapunov exponents and the covariant Lyapunov vectors. Covariant Lyapunov vectors indicate local intrinsic directions of the phase space.

Lyapunov exponents are famous quantifiers of chaos that are able to give information such as sensitivity to perturbations, local entropy production and the Kaplan-Yorke dimension of attractors [57–61]. Algorithms for computing Lyapunov exponents were introduced several decades ago by Shimada and Nagashima [62] as well as Bennetin [63, 64]. Although Lyapunov exponents, provide information about the dynamical structure, the associated directions of perturbation growth are more effective tools for characterizing the local dynamics. Existence of an intrinsic basis for the Lyapunov exponents, the so called covariant Lyapunov vectors was theoretically

shown long time ago [65]. Nevertheless, until recently the only numerically accessible Lyapunov vectors were the so called Gram-Schmidt vectors that are a byproduct of Gram-Schmidt orthogonalization of perturbation vectors in Bennetin method for computing Lyapunov exponents. These vectors, also referred to as Bennetin vectors or backward and forward Lyapunov vectors are time dependent, i.e., as opposed to the Lyapunov exponents which are global quantities, these vectors provide information about the local structure of attractors. However their benefit is very limited. Since they are orthogonal, they can not show the directions of the stable and unstable manifolds. They are norm-dependent and not invariant under time reversal. They are not covariant with the dynamics, i.e.,the linearized dynamics does not map the Gram-Schmidt vector at one point to the Gram-Schmidt vector of the image of that point at another time.

Meanwhile, covariant Lyapunov vectors form an intrinsic basis for the Lyapunov exponents. They point in the direction of the stable and unstable manifolds which are the inherent directions of any dynamical system. They are invariant under time reversal and covariant with the dynamics. Effective algorithms for computing covariant Lyapunov vectors, however, have only become available since 2007 [22–25]. Since then, there has been a growing interest in using the covariant Lyapunov vectors to better understand chaotic dynamics.

However, existing methods of computing the covariant Lyapunov vectors all include iterating the system forward from the far past and backwards from the far future. Therefore using these methods for predicting extreme events is not practical. We develop a new method for estimating the covariant Lyapunov vectors without iterating to the far future. We use this new method in our models and compare the results with the method of Ginelli et al. [23]. During the course of this thesis we will investigate how changes in the finite-time Lyapunov exponents along with the changes in the directions associated with them, i.e., the stable and unstable directions in the phase space represented by the covariant Lyapunov vectors, are linked to the occurrence of extreme events. We investigate critical transitions using models of fast-slow systems. Using different models of fast-slow systems, we show how tangencies between the covariant Lyapunov vectors are a generic property of critical transitions. We show that tangencies between the covariant Lyapunov vectors occur due to temporary switching between the stability of the orthogonal directions in the

phase space and that the sudden change in the stability of the orthogonal directions is a generic sign of critical transitions. Through receiver operating characteristic curves (ROC), we demonstrate that in hyperbolic dynamical systems the angle between the covariant Lyapunov vectors as well as their finite-time growth rates can be more effective precursors of critical transitions than classical precursors such as finite-time variance.

We use principal component analysis (PCA) of covariant Lyapunov vectors to measure the degree of alignment between the covariant Lyapunov vectors in high dimensional systems. We show that the type of extreme events that are tails of event size distributions, the Black Swans, are not reflected in the covariant Lyapunov vectors and therefore, we can not effectively predict them with our dynamical precursors. However, through an example of a coupled chaotic electronic circuit, we demonstrate that our dynamical precursors can predict the Dragon Kings in high-dimensional chaotic systems. We show that a sharp increase in the variance of the first principal component, indicating the main direction of the alignment of the covariant vectors, precedes a Dragon King.

We demonstrate how an increase in the degree of alignment of the covariant vectors announces the system's state entering a region of the phase space in which loss of transverse stability may lead to catastrophes. Temporary loss of transverse stability causes repelling of the trajectory from the invariant manifold. The sudden shift of the trajectory away from the invariant manifold can be temporary, leading to the so called attractor bubbling [66]. However, it can also lead to the system transitioning to another stable state. We show that the dynamical system's deviation from hyperbolicity prior to a transition, reflected in the increase in the variance of the first principal component can be used to predict the transitions. Furthermore, We use our method for estimating the covariant vectors to suppress the Dragon Kings.

2 Fundamentals

In this chapter we introduce the mathematical background needed for this thesis. This background is provided in length in [25]. We investigate growth of perturbations in the tangent space. We describe the notion of singular vectors as optimal directions of perturbation growth. We define the backward and forward Lyapunov vectors also referred to as Benettin vectors or Gram-Schmidt vectors as the infinite time limits of the singular vectors. We introduce the concept of Oseledec Splitting and use it to identify covariant Lyapunov vectors.

2.1 Singular Vectors and Lyapunov vectors

Lyapunov exponents are famous quantifiers of chaos. They represent directions of perturbation growth and can describe the dynamical structure of high-dimensional complex systems. Assume we have a dynamical system described by an ordinary differential equation,

$$\dot{u}(t) = g(u, t), \tag{2.1}$$

where, $u(t)$ is a vector in R^m and $g(u, t)$, is a nonlinear vector function. This system has a trajectory that evolves in the state space whose evolution is determined by eq. (2.1). Assume the trajectory is perturbed by an infinitesimal perturbation. Perturbations live in the tangent space, the space of all possible perturbations to

the system's state. The evolution of perturbations is governed by the following equation,

$$\dot{v} = \boldsymbol{J}(u,t)v, \tag{2.2}$$

where $\boldsymbol{J}(u,t) \in R^{m\times m}$ is the Jacobian matrix and v is the perturbation vector. This equation can be rewritten in the matrix form,

$$\dot{\boldsymbol{M}} = \boldsymbol{J}(u,t)\boldsymbol{M}. \tag{2.3}$$

$\boldsymbol{M}$ is a nonsingular matrix. The columns of $\boldsymbol{M}$ are the perturbations in different directions in the tangent space. The operator that evolves the perturbation matrix from one point in the tangent space to another is the linear propagator, F, that can be represented by the following equation,

$$F(t_1,t_2) = \boldsymbol{M}(t_2)\boldsymbol{M}^{-1}(t_1). \tag{2.4}$$

The evolution of vectors by this operator can be described as,

$$v(t_2) = F(t_1,t_2)v(t_1), \tag{2.5}$$

where $t_2 > t_1$ and the vector $v(t_1)$ has been evolving along the trajectory from point t_1 to point t_2 resulting $v(t_2)$. In order to go backwards in time the operator $\boldsymbol{F}(t_1,t_2)^{-1}$ should be employed. From eq. (2.5) we can deduce that in forward time dynamics the growth of the Euclidean norm of the perturbation vectors is governed by $\boldsymbol{F}(t_1,t_2)^T\boldsymbol{F}(t_1,t_2)$. The same applies to the growth of the perturbation vectors backwards in time and the operator $\boldsymbol{F}(t_1,t_2)^{-T}\boldsymbol{F}(t_1,t_2)^{-1}$. To make this more clear, assume $f_i^+(t_1,t_2)$ are the eigenvectors and $\sigma_i(t_1,t_2)^2$s are the eigenvalues of the operator $\boldsymbol{F}(t_1,t_2)^T\boldsymbol{F}(t_1,t_2)$ where, $\sigma_1(t_1,t_2) \geq \sigma_2(t_1,t_2) \geq ... \geq \sigma_m(t_1,t_2)$.

$$\boldsymbol{F}(t_1,t_2)^T\boldsymbol{F}(t_1,t_2)f_i^+(t_1,t_2) = \sigma_i(t_1,t_2)^2 f_i^+(t_1,t_2), \tag{2.6}$$

and hence,

$$\boldsymbol{F}(t_1,t_2)^{-T}\boldsymbol{F}(t_1,t_2)^{-1}(\boldsymbol{F}(t_1,t_2)f_i^+(t_1,t_2)) = 1/\sigma_i(t_1,t_2)^2(\boldsymbol{F}(t_1,t_2)f_i^+(t_1,t_2)). \quad (2.7)$$

I.e., the eigenvalues of $\boldsymbol{F}(t_1,t_2)^{-T}\boldsymbol{F}(t_1,t_2)^{-1}$ are $1/\sigma_i(t_1,t_2)^2$. We denote its eigenvectors by $f_i^-(t_1,t_2)$ and using eq. (2.7) we have,

$$\begin{aligned} F(t_1,t_2)f_i^+(t_1,t_2) &= f_i^-(t_1,t_2)\sigma_i(t_1,t_2) \\ F^{-1}(t_1,t_2)f_i^-(t_1,t_2) &= f_i^+(t_1,t_2)\sigma_i(t_1,t_2)^{-1} \end{aligned} \quad (2.8)$$

From eq. (2.8) we can see that if a perturbation vector at time t_1 coincides with $f_i^+(t_1,t_2)$, by evolving to time t_2 it will be equal to $f_i^-(t_1,t_2)$ and it's growth will be $\sigma_i(t_1,t_2)$. $\sigma_i(t_1,t_2)$, are called singular values and the $f_i^+(t_1,t_2)$ and $f_i^-(t_1,t_2)$ are the right and left singular vectors. The set of vectors $f_i^+(t_1,t_2)$ which are the eigenvectors of the Hermitian operator $\boldsymbol{F}(t_1,t_2)^T\boldsymbol{F}(t_1,t_2)$ are a set of orthogonal basis for the tangent space. Hence any perturbation vector can be written as a linear combination of them and it's growth rate will also be determined by the growth rates of $f_i^+(t_1,t_2)$. Namely if a perturbation vector coincides with $f_1^+(t_1,t_2)$ its growth ratio will be maximal and equal to $\sigma_1(t_1,t_2)$. Therefore these vectors are also called optimal vectors. The same logic applies to $f_i^-(t_1,t_2)$ and going backwards in time. Thus, these vectors are also called optimal vectors. It is important to emphasize that singular vectors are orthogonal and their orientation is norm-dependent [67]. Moreover in general singular vectors can exhibit degeneracy. In the absence of degeneracy they have unique directions. However, in the presence of degeneracy as well, a set of linearly independent vectors that represent singular vectors can always be found. In other words in the m dimensional tangent space you can always determine a set of orthogonal right singular vectors mapping to the left singular vectors and vice versa.

The singular values determine transformation of volumes in the tangent space. The stretch ratio of a k dimensional volume in the tangent space forward in time from t_1 to t_2 is is the product of the first k, singular values $(\sigma_i(t_1,t_2))$. The stretch ratio

of a k dimensional volume in the tangent space evolving back in time is the product of the first k reciprocal of the singular values $(1/\sigma_i(t_1, t_2))$.

The singular vectors determine the finite-time evolution of the perturbation vectors in the tangent space. However, the Lyapunov vectors determine the directions of growth of perturbations in the infinite limit. The average growth rate of the Lyapunov vectors are independent of time and are characteristic of the attractor the trajectory lies in. Oseledec's multiplicative ergodic theorem [68] proves the existence of the limit of the growth ratios and the singular vectors. To determine these vectors we introduce the *far-future operator* as,

$$W^+(t) = \lim_{t_2 \to \infty} [F(t, t_2)^T F(t, t_2)]^{1/2(t_2 - t)} \tag{2.9}$$

The eigenvectors of the far-future operator are the limits of the right singular vectors $f_i^+(t, t_2)$ with $t_2 \to \infty$. They are denoted by ϕ_i^+ and are referred to as the *forward Lyapunov vectors*. The logarithms of the eigenvalues of the far future operator are the *Lyapunov exponents*, $\lambda_1 \geq \lambda_2 ... \geq \lambda_m$. To determine the evolution of the perturbation vectors in the far past, we define the *far-past operator* as,

$$W^-(t) = \lim_{t_1 \to -\infty} [F(t_1, t)^{-T} F(t_1, t)^{-1}]^{1/2(t - t_1)} \tag{2.10}$$

The eigenvectors of the far-past operator are the limits of the left singular vectors $f_i^-(t_1, t)$ when $t_1 \to -\infty$. They are denoted by $\phi_i^-(t)$ and referred to as *backward Lyapunov vectors*. They are also called the Gram-Schmidt vectors, due to them being a byproduct of the Gram-Schmidt orthogonalization of vectors during the processes of computing Lyapunov exponent which will be explained in section 3.1. Similar to the singular vectors, the backward and forward Lyapunov vectors are orthogonal set of vectors that are norm-dependent. Although the backward and forward Lyapunov vectors are time dependent, the Lyapunov exponents do not depend on time. Rather, they are global properties that facilitate investigation of the dynamical structure. Similar to the singular vectors we can measure the

stretch rate of a k dimensional volume in the tangent space in infinite limit with the Lyapunov exponents. Namely, the stretch of a k dimensional volume in the tangent space evolving forward in time per unit time is equal to $\sum_{i=1}^{k} \lambda^{(i)}$. We will elaborate on this in the upcoming discussions. So far in our discussions we have assumed that the Lyapunov exponents are all distinct. However, in general we have to take into account possible degeneracies. Assume that a system in an m dimensional space has s distinct Lyapunov exponents ($1 \geq s \leq m$). As before we denote the ith distinct Lyapunov exponent with $\lambda^{(i)}(i = 1, ..., s)$, where each exponent has the degeneracy of ν and $\sum_{i=1}^{s} \nu = m$. Namely, there are ν_i forward and ν_i backward Lyapunov vectors associated with the ith Lyapunov exponent $\lambda^{(i)}$. Hereinafter, we will refer to the set of Lyapunov vectors associated with $\lambda^{(i)}$ as $\phi^{\pm}_{\lambda^{(i)}}$ and the jth Lyapunov vector associated with $\lambda^{(i)}$ as $\phi^{\pm}_{\lambda^{(i)},j}$. Similar to singular vectors, in the presence of degeneracy the Lyapunov vectors are not unique and any orthonormal set of vectors asymptotically growing with λ^i can be regarded as $\phi^{\pm}_{\lambda^{(i)}}$.

2.2 Oseledec subspaces and Asymptotic perturbation growth

In this section we will investigate the asymptotic growth rate of arbitrary perturbation vectors in tangent space. In order to do this, we have to identify the perturbation vectors with the subspaces spanned by Lyapunov vectors that they belong to. As mentioned before in the infinite limit the linear propagator $F(t_1, t_2)$ maps the forward Lyapunov vectors to the backward Lyapunov vectors with the stretching rate of the Lyapunov exponents.

We define the Oseledec subspace $S^+_j(t)$,

$$\begin{aligned} S^+_j(t) &= \text{span}\{\phi^+_{\lambda^{(i)}}(t) | i = j, j+1, \ldots, s\}, \\ S^+_s(t) \subset S^+_{s-1}(t) &\subset \cdots \subset S^+_1(t) = R^m \end{aligned} \tag{2.11}$$

Namely $S^+_j(t)$ consists of the subspace spanned by the forward Lyapunov vectors corresponding to the ith distinct Lyapunov exponent, $\phi^+_{\lambda^{(i)}}(t)$, where $i \leq j$. Thus

the dimension of this subspace is $\sum_{i=j}^{s} \nu_i$, ν_i being the multiplicity of $\lambda^{(i)}$. All the vectors belonging to this subspace asymptotically grow forward in time with the rate smaller than or equal to $\lambda^{(j)}$.

Consider an arbitrary vector $v^{(j)}(t)$ belonging to the subspace $S_j^+(t) \backslash S_{j+1}^+(t)$. This is the subspace $S_j^+(t)$ from which all the vectors that also belong to $S_{j+1}^+(t)$ has been subtracted. Hence $S_j^+(t) \backslash S_{j+1}^+(t)$ consists of all the vectors that are orthogonal to $\phi_{\lambda^{(i)}}^+(t)$, $i < j$ and definitely have a nonzero component along $\phi_{\lambda^{(i)}}^+(t)$. The may also have components along $\phi_{\lambda^{(i)}}^+(t)$, $i > j$. Therefore going forward in time the dominant growing component of $v^{(j)}$ is the component growing with $\lambda^{(j)}$ and in the infinite limit the vector $v^{(j)}(t)$ will exponentially grow with the average rate $\lambda^{(j)}$.

We define Oseledec subspaces spanned by the backward Lyapunov vectors,

$$\begin{aligned} S_j^-(t) &= \text{span}\{\phi_{\lambda^{(i)}}^-(t) | i = 1, 2, \ldots, j\} \\ S_1^-(t) \subset S_2^-(t) &\subset \cdots \subset S_s^-(t) = R^m \end{aligned} \tag{2.12}$$

I.e., $S_j^-(t)$ is the subspace spanned by the backward Lyapunov vectors $\phi_{\lambda^{(i)}}^-$ where $i < j$. All the vectors that belong to the subspace $S_j^-(t)$ decay with the exponential rate bigger than $\lambda^{(j)}$. These subspaces are also called Oseledec's splitting since they represent a filtering of evolution of the vectors in the tangents space [64, 67, 68]. Now consider the vector $v^{(j)}(t)$ belonging to the subspace $S_j^-(t) \backslash S_{j-1}^-(t)$. This is the subspace $S_j^-(t)$ from which all the vectors belonging to $S_{j-1}^-(t)$ have been subtracted. Therefore all the vectors in this subspace are orthogonal to $\phi_{\lambda^{(i)}}^-(t)$, $i > j$. They definitely have a nonzero component along $\phi_{\lambda^{(j)}}^-(t)$ and may or may not have nonzero components along $\phi_{\lambda^{(i)}}^-(t)$, $i < j$. Going backwards in time the slowest decaying component will be the component along $\phi_{\lambda^{(j)}}^-(t)$. Therefore, in the infinite limit the vector, $v^{(j)}(t)$ will be exponentially decaying with the rate $\lambda^{(j)}$. To summarize,

$$v^{(j)}(t_1) \in S_j^+(t_1) \backslash S_{j+1}^+(t_1) \Rightarrow \|F(t_1, t_1 + t) v^{(j)}(t_1)\| \sim e^{\lambda^{(j)} t} \tag{2.13}$$

and

$$v^{(j)}(t_1) \in S_j^-(t_1) \backslash S_{j-1}^-(t_1) \Rightarrow \|F(t_1 - t, t_1)^{-1} v^{(j)}(t_1)\| \sim e^{-\lambda^{(j)} t}. \tag{2.14}$$

Any perturbation vector in the tangent space belongs to $S_1^+(t_1)$. Furthermore $S_2^+(t_1)$ is a subspace of $S_1^+(t_1)$ that has a measure zero compared to $S_1^+(t_1)$. Hence, we can claim that almost any vector in the tangent space belongs to $S_1^+(t_1) \backslash S_2^+(t_1)$. Therefore, going forward in time, in the infinite limit, almost any vector exponentially grows with λ^1 and converges to the span of $\phi_{\lambda^1}^-(t)$, i.e., $S_1^-(t)$. For simplicity, assume that there is no degeneracy for now.

Consider a square in the tangent space. Almost any such square has a nonzero intersection with the subspace $S_2^+(t_1)$. There is a set of squares fully embedded in $S_2^+(t_1)$. However, $S_2^+(t_1)$ has a measure zero compared to $S_1^+(t)$ and can be neglected. Almost all the squares that have a nonzero intersection with the subspace $S_2^+(t_1)$ belong to $S_2^+(t_1) \backslash S_3^+(t_1)$ (again we say almost since $S_3^+(t_1)$ has a measure zero compared to $S_2^+(t_1)$ and those intersections completely belonging to $S_3^+(t_1)$ can be neglected). As a results all vectors of this square but one exponentially grow with λ^1 and converge to the span$\phi_{\lambda^1}^-(t)$ asymptotically. However, the one direction that is in the subspace $S_2^+(t_1) \backslash S_3^+(t_1)$, grows with λ^2 and converges to span$\{\phi_{\lambda^2}^-(t)\}$. Therefore the area of this square in the infinite limit exponentially grows with $\lambda^1 + \lambda^2$ and it converges to $S_2^-(t)$. However, if λ^1 is degenerate then almost all squares will be embedded in $S_1^+(t_1) \backslash S_2^+(t_1)$ and in the infinite limit the square will converge to span$\{\phi_{\lambda^1}^-(t)\}$ or $S_1^-(t)$ with exponential growth rate of $2\lambda^1$. Similarly almost any cube in the tangent space (in the absence of degeneracy) will grow asymptotically with the exponential rate of $\lambda^1 + \lambda^2 + \lambda^3$ and will converge to $S_3^-(t)$. In general, a volume of dimension k grows with the exponential rate $\sum_{i=1}^{j} \nu^{(i)} \lambda^{(i)}$, where $\sum_{i=1}^{j} \nu^{(i)} = k$ and converges to $S_j^-(t)$, where $S_{j-1}^-(t) < k \leq S_j^-(t)$, i.e.,

$$F(t_1, t) v_k(t_1) \subset_{t_1 \to -\infty} S_j^-(t) \tag{2.15}$$

$$\dim S_{j-1}^-(t) < k \leq \dim S_j^-(t) \tag{2.16}$$

The same logic applies for backwards iterations. That is, apart from a zero measure fraction of the vectors in tangent space that belong fully to $S_s^-(t_2)$ all the vectors in the tangent space are embedded in the subspace $S_s^-(t_2)\backslash S_{s-1}^-(t_2)$. There for almost any vector iterated infinitely backwards in time will decay with the exponential rate $\lambda^{(s)}$ and converge to span$\{\phi^+_{\lambda^{(s)}}(t)\}$ or S_s^+. Subsequently (in the absence of degeneracy) almost any square in the tangent space has a non-zero intersection with the subspace $S_{s-1}^-(t_2)\backslash S_{s-2}^-(t_2)$. While this intersection decays exponentially with the rate $\lambda^{(s-1)}$ and converges to span$\{\phi^+_{\lambda^{(s-1)}}(t)\}$, all the other sections of the square will decay backwards in time with the rate $\lambda^{(s)}$ and converge to span$\{\phi^+_{\lambda^s}(t)\}$. Hence the whole square will converge to S_{s-1}^+. In general any k dimensional volume in the tangent space, infinitely iterated backwards in time decays exponentially with the rate $\sum_{i=s-j}^{s}\nu^{(i)}\lambda^{(i)}$, where $\sum_{i=s-j}^{s}\nu^{(i)}=k$ and will converges to $S_j^+(t)$, where $S_{j+1}^+(t)<k\leq S_j^+(t)$, i.e.,

$$F^{-1}(t,t_2)v_k(t_2)\subset_{t_2\to\infty} S_j^+(t) \tag{2.17}$$

$$\dim S_{j+1}^+(t)<k\leq \dim S_j^+(t) \tag{2.18}$$

In the next step it is helpful to study the finite-time evolution of backward and forward Lyapunov vectors. Consider, $\phi^+_{\lambda^j}(t_1)$ and $\psi^+_{\lambda^j}(t_2)=F(t_1,t_2)\phi^+_{\lambda^j}(t_1)$. The vector $\phi^+_{\lambda^j}(t_1)$ belongs to the subspace $S_j^+(t_1)\backslash S_{j+1}^+(t_1)$. I.e., it asymptotically grows with exponential rate λ^j. Consequently, the vector $\psi^+_{\lambda^j}(t_2)$ too, asymptotically grows with the exponent λ^j and hence belongs to the subspace $S_j^+(t_2)\backslash S_{j+1}^+(t_2)$. It is important to notice that $\psi^+_{\lambda^j}(t_2)$ is not a Lyapunov vector anymore. The subspaces span$\{\phi^+_{\lambda^{(j)}}(t_2)\}$ and $S_j^+(t_2)\backslash S_{j+1}^+(t_2)$ are not equivalent. Namely the vectors belonging to the subspace $S_j^+(t_2)\backslash S_{j+1}^+(t_2)$ definitely have a nonzero component along the subspace span$\{\phi^+_{\lambda^{(j)}}(t_2)\}$ however, they usually also have non zero components along $\phi^+_{\lambda^{(i)}}(t_2)$, $i>j$. Assume we represent the forward Lyapunov vectors in the matrix form (for simplicity consider there is no degeneracy),

$$\mathbf{\Phi}^+(t)=[\phi_1^+(t),\phi_2^+(t),\ldots,\phi_m^+(t)]. \tag{2.19}$$

The column of matrix $\mathbf{\Phi}^+(t)$ represent the forward Lyapunov vectors, and $\mathbf{\Psi}^+(t_2)$ is the matrix of the finite-time evolved vectors. Notice that the first vector $\psi_1^+(t_2)$ definitely has a nonzero component along $\phi_1^+(t_2)$ and can also have components

along all other Lyapunov vectors. The second vector $\psi_2^+(t_2)$ belongs to the subspace $S_2^+(t_2)\backslash S_3^+(t_2)$ hence is orthogonal to $\phi_1^+(t_2)$, definitely has a non-zero component along $\phi_2^+(t_2)$ and can also have components along any other $\phi_i^+(t_2)$, $i > 2$. With the same logic you can see that $\psi_3^+(t_2)$ is orthogonal to $\phi_1^+(t_2)$ and $\phi_2^+(t_2)$ and so on. Therefore, we can write the relation between $\mathbf{\Phi}^+(t_2)$ and $\mathbf{\Psi}^+(t_2)$ as a QL decomposition, i.e.

$$\mathbf{\Psi}^+(t_2) = \mathbf{\Phi}^+(t_2)\boldsymbol{L}, \tag{2.20}$$

where $\boldsymbol{L}$ is a lower triangular matrix. In the presence of degeneracy, any degenerate Lyapunov exponents is associated with a space of Lyapunov vectors and any orthogonal set of vectors in that space can serve as Lyapunov vectors. That is to say $\mathbf{\Phi}(t_2)$ is not unique thus neither is the decomposition. Nevertheless eq. (2.20) one can always holds true. To summarize the finite-time evolution of a forward Lyapunov vectors are not Lyapunov vectors, i.e., forward Lyapunov vectors are not covariant with the dynamics. Nonetheless the forward Lyapunov vectors can always be recovered by performing a QL decomposition on the finite-time evolved Lyapunov vectors. For future reference it is useful to represent the iterations backwards in time,

$$F^{-1}(t_1, t_2)\mathbf{\Phi}^+(t_2) = \mathbf{\Phi}^+(t_1)\boldsymbol{L}(t_1, t_2). \tag{2.21}$$

Similarly, for iterations of backward Lyapunov vectors backwards in time consider $\phi_{\lambda^j}^-(t_2)$ and $\psi_{\lambda^j}^-(t_1) = F^{-1}(t_1, t_2)\phi_{\lambda^j}^-(t_2)$. The vector $\phi_{\lambda^j}^-(t_2)$ belongs to the subspace $S_j^-(t_2)\backslash S_{j-1}^-(t_2)$ and asymptotically decays backwards in time with exponential rate $\lambda^{(j)}$. Therefore we can conclude that $\psi_{\lambda^j}^-(t_1)$ also belongs to $S_j^-(t_1)\backslash S_{j-1}^-(t_1)$ due to its asymptotic growth rate. Hence $\psi_{\lambda^j}^-(t_1)$ is orthogonal to all $\phi_{\lambda^i}^-(t_1)$, $i > j$. It definitely has a non-zero component along $\phi_{\lambda^j}^-(t_1)$ and can also have non-zero components along all $\phi_{\lambda^i}^-(t_1)$,$i < j$. Therefore we have,

$$\mathbf{\Psi}^-(t_2) = \mathbf{\Phi}^-(t_2)\boldsymbol{R}, \tag{2.22}$$

where $\boldsymbol{R}$ is an upper triangular matrix. The mapping can be represented forward in time as,

$$F(t_1, t_2)\boldsymbol{\Phi}^-(t_1) = \boldsymbol{\Phi}^-(t_2)\boldsymbol{R}(t_1, t_2). \tag{2.23}$$

2.3 Covariant Lyapunov Vectors

As mentioned before the forward and backward Lyapunov vectors are not covariant with the dynamics and not invariant under time reversal. If you compute the Lyapunov vectors at one point and then evolve them in time using the linear propagator the resulting vectors will not be Lyapunov vectors. However, in case a vector asymptotically grows with the exponential rate of $\lambda^{(j)}$, so will its finite-time evolved version. In other words although the finite-time evolution of a Lyapunov vector is not a Lyapunov vector any more, the evolved version will stay in the Oseledec subspace that it was embedded in before the evolution. I.e., the Oseledec subspaces are covariant with the dynamics. This can also be observed in eq. (2.22) and eq. (2.20). Since QR decomposition preserves the subspace spanned by each first k columns of the factorized matrix and QL decomposition preserves the subspace spanned by each last k vectors of the factorized matrix.

$$F(t_1, t_2)S_j^+(t_1) = S_j^+(t_2), \tag{2.24}$$
$$F(t_1, t_2)S_j^-(t_1) = S_j^-(t_2). \tag{2.25}$$

The fact that Oseledec subspaces are covariant with the dynamics and invariant under time reversal leads to the assumption that it is possible to look for a set of vectors within these subspaces that are covariant with the dynamics and can be used as a basis for Lyapunov exponents. We are looking for a set of vectors that fulfill the criteria for asymptotic growth rate with Lyapunov exponents backwards and forward in time. In other words,

$$\|F(t_1, t_1 \pm t)\gamma_j(t_1)\| \sim e^{\pm\lambda_j t} \tag{2.26}$$

for $t \to \infty$, where $\gamma_{\lambda^{(j)}(t)}$, is the covariant Lyapunov vector. Covariant Lyapunov vectors are covariant with the dynamics and invariant under time reversal. Equation (2.26) implies that the covariant vectors are embedded in the subspace of intersection of the Oseledec subspaces, $\gamma_{\lambda^{(j)}}(t) \in \boldsymbol{S_j^+ \bigcap S_j^-(t)}$. The sum of the dimensions of these subspaces is bigger than the dimension of the tangent space, hence, the intersection of these subspaces is always nonzero. This property is the main idea of the method introduced by [22].

An important topic to discuss now is the relation between the forward or backward Lyapunov vectors and the covariant Lyapunov vectors. Consider the matrix $\Gamma(t)$, that is the matrix columns of which represent the covariant Lyapunov vectors $\gamma_{\lambda^{(j)}(t)}$. For the sake of simplicity assume that there is no degeneracy. Iterating $\Gamma(t)$ forward in time the first column is supposed to grow asymptotically with exponential rate λ^1, hence it belongs to the subspace $S_1^+(t)\backslash S_2^+(t)$. That is to say, it has a component along the first forward Lyapunov vector $\phi_1^+(t)$ and may also have components along all the other $\phi_i^+(t)$s. Similarly the ith column exponentially grows with λ_i and is embedded in the subspace $S_i^+(t)\backslash S_{i+1}^+(t)$. Therefore it is orthogonal to $\phi_j^+(t)$, $j < i$, definitely has a non-zero component along $\phi_i^+(t)$, and possibly has nonzero components along other $\phi_j^+(t)$, $j > i$. Therefore, we have,

$$\boldsymbol{\Gamma}(t) = \boldsymbol{\Phi}^+(t)\boldsymbol{A}^+(t), \tag{2.27}$$

where $\boldsymbol{A^+(t)}$ is a lower-triangular matrix.

Now let's study the evolution of the covariant vectors backwards in time. The first column of the matrix is $\Gamma(t)$ is the first covariant vector and hence going backwards in time it decays with the exponential rate λ^1 and belong to the subspace $S_1^+(t)$, therefor, it is tangent to the first backward Lyapunov vector, $\phi_1^-(t)$ and orthogonal to $\phi_j^-(t)$, $j > 1$. Similarly the ith column of $\Gamma(t)$ is the ith covariant Lyapunov vector

and decays with the exponential rate $\lambda^(i)$ and belongs to the subspace $S_i^-(t) \backslash S_{i-1}^-(t)$. That is to say it is orthogonal to $\phi_j^-(t)$, $j > i$, has a non-zero component along $\phi_i^-(t)$ and possibly has non-zero components along $\phi_j^-(t)$, $j < i$. Therefore, we have,

$$\boldsymbol{\Gamma}(t) = \boldsymbol{\Phi}^-(t)\boldsymbol{A}^-(t), \tag{2.28}$$

where $\boldsymbol{A^-(t)}$ is an upper-triangular matrix.

The same logic applies to the case with degenerate Lyapunov exponents and leads to eq. (2.27) and eq. (2.28). The only difference is that the matrices would not be unique and any set of linearly dependent vectors spanning the subspace corresponding to the exponent $\lambda^{(j)}$ would be appropriate as covariant vectors.

In the next step we investigate the finite-time evolution of the covariant Lyapunov vectors,

$$F(t_1, t_2)\boldsymbol{\Gamma}(t_1) = \boldsymbol{\Gamma}(t_2)\boldsymbol{C}(t_1, t_2). \tag{2.29}$$

Undoubtedly $C(t_1, t_2)$ should be diagonal in order to fulfill the covariance criteria of $\Gamma(t)$. Below we show why this is the case. Inserting eq. (2.27) in eq. (2.29) and using eq. (2.21) we have,

$$\boldsymbol{L}(t_1, t_2)\boldsymbol{A}^+(t_2)\boldsymbol{C}(t_1, t_2) = \boldsymbol{A}^+(t_1) \tag{2.30}$$

In eq. (2.30) all the matrices apart from $C(t_1, t_2)$ are lower-triangular, hence, $C(t_1, t_2)$, is lower triangular as well. Inserting eq. (2.28) in eq. (2.29) and using eq. (2.23) we have

$$\boldsymbol{R}(t_1, t_2)\boldsymbol{A}^-(t_1) = \boldsymbol{A}^-(t_2)\boldsymbol{C}(t_1, t_2). \tag{2.31}$$

In eq. (2.31) all the matrices apart from $C(t_1, t_2)$ are upper-triangular, hence, $C(t_1, t_2)$ is upper-triangular as well. Since $C(t_1, t_2)$, has to be simultaneously upper and lower-triangular it can only be diagonal. The diagonal elements of $C(t_1, t_2)$ represent the finite-time growth rate of the covariant Lyapunov vectors aka finite-time Lyapunov exponents. Equation (2.29) indicates that once the covariant vectors have been computed, they can be computed at other times by evolving by the linear propagator. Although, this is true in theory, in practice the accumulation of numerical error makes the vectors diverge from the direction of covariant vectors and all will converge to the fastest growing direction that corresponds to the first Lyapunov exponent. The numerical methods for computing the Lyapunov exponents and covariant Lyapunov vectors is the subject of the following sections.

3 Computational methods

This chapter is dedicated to the main computational methods used in the thesis. We briefly explain the Bennetin method for computing the Lyapunov exponents as well as the Backward and forward Lyapunov vectors. We present the available methods for computing covariant Lyapunov vectors and give a detailed explanation of the Ginelli et al.'s method that is used through out this thesis. Further we introduce a new method for estimating the covariant Lyapunov vectors that makes it possible to measure the vectors with out iterating the system to the far future. This method enables us to use the covariant Lyapunov vectors for prediction purposes. Throughout this thesis we will compare the two methods by using them on different models.

3.1 Computation of Lyapunov Exponents, Backward and Forward Lyapunov Vectors, Bennetin's Method

The effective algorithms for computing the backward Lyapunov vectors and the Lyapunov exponents was introduced almost simultaneously by Bennetin et al. [63, 64] and by Shimada et al. [62]. The main idea is to employ eq. (2.23) which governs the evolution of the backward Lyapunov vectors forward in time. The basis of this method is the assumption that a random orthogonal set of vectors iterated forward in time with eq. (2.23) will converge to the backward Lyapunov vectors. The reason for this convergence is eq. (2.15). This equation indicates that a k dimensional volume evolved forward in time with the linear propagator will in the infinite limit converge

to the Oseledec subspace $S_j^-(t)$ where $j \leq k$ depending on the degeneracy of the Lyapunov Exponents. We also know that in practice due to numerical noise every such volume will converge to the subspace spanned by the first Lyapunov exponent if we use eq. (2.15). However, using eq. (2.23) while evolving the vectors forward in time we preserve the subspace spanned by them and prevent the subspace they span from collapsing on $S_1^-(t)$. This processes is equivalent to the Gram-Schmidt Orthogonalization procedure.

A more practical explanation of the method is as follows: First, we need to initialize the perturbation vectors to represent the volume that is going to asymptotically converge to the span of the backward Lyapunov vectors through evolution via the linear propagator. It would be enough to initialize any random orthogonal matrix $\boldsymbol{Q}(t_1)$. Second, we evolve $\boldsymbol{Q}(t_1)$ forward in time using the linear propagator,

$$\boldsymbol{V}(t_2) = \boldsymbol{F}(t_1, t_2)\boldsymbol{Q}(t_1). \tag{3.1}$$

The resulting matrix will consist of a set of vectors that are no longer orthogonal. Using this matrix we want to find the matrix of the $\boldsymbol{Q}(t_2)$. We do not change the first vector, we let it grow with the linear propagator. After long enough transient time this vector will grow in the direction of the first backward Lyapunov vector. We only have to normalize it to prevent overflow. The growth of this vectors during each interval is the first finite-time Lyapunov exponent.

According to eq. (2.23) in the absence of degeneracy the subspace spanned by the first and the second vector will converge to S_2^-, The only thing we need to do is to prevent the subspace from collapsing on S_1^-. This is possible by subtracting the projection of the second vector $v_2(t_2)$ on $v_1(t_2)$ from $v_2(t_2)$. While this orthogonalization procedure preserves the subspace spanned by the two vectors it prevents $q_2(t_2)$ from collapsing on $q_1(t_2)$. In the next step we need to normalize the second vector. The normalization coefficient will be the second finite-time Lyapunov exponent. Although in case λ_1 is degenerate this processes is not needed for defining the second vector, this method is still valid and can be applied specifically since, unless we have prior knowledge, it is very difficult to identify degeneracy in the

Lyapunov exponents. As for the third vector we can say that the subspace spanned by the first three vectors converges to S_3^-, in the absence of degeneracy. That is the case however, only if we prevent collapsing of this subspace. Same as before we do this by subtracting the projections of $v_3(t_2)$ on $v_1(t_2)$ and $v_2(t_2)$. This way, while preserving the subspace spanned by the three vectors we prevent the third vector from collapsing on the subspace of the first and the second vector. We continue this process until we have the complete matrix $\boldsymbol{Q}(t_2)$. To go forward in time we apply the linear propagator on the matrix $\boldsymbol{Q}$ again, and repeat the same orthogonalization process.

Let's have a closer look at the processes of building $\boldsymbol{Q}$ from $\boldsymbol{V}$. The orthogonalization processes we described means that the first column of $\boldsymbol{V}$, that is the vector v_1, has the same direction as the first column of $\boldsymbol{Q}$, i.e., q_1. The second vector v_1 has only nonzero projections onto q_1 and q_2 and so on. That is to say $\boldsymbol{V}$ can be written as the multiplication of the matrix $\boldsymbol{Q}$ with an upper triangular matrix $\boldsymbol{R}$,

$$\boldsymbol{V}(t_2) = \boldsymbol{Q}(t_2)\boldsymbol{R}(t_1, t_2). \tag{3.2}$$

I.e. $\boldsymbol{Q}$ can be recovered after evolution by the linear propagator through QR-decomposition. The finite time Lyapunov exponents will be diagonal elements of $\boldsymbol{R}$, the average of which yields the Lyapunov Exponents.

3.2 Computing Covariant Lyapunov vectors

Effective algorithms that make computation of covariant Lyapunov vectors possible, were introduced simultaneously by Ginelli et al. [23] and by Samelson and Wolfe [22] in 2007. Later Kuptsov and Parlitz [25] introduced the new method of LU factorization. In the following we explain the method of Ginelli et al. [23] and introduce a new method for estimating the covariant Lyapunov vectors.

3.3 Computing Covariant Lyapunov Vectors Using Ginelli et al.'s Method

The method presented by Ginelli et al. is based on the asymptotic behavior of the covariant Lyapunov vectors. The covariant Lyapunov vectors grow exponentially backwards and forward in time with the Lyapunov exponents, eq. (2.26). Ginelli et al.'s method suggested that performing iterations backwards in time on a random set of vectors, while confining them to the space of projections on the backward Lyapunov vectors, will lead to the convergence of the set to the covariant Lyapunov vectors.

In this method eq. (2.31) is considered as the stable dynamics to which any random upper-triangular matrix will converge after sufficient transient time. To consider the method in more detail let's take another look at eq. (2.14). If we compute the backward vectors and hence the Oseledec subspaces, any vector initialized within the corresponding Oseledec subspace as in eq. (2.14) and iterated backwards will converge to the corresponding covariant Lyapunov vector. However this is only true in theory. In practice due to numerical noise all the vectors will converge to the subspace $S_m^-(t) \backslash S_{m-1}^-(t)$ and grow with the smallest Lyapunov exponent, λ_m.

The solution to this problem offered by Ginelli et al. was to iterate these vectors backwards in time, in the space of projections on to the backward Lyapunov vectors in order to confine them to their corresponding Oseledec subspaces and prevent them from collapsing on the subspace $S_m^-(t) \backslash S_{m-1}^-(t)$.

Te following is a recipe for this method:

The first step is the same as the process of computing the Lyapunov exponents. Start with a random set of orthogonal vectors as the initial set of perturbation vectors. Evolve the system forward in time. Evolve the perturbation vectors forward in time using the Jacobian matrix. Let the perturbation vectors evolve several time steps and then perform QR factorization to orthogonalize them again. After a transient time that should be sufficiently long you can assume that the perturbation vectors, i.e., the columns of the matrix $\boldsymbol{Q}(t_n)$ of the QR decomposition have converged to the backward Lyapunov vectors. From this point on you can start storing the backward

vectors $\boldsymbol{Q}(t_n)$ and the matrix $\boldsymbol{R}(t_n, t_{n+1})$ that is derived from the QR decomposition. Remember that the upper-triangular matrix $\boldsymbol{R}(t_n, t_{n+1})$ is the matrix form eq. (2.23) here we have,

$$F(t_n, t_{n+1})\boldsymbol{\Phi}^-(t_n) = \boldsymbol{\Phi}^-(t_{n+1})\boldsymbol{R}(t_n, t_{n+1}). \tag{3.3}$$

As is evident from eq. (3.3), the matrix $\boldsymbol{R}(t_n, t_{n+1})$ determines the evolution of perturbations that are confined to the space of backward vectors between t_n and t_{n+1}. Hence for the backward iterations you only need the matrix $\boldsymbol{R}$ to evolve the perturbations. Continue storing the backward Lyapunov vectors and $\boldsymbol{R}$ for the entire interval of which you need the covariant Lyapunov vectors. Once you reach the end of the interval you need to go forward in time to have a second transient for the backwards iterations. However since you don't need the covariant vectors for this transient only store the $\boldsymbol{R}$. This transient time need to be long enough for the vectors to converge to the covariant Lyapunov vectors.

After sufficient time you can start the backward iterations. As previously mentioned the main idea of this method is to confine a random set of vectors in the space of the projections onto the backward Lyapunov vectors and iterate backwards to reach the covariant Lyapunov vectors. Reorganizing eq. (2.31) we have the dynamic rule for the evolution of the covariant vectors backward in time,

$$\boldsymbol{R}(t_n, t_{n+1})^{-1}\boldsymbol{A}^-(t_n + 1) = \boldsymbol{A}^-(t_n)\boldsymbol{C}(t_n, t_{n+1})^{-1}, \tag{3.4}$$

where $\boldsymbol{A}^-(t)$ is an upper-triangular matrix that is the matrix of the projections of the covariant Lyapunov vectors on the backward vectors and $\boldsymbol{C}(t_n, t_{n+1})$ is a diagonal matrix, the elements of which are the finite-time covariant Lyapunov exponents. Knowing the dynamical rule of eq. (3.4) you can perform the backward iterations. In order to start you can use any random upper-triangular matrix, $\boldsymbol{A}$ and start iterating backwards using the matrices $\boldsymbol{R}$ previously stored, by the end of the transient time the matrices $\boldsymbol{A}^-$ have converged to the covariant Lyapunov vectors in the basis of the backward vectors. In case the covariant Lyapunov vectors are needed in the

same basis as the backward vectors, it suffices to multiply them with the stored matrix of the backward Lyapunov vectors, see eq. (2.28).

3.4 Estimating the vectors without going to the Far Future

This thesis is dedicated to investigation of the behaviors of the covariant Lyapunov vectors during and prior to extreme events and critical transitions. Our goal is to use the covariant Lyapunov vectors to show the changes in the dynamical structure of the systems that lead to extreme events and critical transitions. However, apart from giving a qualitative description of structural changes leading to extreme events and critical transitions, we would like to introduce the changes in the covariant Lyapunov vectors as practical candidates for predicting extreme events and critical transitions. We would also like to compare their predictive powers with other classical predictors such as the finite-time variance. Nonetheless, the methods of computing covariant Lyapunov vectors introduced so far all require evolving the perturbation vectors backwards from the far future. Using the recordings from the future makes these methods practically useless for our prediction purposes.

Consequently, we devise a method for estimating the covariant Lyapunov vectors without using data from the far future. This method only uses the data from the past and the immediate future. The main idea is, first to evolve the covariant Lyapunov vectors computed in the preceding point forward, in the space of the projections onto the backward Lyapunov vectors to the present, then evolve the resulting vectors from the immediate future backwards to the present repeatedly.

That is to say, same as Ginelli et al.'s method we utilize the asymptotic behavior of the covariant Lyapunov vectors and confine the evolution of the perturbation vectors to the space of projections onto the backward Lyapunov vectors. However, instead of using a random matrix as the initial set of perturbations we evolve the covariant Lyapunov vectors computed in the preceding point with the linear propagator while confined to the space of projections onto the backward Lyapunov vectors. Assuming we have no access to the far future we then evolve the vectors backwards in time

repeatedly, i.e., we use the linear propagator of the immediate future that we know, as an estimate for the propagator of the more distant future. Say you need to compute the covariant Lyapunov vectors at time t_1 and you only have the data until t_2 where $t_2 > t_1$. $t_2 - t_1 \geq \Delta$ can be as small as desired. The minimum amount is one orthogonalization step , Δ, i.e., the distance between two QR decompositions. In fact for all our systems in which we use this method we assumed $t_2 - t_1$ to be one orthogonalization step. In this method we use two transient times both of which are in the far past. The first transient is for the perturbation vectors to converge to the backward vectors and the second is for them to converge to the covariant vectors.

Here is a more detailed explanation of the practical implementation of the method: Start in the far past and evolve the system and the perturbation vectors, orthogonalizing every several time steps as explained in section 3.1. After a long enough transient time you can assume that the perturbation vectors have converged to the backward Lyapunov vectors. The next step is to compute the vectors that, through the second transient, will converge to the covariant Lyapunov vectors. The second transient doesn't need to be long. It can be as short as the available data allows.

First, let's have another look at the evolution of the covariant Lyapunov vectors backwards and forward in time, in the space of projections onto the backward Lyapunov vectors. The evolution of the covariant Lyapunov vectors forward in time is governed by the following equation,

$$\boldsymbol{R}(t_1, t_2)\boldsymbol{A}^-(t_1) = \boldsymbol{A}^-(t_2)\boldsymbol{C}(t_1, t_2). \tag{3.5}$$

We also know that reorganizing eq. (3.5) gives us the evolution of the covariant Lyapunov vectors backwards in time,

$$\boldsymbol{R}(t_1, t_2)^{-1}\boldsymbol{A}^-(t_2) = \boldsymbol{A}^-(t_1)\boldsymbol{C}(t_1, t_2)^{-1}. \tag{3.6}$$

Knowing the dynamics of the backwards and forward transformation in the space of projections onto backward Lyapunov vectors you can start the second transient. Assume your starting point to be t_n. The idea here is to use only information from t_n

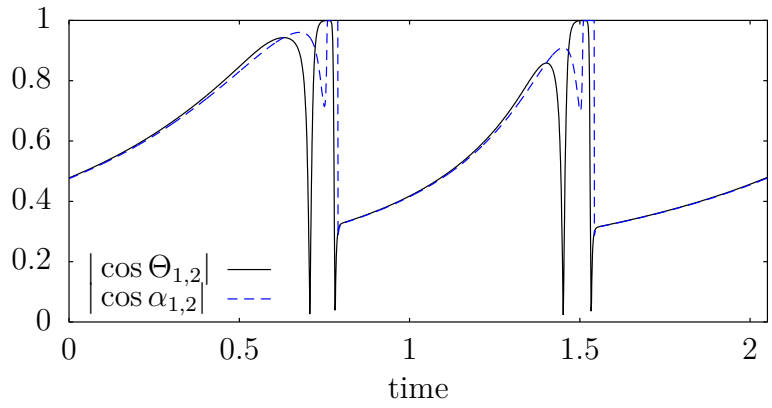

Figure 3.1: Estimating approximations of covariant Lyapunov vectors with the repetitive iteration method yields results which mimic the dynamics of covariant Lyapunov vectors computed through Ginelli et al.'s method. The absolute value of the cosine of the angle between the first and the second covariant Lyapunov vectors computed with Ginelli et al.'s method, solid black line, are compared with the results from the repetitive iteration method, dashed blue line, for a FitzHugh-Nagumo model with $a = 0.4$, $b = 0.3$, $e = 0.01$ and $D = 0$.

to $t_n+\tau$ for computing the covariant vectors, where, τ, can be as small as need be. In all our computations we assumed τ to be equal to one orthogonalization step, Δ, that is the minimum value it can take. In the next step evolve the perturbation vectors from t_n to $t_n+\tau$ and record $\boldsymbol{R}(t_n, t_n+\tau)$. Compute the inverse, $\boldsymbol{R}(t_n, t_n+\tau)^{-1}$ and multiply it with a random upper-triangular matrix $\boldsymbol{A}_{\boldsymbol{R}}(t_n)$ according to eq. (3.6). Repeat multiplying the result with $\boldsymbol{R}(t_0, t_0+\tau)^{-1}$, N times.

$$\boldsymbol{A}^{'}(t_n) \propto \boldsymbol{R}(t_n, t_n+\tau)^{-N} \boldsymbol{A}_{\boldsymbol{R}}(t_n). \tag{3.7}$$

The value of N depends on the specific model and should be chosen accordingly. Applying the resulting matrix to the backward vectors computed at time t_n gives us an estimate of the covariant Lyapunov vectors.

However, after evaluating the vectors for the very first point, t_n, we don't have to use random matrices any more. As a matter of fact we can improve our estimate of the covariant vectors by evolving the vectors computed in the previous points. That is to say we use the basic property of the covariant Lyapunov vectors that is their

covariance with the dynamics to evolve them from the previous to the next point. Nonetheless since we don't have the exact covariant vectors and accumulation of numerical errors will also make it impossible for the vectors to remain covariant we can only get a good estimate of the vectors through repeated evolution backwards in the space of projections onto the backward Lyapunov vectors.

In more detail, knowing $\boldsymbol{A}^{'}(t_n)$, the matrix $\boldsymbol{A}^{'}(t_{n+1})$ for the next time step $t_{n+1} = t_n + \Delta$, can be obtained by evolving $\boldsymbol{A}^{'}(t_n)$ from t_n to $t_{n+1}+\tau$, in the space of projections onto the backward vectors using eq. (3.5), and then using the evolved matrix to iterate backwards from $t_{n+1}+\tau$ to t_{n+1}, N times. Since $\boldsymbol{R}(t_n, t_{n+1})^{-1}\boldsymbol{R}(t_n, t_{n+1}) = 1$ we have,

$$\boldsymbol{A}^{'}(t_{n+1}) \propto \boldsymbol{R}(t_{n+1}, t_{n+1}+\tau)^{-(N-1)}\boldsymbol{R}(t_n, t_{n+1})\boldsymbol{A}^{'}(t_n), \tag{3.8}$$

In other words, using information of the vectors computed in the past one can improve the estimate of the vectors in the present. Therefore using matrices $A^{'}(t_p)$ from the past to successively compute $A^{'}(t_n)$ with $t_p < t_n$, gradually improves the precision of the estimates during the time steps of the second transient .

Using the $A^{'}$ from the past to compute the $A^{'}$ gradually improves the precision of your estimates. After a short transient you can assume that the matrix $\boldsymbol{A}^{'}$ has converged to an estimate of $\boldsymbol{A}^{-}$, that is the matrix of projection of the covariant Lyapunov vectors onto the backward vectors. Multiplying this matrix with the matrix of backward vectors gives you an estimate of the covariant Lyapunov vectors. Figure 3.1 shows the angle between the first and the second covariant vector of a FitzHugh-Nagumo oscillator computed with Gienlli et al.'s method and the estimating method.

A difficulty that can occur with this method in systems with highly expanding directions is that $\boldsymbol{A}^{'}$ becomes ill-conditioned and several vectors collapse on each other. The solution in that case is to randomize the matrix $\boldsymbol{A}^{'}$ again. Ill-conditioned $\boldsymbol{A}^{'}$ can also occur during repeated iterations. This problem usually occurs if N is too large. In this case it suffices to reduce N to a value that is large enough to guarantee convergence of the vectors to the covariant directions and small enough not to cause singularities in $\boldsymbol{A}^{'}$.

Note that if one has enough data in the past one can use any "standard" method to covariant vectors (e.g. Ginelli et al.'s) until the near past and then use the approximative method described above to compute a present estimate of covariant vectors. Moreover, bear in mind that this method only yields estimates of the covariant Lyapunov vectors and not the exact vectors. Nonetheless it seems to be leading to effective approximations of the vectors without asymptotic backwards iterations. The advantage of this method as mentioned before is that it enables us to compute the covariant Lyapunov vectors at any point without using data from the future. This will prove to be important in the later stages of this work.

4 Critical Transitions

This chapter is dedicated to critical transitions in models of dynamical systems. Critical transitions represent a large classes of extreme events. We use the mathematical framework of fast-slow systems to explore critical transitions. Our models of fast-slow systems include, FitzHugh-Nagumo oscillator, Van der Pol oscillator, Josephson junction and Hindmarsh-Rose model. We compute the covariant Lyapunov vectors with the Ginelli et al.'s method as well as the repetitive iteration method and analyze the changes in the covariant Lyapunov vectors prior to critical transitions.

4.1 Mathematical framework

From financial market crashes [69, 70] to the climate [13, 71], from earth systems [72, 73] to medical conditions [74–76], a wide range of extreme events in complex systems are considered to be critical transitions. During a critical transition the system undergoes an abrupt shift from one state to another. Systems undergoing critical transitions exhibit generic properties that can be used for prediction of the transition [77]. The most famous symptom of a critical transition is the system's slow recovery from perturbations before a tipping point, a phenomenon referred to as *critical slowing down* [78, 79]. It has been shown in different systems that critical slowing down starts prior to a critical transition and the recovery rate from perturbations gradually goes to zero as the system approaches the tipping point [80]. Critical slowing down manifests itself in different observables such as in the increased variance. As the system approaches the tipping point decreased recovery rate from perturbations implies that the impact of fluctuations does not disappear

[81]. The accumulation of fluctuations leads to an increased variance [82, 83]. Other signs of critical slowing down include increased autocorrelation [84–86], skewness and flickering, i.e., increased asymmetry in the fluctuations [87–89] before transitions.

Critical transitions occur in dynamical systems that gradually move towards a tipping point. Typically there are one or several parameters that move slowly until the critical point, i.e., the bifurcation parameters. Therefore a typical mathematical model to describe critical transition is fast-slow systems. A general fast-slow system can be written as,

$$\begin{aligned} \epsilon \dot{x} &= f(x, y) \\ \dot{y} &= g(x, y), \end{aligned} \tag{4.1}$$

where $\epsilon \ll 1$. Fast-slow systems exist in multiple time scales and the slow variables can be considered as the bifurcation parameters pushing the system towards a tipping point. We will investigate different fast-slow systems and compute their covariant Lyapunov vectors using the Ginelli et al.'s method and our own repetitive iteration method in order to see how critical transitions are reflected in the changes in the covariant Lyapunov vectors and the Lyapunov exponents. We will then use the angle between the covariant Lyapunov vectors as well as the finite-time Lyapunov exponents to predict critical transitions with different lead times and compare the results to predictions made by the finite-time estimates of variance as a typical variable used for predicting critical transitions.

4.2 FitzHugh-Nagumo Oscillators

The FitzHugh-Nagumo model is s two dimensional simplification of the Hodgkin-Huxley model for neural activity introduced by Richard FitzHugh [90–92]. Later Nagumo et al. [93] developed and explored an electric circuit equivalent of this model. The rich dynamics of this model makes it a good candidate for excitable dynamics and relaxation oscillators, not only in neuroscience but also in other areas

of physics. The basic model is a two dimensional system with continuous time dynamics that is represented by two nonlinear, ordinary differential equations.

$$\epsilon \dot{x} = x - \frac{x^3}{3} - y, \tag{4.2}$$

$$\dot{y} = x + a - by + \sqrt{2D}\eta(t). \tag{4.3}$$

The variable x depicts the membrane voltage and y is the recovery variable describing the inactivation of the sodium and potassium channels [94, 95]. In order to have relaxation oscillations, ϵ should be much smaller that one. This way the two variables x and y will act in two different time scales. x will be the fast variable and y will be the slow control parameter. Parameters a and b determine the position of the fixed point and the average duration of an excitation. The stochastic term in the second variable $\eta(t)$ is white noise representing the random fluctuations in the sodium and potassium channels. Nagumo et al. [93, 94] described this model with an electric circuit including a capacitor, a tunnel diode, a resistor, an inductor, and a battery. The capacitor represents the membrane capacitance, the tunnel diode describes the nonlinear dynamics of the fast membrane current and the resistor depicts the resistance of the channels. Understanding this system is easy by looking at the nullclines of the variables. As previously mentioned the x and the y variable live on two different time scales. Therefore any point that is not on the x-nullcline is attracted to the x-nullcline without significant change in the y variable. Once it lands on the x-nullcline, $\dot{x}$ becomes zero. However small but non-zero value of $\dot{y}$ forces the trajectory to gradually crawl up the left branch or down the right branch. If it reaches one of the knees (the maximum or the minimum of the x nullcline) it will be detached from the x-nullcline. At this point $\dot{x}$ starts to rapidly increase. The trajectory travels from one branch to the other in a very short time. Due to the small value of $\dot{y}$ there is no significant change in y during this transition. Also note that $\dot{x}$ depends on the vertical distance of the trajectory from the x-nullcline. Therefore the rapid increase in the first half of the transition, as it is moving towards the extremum of the x-nullcline is followed by a fast decrease of $\dot{x}$ as it moves past the extremum. This rapid transition from one branch to the other depicts a neural

spiking.

The spiking behavior of the oscillator is determined by the relative position of the fixed point. A fixed point located on the left branch is a stable fixed point. In this case, in the absence of any perturbation, $D = 0$, the system remains in the fixed point and no spike will be generated, hence only noise induced transitions can happen. By decreasing a, however, the location of the fixed point can shift to the right, once it reaches the left knee it undergoes a Hopf bifurcation and a limit cycle emerges. The fixed point in the middle branch is unstable and the system in this case regularly spikes. Figure 4.1 shows the oscillators in both excitable spiking and regular or tonic spiking regime. In the absence of external input in the excitable oscillator only one transition happens, that is when the trajectory flies from the right branch to the left one to reach the stable fixed point and rest there (fig. 4.1 left). However in an oscillator with the unstable fixed point, regular transitions happen even in the absence of any perturbation (fig. 4.1 right). Figure 4.2 shows that the trajectories starting in different states in the phase space are attracted to the nullclines in both regimes.

We computed the covariant Lyapunov vectors and the finite-time Lyapunov exponents for the FitzHugh-Nagumo oscillator in both spiking regimes. Figure 4.3 and fig. 4.4 present the results using Ginelli et al.'s [23] method. We chose the integration step of $\delta t = 0.001$ and the orthogonalization interval of $\Delta = 0.01$. Figure 4.3 shows the results for, $a = 1, b = 0.3, \epsilon = 0.01$ and $D = 0.2$, i.e, noise induced transition regime.

The first covariant vector is the same as the first backward vector and corresponds to the largest Lyapunov exponent, i.e., the fastest growing direction. As the trajectory slowly moves along one of the branches, this direction would be the neutral direction. That is to say, perturbations along this direction neither shrink nor grow, therefore the first finite-time Lyapunov exponent would be zero. Figure 4.3(e) shows the first finite-time Lyapunov exponent. As depicted in the figure while the system is not undergoing any transition the first finite-time Lyapunov exponent remains close to zero. Very close to the transition, the first finite-time Lyapunov exponent rapidly increases and becomes positive enabling the transitions. As the trajectory traverses to the other branch, any perturbation along the trajectory will also rapidly grow

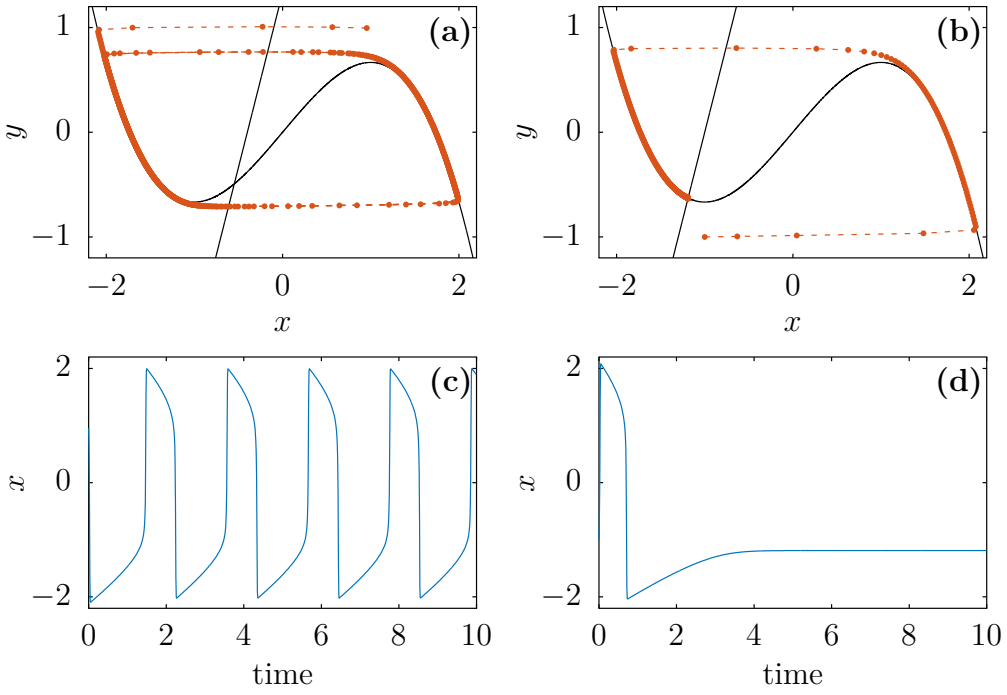

Figure 4.1: Spiking pattern of a FitzHugh-Nagumo Oscillator depends on the position of the fixed point. The black lines are the nullclines and the red lines are typical trajectories in the absence of noise. The blue lines are the time series of the trajectory. (a) Phase space portrait of a FitzHugh-Nagumo oscillator in the regular spiking regime. (b) Phase space portrait of a FitzHugh-Nagumo oscillator in the quiescent regime. (c) Time-series of the fast variable in the regular spiking regime. (b) The time-series of the fast variable in the quiescent regime.

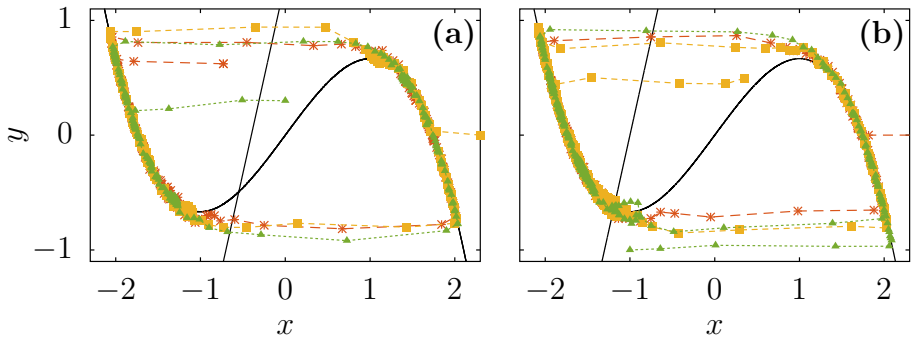

Figure 4.2: Sample trajectories of a FitzHugh-Nagumo oscillator starting at different regions of phase space, (a) in the regular spiking regime and (b) in the excitable regime.

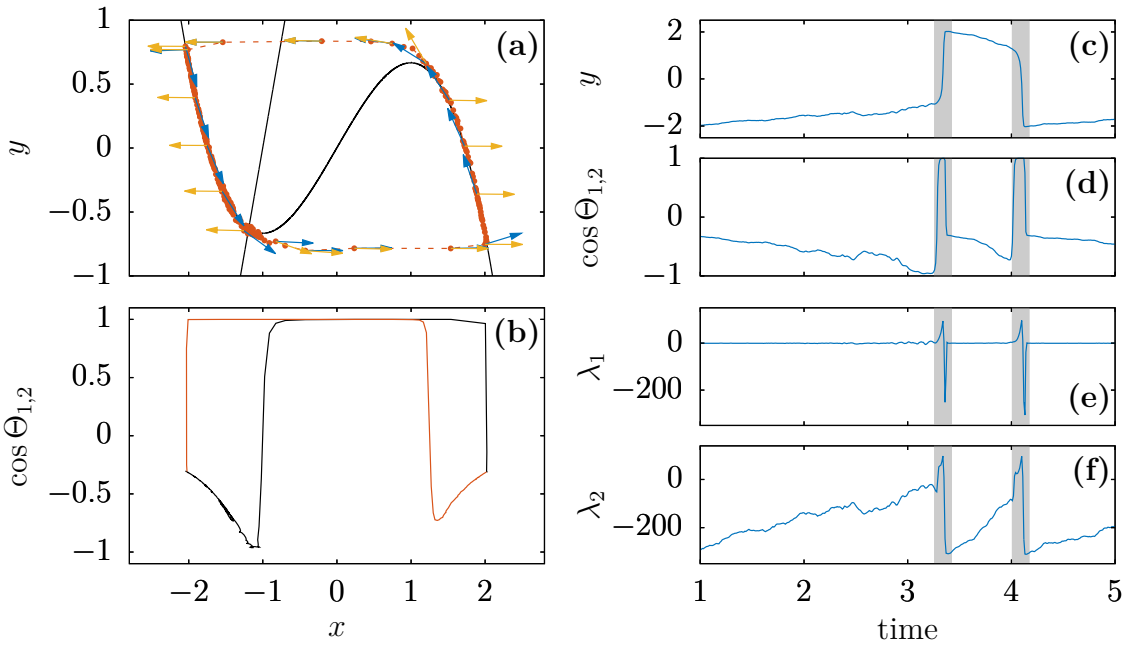

Figure 4.3: Alignment of covariant Lyapunov vectors during noise-induced transitions in a FitzHugh-Nagumo oscillator with $a = 1$, $b = 0.3$, $\epsilon = 0.01$ and $D = 0.2$, i.e., excitable regime. Vectors are computed via Ginelli et al.'s method. (a) The red line indicates a typical trajectory in the phase space. The blue and the yellow vectors show the first and the second covariant Lyapunov vector respectively, both vectors align during transitions. (b) The angle between the first and the second vector is shown while the system is drifting on the left and transitioning to the right branch (black line) and drifting on the right and transitioning to the left branch (red line). (c) Time series of the fast variable, i.e., the observable of the system. (d) Time series of the cosine of the angle between the first and the second vector. (e) Time series of the first finite-time Lyapunov exponent. (f) Time series of the second finite-time Lyapunov exponent.

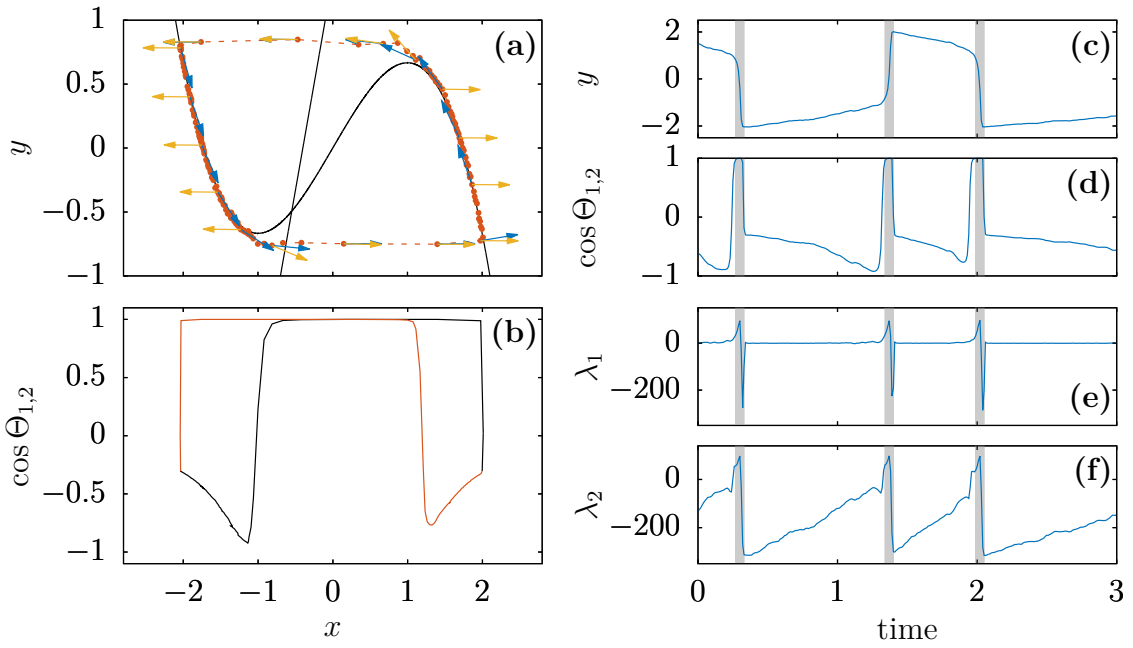

Figure 4.4: Alignment of covariant Lyapunov vectors in a single FitzHugh-Nagumo oscillator with $a = 0.4$, $b = 0.3$, $\epsilon = 0.01$ and $D = 0.2$ during transitions in the regularly spiking regime. Vectors are computed via Ginelli et al.'s method. (a) The red line indicates a typical trajectory in the phase space. The blue and yellow vectors show the first and the second covariant Lyapunov vector respectively, both vectors align during transitions. (b) The angle between the first and the second vector is shown while the system is drifting on the left and transitioning to the right branch (black line) and drifting on the right and transitioning to the left branch (red line). (c) Time series of the fast variable, i.e., the observable of the system. (d) Time series of the cosine of the angle between the first and the second vector. (e) Time series of the first finite-time Lyapunov exponent. (f) Time series of the second finite-time Lyapunov exponent.

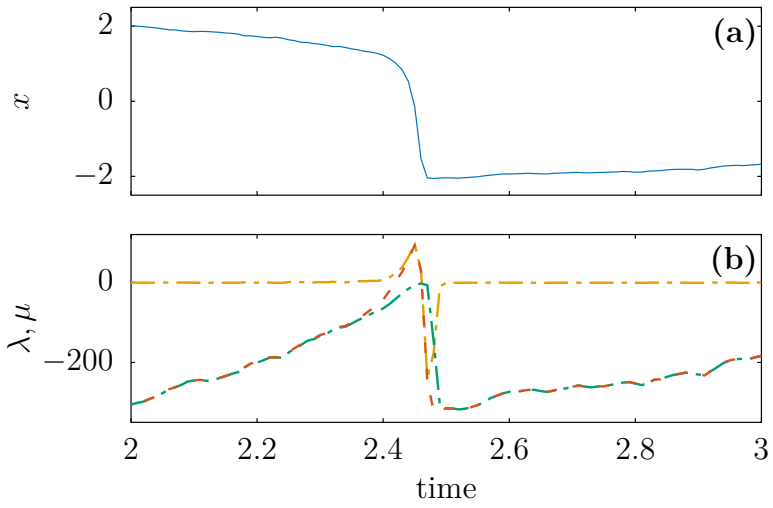

Figure 4.5: While the trajectory is slowly drifting on the nullcline the growth rate of the second covariant vector (red line) is similar to the second finite-time Lyapunov exponent (green line). Merging of the first and the second covariant Lyapunov vector during the transition manifests itself in converging of the growth rate of the second covariant vector to the first finite-time exponent (orange line). Note that the growth rate of the first covariant Lyapunov vector is by definition the same as the first finite-time Lyapunov exponent $\lambda_1(t) = \mu_1(t)$. (a) Time series of the fast variable of a single FitzHugh-Nagumo oscillator in the noise induced transitions regime. (b) The first (orange line) and the second (green line) finite time Lyapunov exponent, $\lambda_1(t)$ and $\lambda_2(t)$ are compared to the finite-time growth rate of the second covariant Lyapunov vector (red line), $\mu_2(t)$. The growth rate of the second vector is computed via Ginelli et al.'s method.

as the trajectory is moving further away from the x-nullcline. However, during the second half of the transition, any perturbation along the trajectory will shrink rapidly as the fast variable is decelerating prior to arriving at the other branch. At the end of the transition, arriving again at the x-nullcline, the first finite-time Lyapunov exponent approaches zero once more.

The second finite-time Lyapunov exponent corresponds to the growth rate of the second backward vector that is orthogonal to the first backward vector (which is the first covariant Lyapunov vector). While the trajectory is crawling up or down one of the branches perturbations along the direction orthogonal to the trajectory die fast therefore the second finite-time Lyapunov exponent is highly negative ,as seen in fig. 4.3(f). During the transition however any perturbation orthogonal to the trajectory neither shrinks nor grows, therefore, during the transition the second finite-time Lyapunov exponents stays zero.

The transition is also reflected in the angle between covariant Lyapunov vectors, i.e., here, the angle between first and second covariant Lyapunov vector, $\theta_{1,2}$. The angle decreases as the system moves towards a transition on the nullcline since the angle between the trajectory and the unstable direction is decreasing (fig. 4.3(a) and (fig. 4.3(b))) Beginning of the transition is marked by the trajectory becoming completely tangent to the direction of the second covariant Lyapunov vector (fig. 4.3(a)). Note that this implies that the system is effectively one-dimensional during the transition to the other section of the manifold. That is to say, there is only one effective dimension in this dynamical system during the transition and that is the direction of the trajectory moving across the branches.

The alignment of the covariant Lyapunov vectors is a generic sign of critical transitions. In general temporary switching between the stability of the orthogonal directions causes alignment between the covariant Lyapunov vectors. Although tangencies between the vectors are not exclusive to critical transitions, we argue that these transitions are typically accompanied with tangencies between the covariant Lyapunov vectors. Covariant Lyapunov vectors as mentioned before grow asymptotically with the rate of the Lyapunov exponents backwards and forward in time their finite time growth rate $\mu_i(t)$, however, can be different from the finite-time Lyapunov exponents. The fact that they are not orthogonal makes it possible for them

to align with invariant manifolds and deviation of the dynamics from hyperbolicity manifests itself in tangencies between the covariant Lyapunov vectors.

Going backwards in time, the j-th covariant Lyapunov vector can be regarded as a vector belonging to the subspace $S_j^-(t)\backslash S_{j-1}^-(t)$. Therefore it is a linear combination of the first j backward vectors with a nonzero component along the j-th backward vector and it is orthogonal to backward vectors of order higher than j (see eq. (2.28)). Therefore going backwards in time it asymptotically decays with the rate λ_j, i.e, the smallest Lyapunov exponent of the exponents λ_i, $i = 1 \dots j$.

Although Lyapunov exponents λ_i, computed in the asymptotic limit of infinite-time are well ordered by value, their finite-time counterparts, the finite-time Lyapunov exponents $\lambda_i(t)$, can fluctuate and exchange order. That is to say the direction corresponding to $\lambda_i(t)$ (the i-th backward Lyapunov vector $\phi_i^-(t)$) where $i < j$, may temporarily become more stable than the direction corresponding to $\lambda_j(t)$. In other words $\lambda_i(t)$ may temporarily decrease below $\lambda_j(t)$. In case for any reason the order between finite-time Lyapunov exponents is temporarily lost, any covariant vector of the order between i and j, will have a dominant component along the i-th backward vector and tend to converge to the subspace $S_i^-(t)\backslash S_{i-1}^-(t)$, forming tangencies with the i-th covariant vector. In this contribution we argue that this temporary change in the stability of stable and unstable or neutral directions is a generic behavior in critical transitions that leads to tangencies between stable and unstable (or marginal) manifolds.

In the case of the FitzHugh-Nagumo, as the system slowly moves towards a transition point, the increase in the second finite-time Lyapunov exponent leads to a decrease of the angle between the first and the second covariant Lyapunov vector. That is to say the smaller the difference between the first and the second finite-time Lyapunov exponents the closer the stability of the corresponding orthogonal directions will be and hence the more the component of the second covariant vector along the first covariant vector will grow.

Right before and at the very beginning of the transition, the marginal direction becomes highly unstable, enabling the transition. The sudden rise of the first Lyapunov exponent making this exponent much larger than the second finite-time Lyapunov exponent that is close to zero, leads to a fast increase in the angle between the

two vectors. However this sudden rise is followed by a sharp decrease way below the value of the second finite-time Lyapunov exponent during the transition. The first Lyapunov exponent becoming the more negative exponent, is like a switching between the stability of the orthogonal directions of the finite-time Lyapunov exponents. That is to say the direction of the first finite-time Lyapunov exponent has temporarily become more stable than the direction orthogonal to it. Therefore the second covariant vector that tends to align with the more stable direction will collapse on the direction parallel to the previously marginal manifold.

Figure 4.5 demonstrates the first and the second finite-time Lyapunov exponents along with the finite-time growth rate of the second covariant Lyapunov vector or the second finite-time covariant Lyapunov exponent in the noise induced regime. Note that the first covariant Lyapunov vector is the same as the first backward vector, therefore the first finite-time Lyapunov exponent is the same as the growth rate of the first covariant Lyapunov vector. The changes in the growth rate of the second covariant vector however is interesting as it switches between the first and the second finite-time Lyapunov exponent during the transition. While the trajectory is crawling along a branch of the nullcline the most stable direction along which the perturbations shrink fastest is the direction parallel to the x axis that is also the direction of the second covariant vector. The growth rate of the second covariant vector is therefore highly negative. The direction orthogonal to the trajectory corresponding to the second finite-time Lyapunov exponent can be regarded as a linear combination of the two covariant Lyapunov vectors. Growth rate of perturbations along the first covariant Lyapunov vector however is zero, hence only the component along the second covariant vector, i.e., the shrinking direction changes. Consequently the second finite-time Lyapunov exponent, is also highly negative and equal to the finite-time growth rate of the second covariant vector, that is to say $\mu_2(t) = \lambda_2(t)$ before the transition. However as the transition point comes closer, the first finite-time Lyapunov exponent becomes positive, therefore the growth rate of the second covariant Lyapunov vector deviates from the second finite-time Lyapunov exponent. During the transition the second vector is tangent to the first vector, hence the finite-time growth rate of the second covariant Lyapunov vector becomes identical to the first Lyapunov exponent $\mu_2(t) = \lambda_1(t)$. Meanwhile as stated before perturbations orthogonal to the trajectory neither shrink nor grow during the

transition, therefore the $\lambda_2(t)$ remains zero throughout the transition. The discrepancy between the second finite-time Lyapunov exponent and the growth rate of the second covariant Lyapunov vector is also a precursor of critical transitions in this model.

We also computed the covariant Lyapunov vector and the Lyapunov exponents for $a = 0.3$, that is the regular spiking regime with a stochastic term added to the bifurcation parameter. The results were qualitatively similar concerning the dynamics of the angle between the covariant Lyapunov vectors and the finite-time Lyapunov exponents. The results are presented in fig. 4.4. Although not presented here, finite-time growth rate of the second covariant vector in the regular spiking regime exhibits the same behavior as in the noise induced regime.

In order to compare the predictive powers of the covariant Lyapunov vectors with a classical precursor of extreme events we computed estimates of the covariant Lyapunov vectors using the repetitive iteration method introduced in section 3.4. Find the results of computing the covariant Lyapunov vectors via the repetitive iteration method for noise induced transition regime in fig. 4.6 fig. 4.7 and in fig. 4.8 for the regular spiking regime. We used integration step $\delta t = 0.001$ and orthogonalization interval, $\Delta = 0.01$. We chose the interval of repetitive iteration τ to be equal to one orthogonalization step Δ, i.e. 0.01 and the number of repeated iterations for each $N = 10$.

The results using the iterative method are qualitatively the same as the results with Ginelli' et al.'s method. Nonetheless there are differences between the results of the two methods. For instance fig. 4.7 shows the finite-time Lyapunov exponents and the finite-time growth rate of the covariant vectors in the noise induced transition regime as computed with the repetitive iteration method. Comparing fig. 4.7 and fig. 4.5 you will notice that the results with both methods show, as discussed before that the growth rate of the second vector is close to the second finite-time Lyapunov exponent while the trajectory is on one of the branches. During the transition however the growth rate of the second covariant Lyapunov vector converges to the first Lyapunov exponent. With the repetitive iteration method this convergence corresponds exactly to the instance that the first finite-time Lyapunov exponent becomes smaller than the second finite-time Lyapunov exponent, which agrees with

our discussion above. As for the Ginelli et al.'s method they seem to converge earlier. The reason for that is in the repetitive iteration method, repeated iteration of the same interval at present amplifies the changes in the local dynamics, while in Ginelli et al.'s method iterating backwards from the far future will lead to a delay in exhibiting the changes in the local dynamics. Although not presented here, finite-time growth rate of the second covariant vector in the regular spiking regime exhibits the same behavior.

We argue that the rapid change from one stable state to another which results the marginal or unstable manifold becoming tangent to the stable manifolds is a generic property of critical transitions. The temporary switching of the stability of the orthogonal backward vectors a.k.a Gram-Schmidt directions is generic to critical transitions in hyperbolic dynamical systems. Hyperbolic dynamical systems typically have distinct stable and unstable directions that is to say they do not have intersecting finite-time Lyapunov exponents. However as the system moves close the critical transition as the trajectory approaches a tipping point the marginal manifold parallel to the trajectory will become highly unstable enabling the transition to the other metastable state. However while the trajectory is slowing down approaching the next metastable state the exponent corresponding to the marginal direction will decrease rapidly being attracted by the next stable state. while the perturbations along this direction rapidly shrink the other orthogonal directions become more neutral during this transition as the only possible change allowed is towards the other metastable state. This rapid change in the stability of the directions leads to the tangencies between the covariant Lyapunov vectors. We further claim that this footprint of the critical transition in the dynamical structure of the system can be used to predict critical transitions. However to show the generality of this phenomenon we have to show that it holds true for other models of critical transitions and to use it as precursors we have to be able to test for it's statistical relevance and measure it's performance compared to other classical precursors of critical transitions.

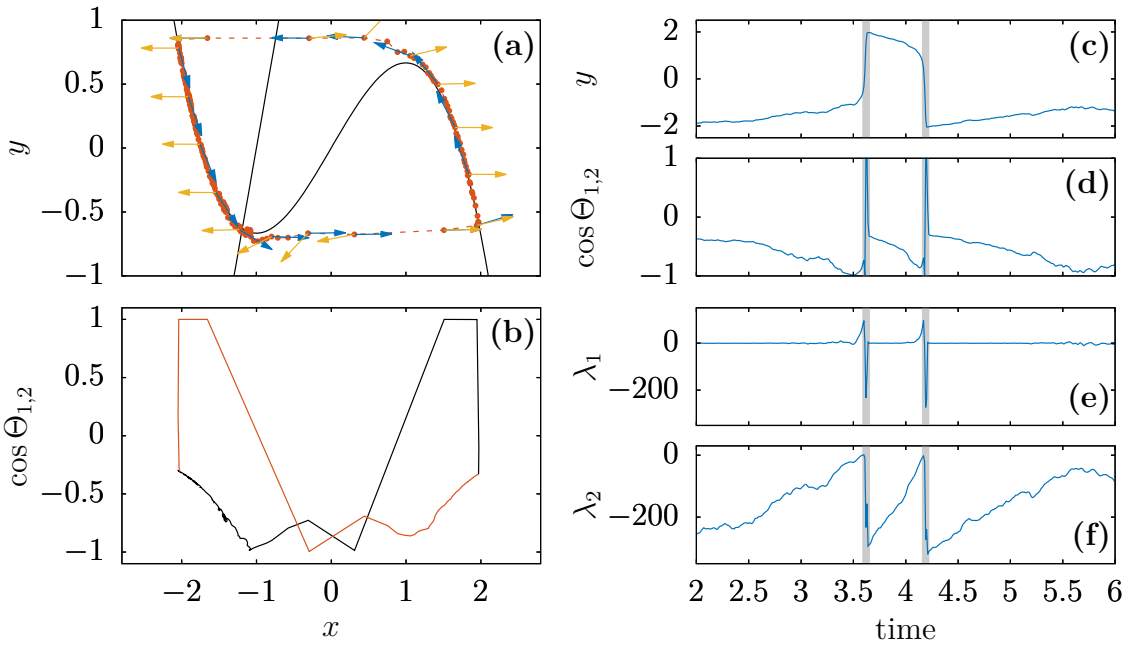

Figure 4.6: Covariant Lyapunov vectors in a single FitzHugh-Nagumo oscillator with $a = 1$, $b = 0.3$, $\epsilon = 0.01$ and $D = 0.2$, i.e., noise induced transition regime, estimated with the repetitive iteration method, confirm the results obtained with Ginelli et al.'s method. (a) The red line indicates a typical trajectory in the phase space. The blue and yellow vectors indicate the first and the second covariant Lyapunov vector respectively, both vectors align during transitions. (b) The angle between the first and the second vector is shown while the system is drifting on the left and transitioning to the right branch (black line) and drifting on the right and transitioning to the left branch (red line). (c) Time series of the fast variable, i.e., the observable of the system. (d) Time series of the cosine of the angle between the first and the second vector. (e) Time series of the first finite-time Lyapunov exponent. (f) Time series of the second finite-time Lyapunov exponent.

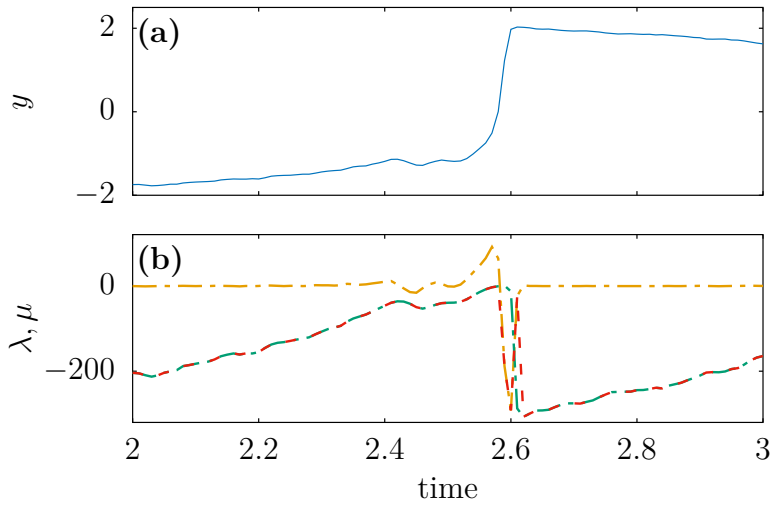

Figure 4.7: Estimates of the covariant vectors computed via the repetitive iteration method are more sensitive to the local dynamics the than the vectors computed with the Ginelli et al.'s method, i.e., merging of the finite-time growth rate of the second covariant vector (red line) and the first finite-time Lyapunov exponent (orange line) occurs exactly at the time when the first finite-time Lyapunov exponent decreases below the second finite-time Lyapunov exponent (green line). (a) Time series of the fast variable of a FitzHugh-Nagumo oscillator in the noise induced transition regime i.e. $a = 1$, $b = 0.3$, $D = 0.2$. (b) The first and the second finite-time Lyapunov exponent, $\lambda_1(t)$ and $\lambda_2(t)$ and the finite-time growth rate of the second covariant Lyapunov vector $\mu_2(t)$. Note that by definition $\lambda_1(t) = \mu_1(t)$.

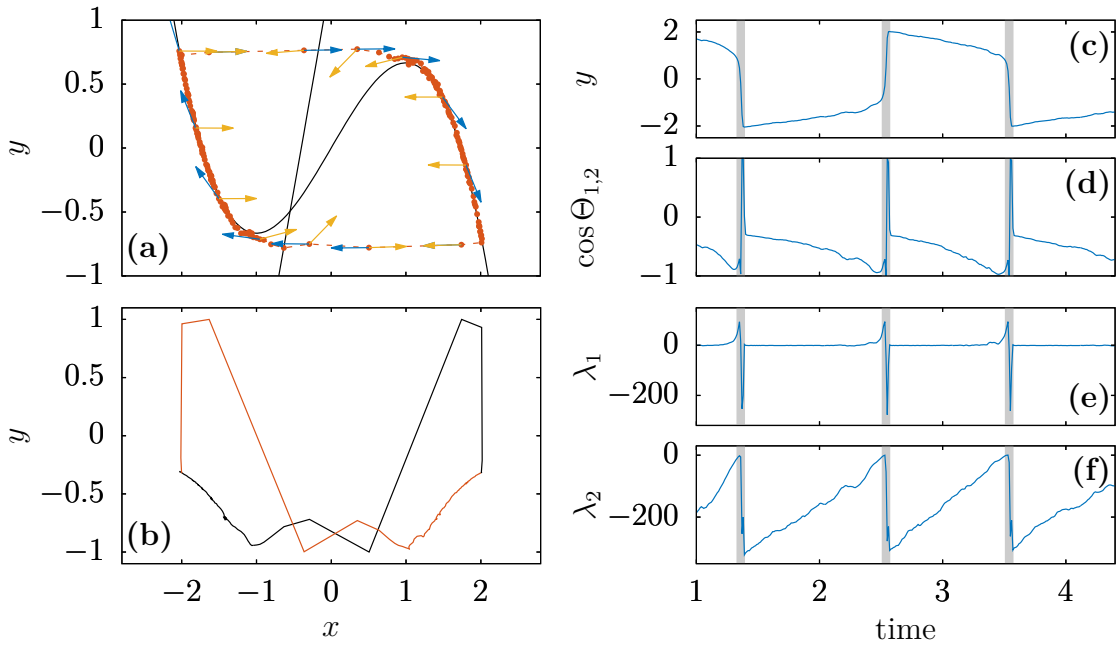

Figure 4.8: Alignment of covariant Lyapunov vectors in a single FitzHugh-Nagumo oscillator with $a = 0.4$, $b = 0.3$, $\epsilon = 0.01$ and $D = 0.2$, i.e., regular spiking regime estimated with the repetitive iteration method, confirm the results obtained with Ginelli et al.'s method. (a) The red line indicates a typical trajectory in the phase space. Green and purple vectors show the first and the second covariant Lyapunov vector respectively, both vectors align during transitions. (b) The angle between the first and the second vector is shown while the system is drifting on the left and transitioning to the right branch (black line) and drifting on the right and transitioning to the left branch (red line). (c) Time series of the fast variable, i.e., the observable of the system. (d) Time series of the cosine of the angle between the first and the second vector. (e) Time series of the first finite-time Lyapunov exponent. (f) Time series of the second finite-time Lyapunov exponent.

4.3 Van der Pol Oscillator

The Van der Pol oscillator similar to FitzHugh-Nagumo oscillator is an oscillator with non-linear damping [96–98]. We use a modified version of it here, with stochastic driving of the bifurcation parameter,

$$\begin{aligned} \epsilon\dot{x} &= y - \frac{27}{4\delta^3}x^2(x+\delta) \\ \dot{y} &= -\frac{\delta}{2} - x + \sqrt{2D}\eta(t). \end{aligned} \tag{4.4}$$

We chose $\delta = 1.5$ and $\epsilon = 0.01$. In this parameter range the system exhibits regular spiking. Adding noise, $\eta(t)$ will lead to stochastic spiking. Figure 4.9 shows the results of the computation of the covariant Lyapunov vectors and the Lyapunov exponents using Ginelli et al.'s method with $D = 0.1$. Figure 4.9(a) demonstrates the phase space portrait of the system. The x-nullcline is the polynomial curve and the y-nullcline is the vertical black line. y is the slow moving bifurcation parameter. The trajectory slowly moves up the left branch until it reaches the tipping point which is followed by a rapid transition to the right branch. The first covariant Lyapunov vector is parallel to the trajectory. The second covariant Lyapunov vector, points to the shrinking direction, i.e., the direction parallel to the axis corresponding to the fast variable, x. As the system slowly approaches the tipping point the difference between the finite-time Lyapunov exponents and hence the angle between the two covariant Lyapunov vectors decreases. The start of the transition is marked by a rapid increase in the first finite-time Lyapunov exponent and increased hyperbolicity. I.e., the angle between the covariant vectors increases. This rapid increase however is followed by a sharp decrease of the first finite-time Lyapunov exponent beyond the second finite-time Lyapunov exponent. The switching between the stability of the orthogonal directions causes merging of the covariant vectors. As the trajectory approaches the other branch towards the end of the transition the vectors separate again.

As is evident from fig. 4.10 the same as FitzHugh-Nagumo, deviation between the finite-time growth rate of the second covariant Lyapunov vector and the second finite-time Lyapunov exponent precedes a critical transition.

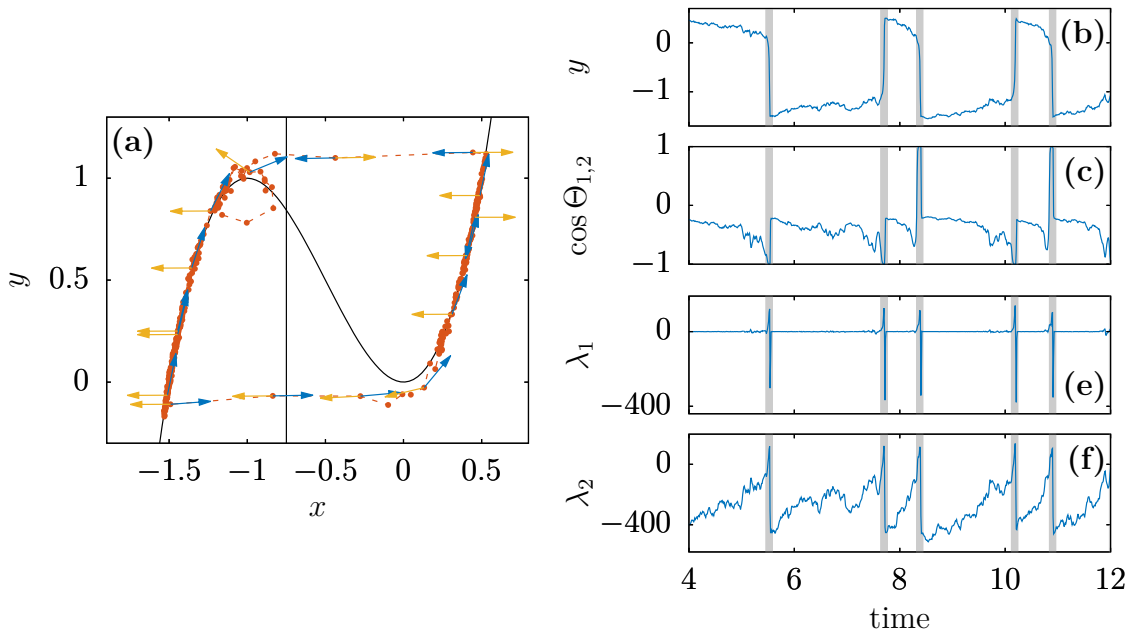

Figure 4.9: Alignment of covariant Lyapunov vectors in a Van der Pol oscillator with $\delta = 1.5$, $\epsilon = 0.01$ and $D = 0.1$, computed with the Ginelli et al.'s method. (a) The red line indicates a typical trajectory in the phase space. Blue and yellow vectors show the first and the second covariant Lyapunov vector respectively, both vectors align during transitions. (b) Time series of the fast variable, i.e., the observable of the system. (c) Time series of the cosine of the angle between the first and the second vector. (d) Time series of the first finite-time Lyapunov exponent. (e) Time series of the second finite-time Lyapunov exponent.

The results of the covariant Lyapunov vectors of the Van der Pol oscillator computed with the repetitive iteration method although not shown here, are consistent with the results from the Ginelli et al.'s method and later will be used to predict the transitions.

4.4 Josephson Junctions

Josephson junction is a device that consists of two superconducting materials with a thin layer of non-superconducting material in the middle. Brian David Josephson was the first person to study the properties of a non-superconducting junction between two superconductors. He predicted the tunneling of pairs of electrons through

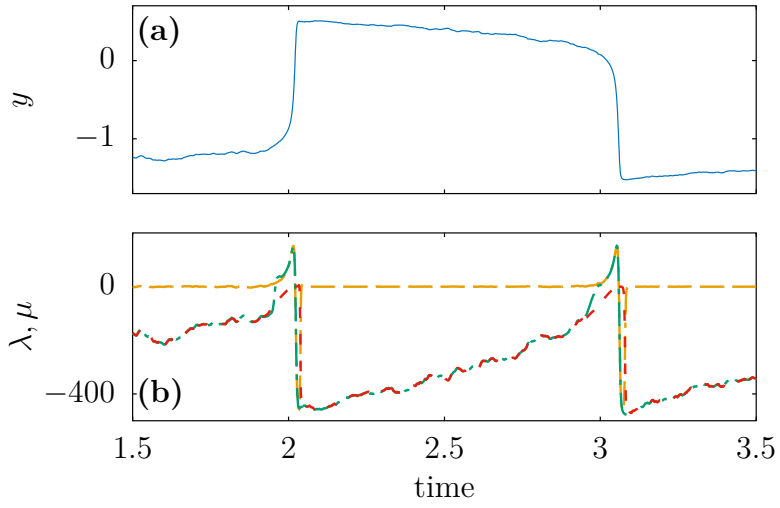

Figure 4.10: While the finite-time growth rate of the second covariant vector, $\mu_2(t)$, and the first finite-time Lyapunov exponent, $\lambda_1(t)$, are the same prior to a transition, divergence of the two is a precursor of a transition. Note that the growth rate of the first covariant Lyapunov vector is by definition the same as the first finite-time Lyapunov exponent $\lambda_1(t) = \mu_1(t)$. (a) Time series of the fast variable of a single Van der Pol oscillator. (b) The first (orange line) and the second (green line) finite time Lyapunov exponent, $\lambda_1(t)$ and $\lambda_2(t)$ are compared to the finite-time growth rate of the second covariant Lyapunov vector (red line),$\mu_2(t)$. The growth rate of the second vector is computed with Ginelli et al.'s method.

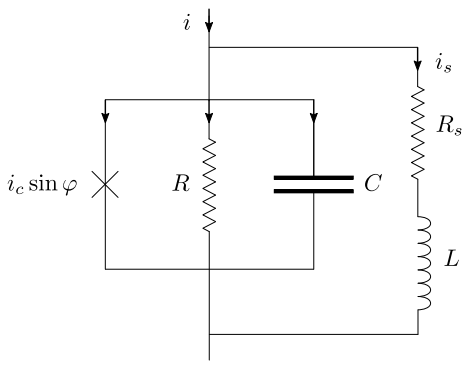

Figure 4.11: The resistive-capacitive-inductively shunted model of a Josephson junction.

the barrier and derived the current voltage dynamics of the junction for which he was awarded the Nobel prize in 1973 [99, 100].

The state of the Josephson junction is described by the Josephson phase, ϕ, i.e., the phase difference of complex wave functions of the Cooper pairs of the electrons formed in the superconductors. In theory in the superconducting phase the electrons travel freely without any resistance and tunnel across the barrier and the Josephson phase will remain constant. Note that the barrier needs to be very thin. If the barrier is an insulator it has to be as thin as a 30 angstroms. If the barrier is a non-superconducting metal it can get as tick as a2 few microns. In the superconducting phase the electrons tunnel through the barrier without any resistance. After the critical current is reached however the junction enters the resistive phase in which a time dependent voltage develops across the junction. In this case the Josephson phase, ϕ, is no longer constant and the voltage across the junction is proportional to $\dot{\phi}$. Josephson effect is highly sensitive to external magnetic fields. Therefore it is used in magnetometers that measure extremely weak magnetic fields such as superconducting quantum interference devices (SQUIDs).

In practice, The Josephson junctions will exhibit parasite resistance capacitance and inductance. The model we use here to investigate the dynamics of the Josephson junction is the resistive-capacitive-inductively shunted junction (RCLSJ). Figure 4.11 shows the equivalent circuit of the model [101]. The elements of the circuit, model the imperfections of the junction. The voltage across the junction is related to the phase as $\hbar/2e\dot{\phi}$. Kirchhoff's law for the circuit results [102],

$$\begin{aligned} i &= C\dot{v} + \frac{v}{R} + i_c \sin\phi + i_s, \\ v &= \hbar/2e\dot{\phi} = L\dot{i_s} + i_s R_s, \end{aligned} \tag{4.5}$$

where i is the total current across the junction, ϕ is the Josephson phase, i.e., the phase difference between the wave functions of the Cooper pairs of the two superconductors. i_s, is the shunt current passing the shunt resistance R_s, and the

shunt inductance, L. Rearranging the equations by rescaling time and changing to dimensionless variables have,

$$\begin{aligned} \beta\gamma^2\ddot{\phi} + \gamma\dot{\phi} + \sin\phi &= J - I_s, \\ \dot{\phi} &= \alpha\dot{I}_s + I_s, \end{aligned} \tag{4.6}$$

where $\gamma = R_s/R$. $\beta = 2ei_cR^2C/\hbar$ is the Stewart-McCumber parameter, the inverse of which represents dissipation. $J = i/i_c$, $I_s = i_s/i_c$ and $\alpha = 2ei_cL/\hbar$ are dimensionless. In the next step if we introduce a new variable, u,

$$u = J - I_s + \frac{1+\gamma}{\alpha}\phi + \frac{\beta\gamma^2}{\alpha}\dot{\phi}, \tag{4.7}$$

the dynamical equation for the junction can be rewritten as,

$$\begin{aligned} \beta\gamma^2\ddot{\phi} + (1 + \frac{\beta\gamma}{\alpha})\gamma\dot{\phi} + \frac{1+\gamma}{\alpha}\phi + \sin\phi &= u, \\ \alpha\dot{u} &= J - \sin\phi, \end{aligned} \tag{4.8}$$

yet another rearranging and scaling time by the factor, α and setting $\epsilon = \gamma/\alpha$, we have,

$$\begin{aligned} \beta\epsilon\dot{\phi} &= \psi - (1 + \beta\epsilon)\phi, \\ \epsilon\dot{\psi} &= u - \hat{\alpha}^{-1}\phi - \sin\phi, \\ \dot{u} &= J - \sin\phi \end{aligned} \tag{4.9}$$

where $\hat{\alpha}^{-1} = \alpha^{-1} + \epsilon$. Given $\epsilon \ll 1$, eq. (4.9) represents a three dimensional fast-slow system. If $\hat{\alpha} > 1$ this system allows multiple stable and unstable branches. The

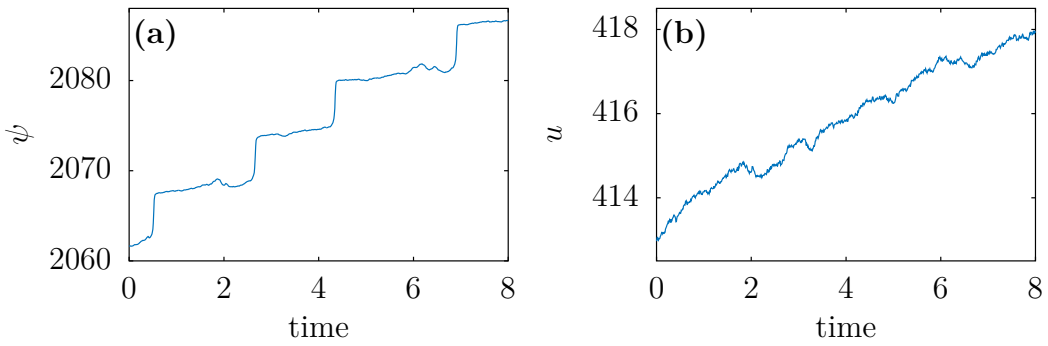

Figure 4.12: Time series of the variables of highly dissipative resistive-capacitive-inductively shunted model of a Josephson junction (a) The Josephson phase, i.e., the fast variable ψ.(b) the bifurcation variable, u.

limit we would like to explore first, is the highly dissipative limit, i.e., $\beta \ll 1$. In this case, the variable ϕ, growing at least an order of magnitude faster than ψ, converges to ψ and the system can be reduced to 2 dimensions.

$$\begin{aligned} \epsilon\dot{\psi} &= u - \hat{\alpha}^{-1}\psi - \sin\psi, \\ \dot{u} &= J - \sin\psi + \sqrt{2D}\eta(t), \end{aligned} \tag{4.10}$$

We have added a stochastic term to the bifurcation parameter that makes the transitions stochastic.

We computed the covariant Lyapunov vectors and the Lyapunov exponents of the Josephson junction with strong damping to see if we can identify the same characteristics in this fast-slows system. Figure 4.12 shows the system for $\hat{\alpha}^{-1} = 0.2, J = 0.1, \epsilon = 0.01$ and $D = 0.2$. The bifurcation variable, has the slow dynamics and it's gradual increase enables the fast variable, ψ, to go through transitions from one stable section of the nullcline to another. Figure 4.13 shows the results of computing the covariant vectors with the method of Ginelli et al.f Figure 4.13(a), shows the system in the phase space, the first and the second covariant Lyapunov vectors. Same as the FitzHugh-Nagumo oscillator, the first vector is parallel to the marginal manifold and The second covariant Lyapunov vector, is parallel to the axis of the bifurcation parameter which is the contracting direction along which perturbations die fastest. Figure 4.13(b) shows the cosine of the angle between the two covariant

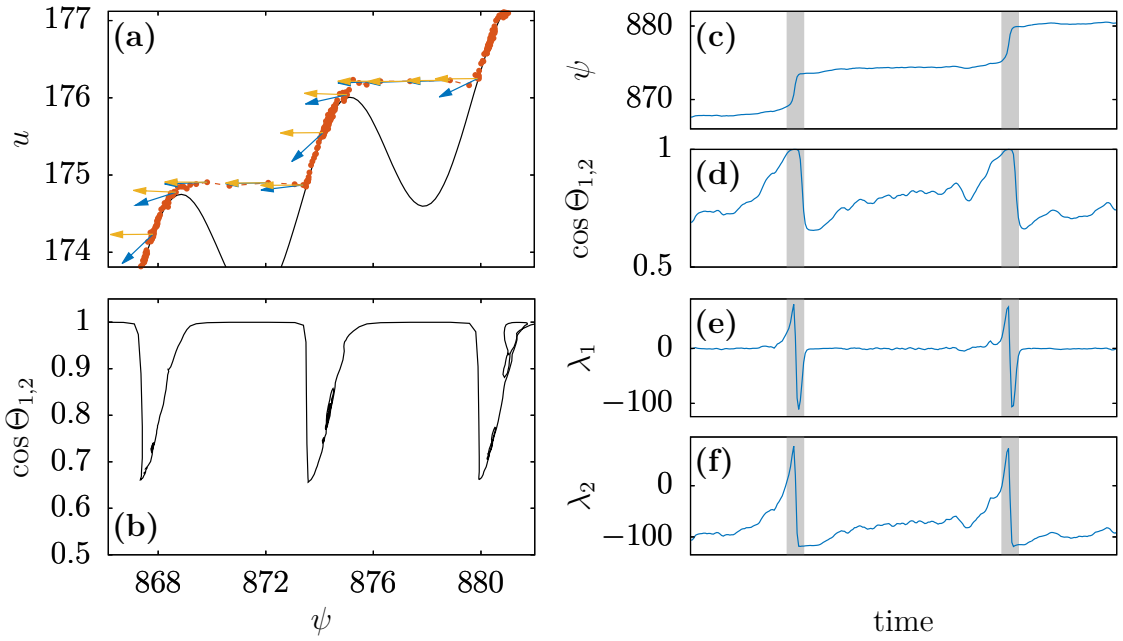

Figure 4.13: Alignment of covariant Lyapunov vectors in a highly dissipative resistive-capacitive-inductively shunted model of a Josephson junction ,with $\hat{\alpha}^{-1} = 0.2, J = 0.1, \epsilon = 0.01$ and $D = 0.2$, during transitions. Vectors are computed via Ginelli et al.'s method (a) The dotted red line indicates a typical trajectory in the phase space. The blue and the purple vectors show the first and the second covariant Lyapunov vector respectively. (b) The angle between the first and the second vector is shown vs the Josephson phase ψ. (c) Time series of the fast variable, ψ. (d) Time series of the cosine of the angle between the first and the second vector. (e) Time series of the first finite-time Lyapunov exponent (f) Time series of the second finite-time Lyapunov exponent.

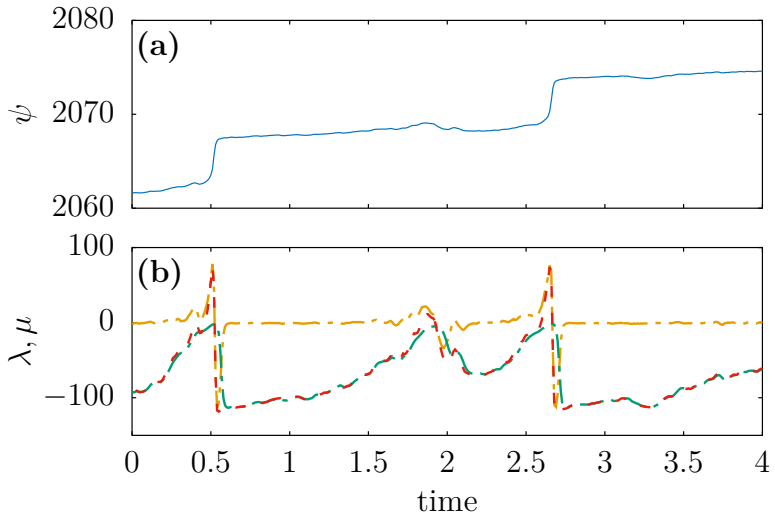

Figure 4.14: While the growth rate of the second covariant vector (red line) in a 2-D Josephson junction is the same as the second finite-time Lyapunov exponent (green line) in the absence of transitions, divergence of the two anticipates a critical transition. During a transition the growth rate of the second covariant vector converges to the first finite-time Lyapunov exponent (yellow line). (a) Time series of the fast variable. (b) The finite-time Lyapunov exponents and the finite-time growth rate of the second covariant vector. The covariant vector is computed via Ginelli et al.'s method.

Lyapunov vectors versus the fast variable. As can be seen from fig. 4.13(b) and fig. 4.13(d) the covariant vectors are aligned during the transition. The flipping of the second vector due to the rise of the first Lyapunov exponent, however, is not visible here. This may be the case since the rise of the first finite-time Lyapunov exponent is not high enough to change the direction of the vector. The rise of the first finite-time exponent demonstrates the temporal instability of the marginal manifold that precedes the critical transition. The overshoot of the first Lyapunov exponent to highly negative values, followed by a rapid rise to it's original value, marks the end of the transition. The second Lyapunov exponent is highly negative and gradually increases. During the transition, it is zero and by the end of the transition it rapidly falls back to it's highly negative value.

Figure 4.14, shows the first and the second finite-time Lyapunov exponent and the growth rate of the second covariant vector. Similar to the FitzHugh-Nagumo oscillator while the trajectory is moving slowly up the nullcline the second finite-time Lyapunov exponent is almost equal to the growth rate of the second covariant

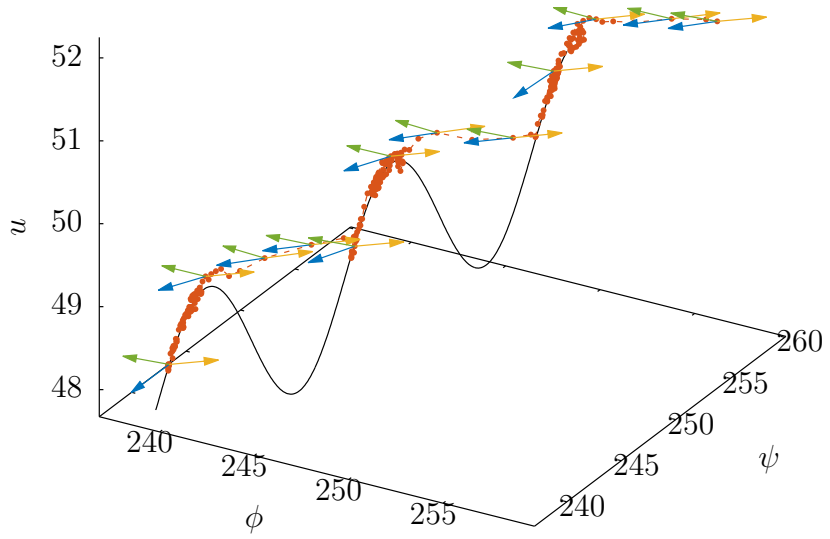

Figure 4.15: Phase space portrait of the 3-D model of Josephson junction in the highly dissipative limit. $\beta = 0.1, D = 0.2, \hat{\alpha}^{-1} = 0.2$. In this parameter range the system is similar to its reduced model. The blue, yellow and the green vectors are the first,second and the third covariant vectors respectively.

vector. This is the state in which the second finite-time exponent is highly negative and much smaller than the first Lyapunov exponent. In this state there are two clear marginal and stable directions forming an acute angle with each other. During the transition however the second finite-time Lyapunov exponent remains zero, while the change in the stability of the directions forces the second covariant Lyapunov vector to become tangent to the direction related to the first Lyapunov exponent, i.e., the trajectory.

We also estimated the covariant Lyapunov vectors using the repetitive iteration method. The vectors computed with the repetitive iteration method qualitatively exhibit the same behavior as the vectors computed with the Ginelli et al.'s method. In order to avoid this essay becoming too long, we will only represent the results of the repetitive iteration method for the three dimensional Josephson junction model.

The two dimensional model of the Josephson junction is in agreement with our finding from the FitzHugh-Nagumo model. But what happens if there is less dissipation and hence β is larger? What happens during a transition in a three dimensional

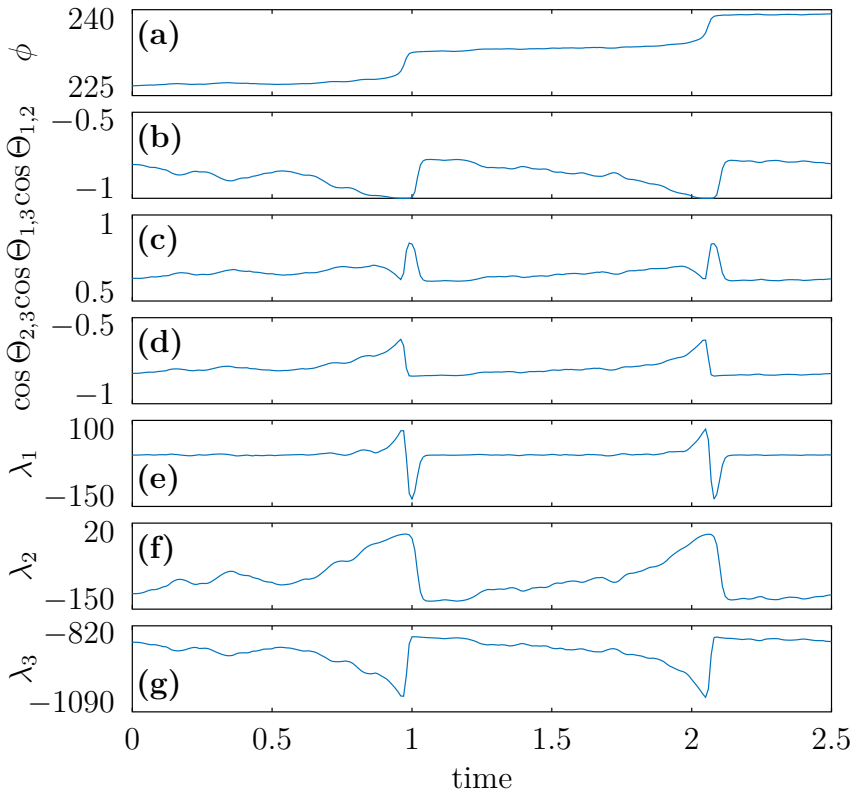

Figure 4.16: The three dimensional Josephson junction with small enough β is almost identical to the two dimensional model. $\beta = 0.1, D = 0.2, \hat{\alpha}^{-1} = 0.2$. The covariant vectors are computed using Ginelli et al.'s method. (a) A typical trajectory of the fast variable, ϕ. (b) Time series of the cosine of the angle between the first and the second covariant Lyapunov vector. The first and the second covariant Lyapunov vector are tangent during the transition. (c) Time series of the cosine of the angle between the first and the third covariant Lyapunov vector. Although the transition is announced in the change of the angle between the first and the second vector, they are not tangent during the transition. (d) Time series of the cosine of the angle between the second and the third covariant Lyapunov vector. The angle between the second and the third vector changes prior to the transition. However they never align. (e) Time series of the first finite-time Lyapunov exponent. (f) Time series of the second finite-time Lyapunov exponent. (g) Time series of the third finite-time Lyapunov exponent.

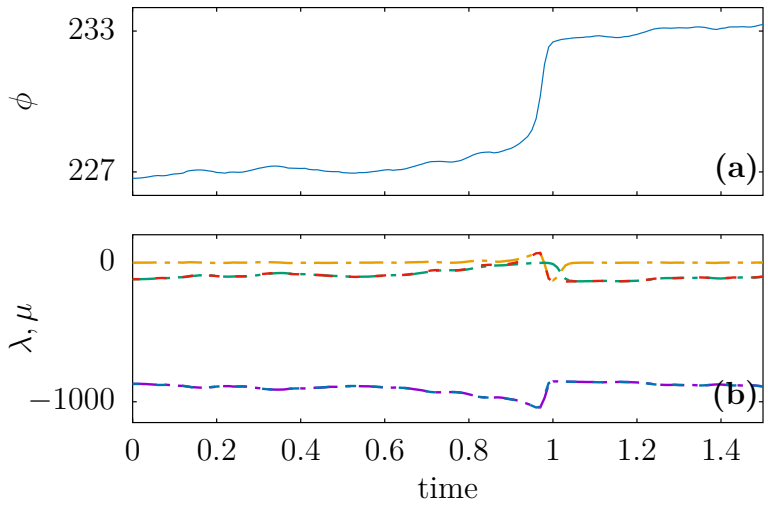

Figure 4.17: The finite-time growth rate of the second covariant vector (red line) diverges from the second finite-time Lyapunov exponent (green line) prior to and converges to the first finite-time Lyapunov exponent (orange line) during a transition. The finite-time growth rate of the third covariant Lyapunov vector (purple line), however, is always the same as the third finite-time Lyapunov exponent (blue line). (a) Josephson phase, ϕ in a 3-D model with $\beta = 0.1, D = 0.2, \hat{\alpha}^{-1} = 0.2$. (b) The three finite-time Lyapunov exponents along with the finite-time growth rate of the second and the third covariant Lyapunov vector.

Josephson junction model? We started with a three dimensional Josephson junction model with $\beta \ll 1$ and computed the covariant vectors for the three dimensional system. Figure 4.15 and fig. 4.16 show a three dimensional Josephson junction model with $\beta = 0.1, D = 0.2$, and $\hat{\alpha}^{-1} = 0.2$. As can be seen from the figures, this system is very similar to the reduced two dimensional model. The third vector points at the very stable direction and corresponds to the third highly negative finite-time Lyapunov exponent. Figure 4.16(b), shows that the first and the second covariant Lyapunov vectors merge during a transition. Their behavior is very similar to that of the two dimensional model studied earlier. The angle between the first and the third and the second and the third covariant Lyapunov vector is clearly affected by the transition. However they do no become tangent during the transition. The reason can be understood from fig. 4.17.

Figure 4.17 demonstrates the finite-time Lyapunov exponents and the finite-time growth rates of the covariant Lyapunov vectors. Note that the finite-time growth rate of the first covariant Lyapunov vector is not shown since it is by definition the same as the first finite-time Lyapunov exponent. The rapid change in the stability of the marginal manifold leading to the transition, leads to the intersection of the first and the second finite-time Lyapunov exponent. The alternation between the stability of the first and the second invariant manifold as discussed before, leads to the merging of the first and the second covariant vector. The third finite-time Lyapunov exponent as well rises during the transition leading to a change in the angle between the third and the first and the second covariant Lyapunov vector. However, despite the rise in the third finite-time exponent it always stays far more stable than the other manifolds. Therefore merging of the vectors doesn't happen in the direction of the third finite-time Lyapunov exponent. That is to say violation of hyperbolicity doesn't happen in that direction.

Upon increasing β, the Josephson junction exhibits a more complex dynamics. With slightly increased β, the system will continue to be a fast-slow system exhibiting transitions. By gradually increasing β, the covariant vectors and the finite-time Lyapunov exponents will exhibit oscillations after each transition. Figure 4.18 shows the results for $\beta = 0.3$ computed with Ginelli et al.'s method. Figure 4.18(f) and (g), show that although the second finite-time Lyapunov exponent is of the same order of the second finite-time Lyapunov exponent of the system with $\beta = 0.1$,

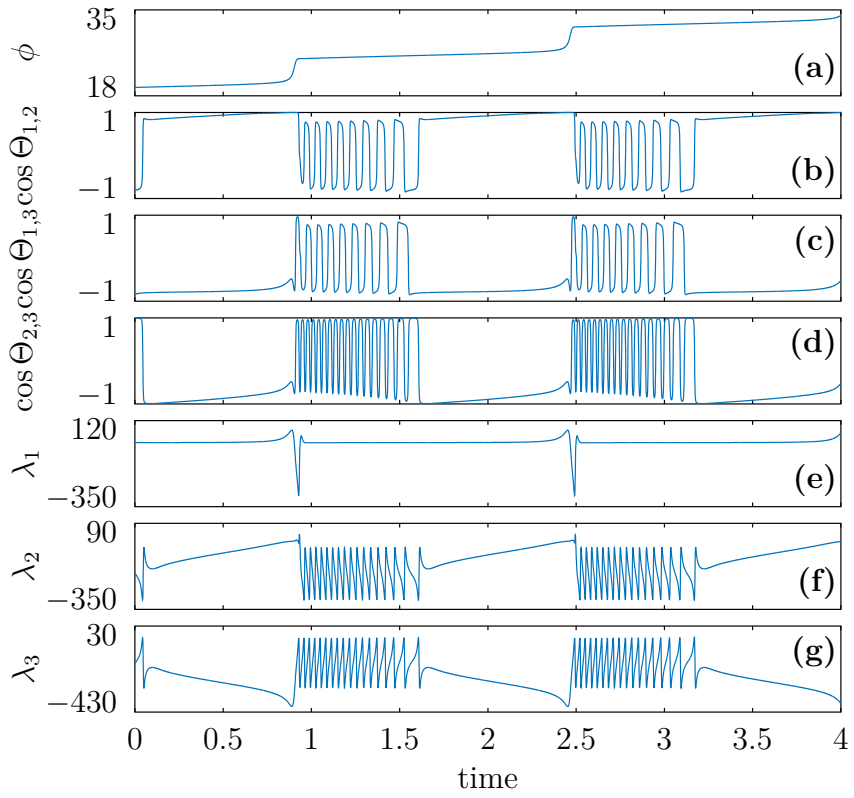

Figure 4.18: The three dimensional Josephson junction $\beta = 0.3, D = 0, \hat{\alpha}^{-1} = 0.2$. The covariant vectors computed using Ginelli et al.'s method, show tangencies between the first and the second and the first and the third covariant vector during a transition. The second and the third vector are frequently tangent. (a) A typical trajectory of the fast variable ϕ. (b) Time series of the cosine of the angle between the first and the second covariant Lyapunov vector. (c) Time series of the cosine of the angle between the first and the third covariant Lyapunov vector. (d) Time series of the cosine of the angle between the second and the third covariant Lyapunov vector. (e) Time series of the first finite-time Lyapunov exponent. (f) Time series of the second finite-time Lyapunov exponent. (g) Time series of the third finite-time Lyapunov exponent.

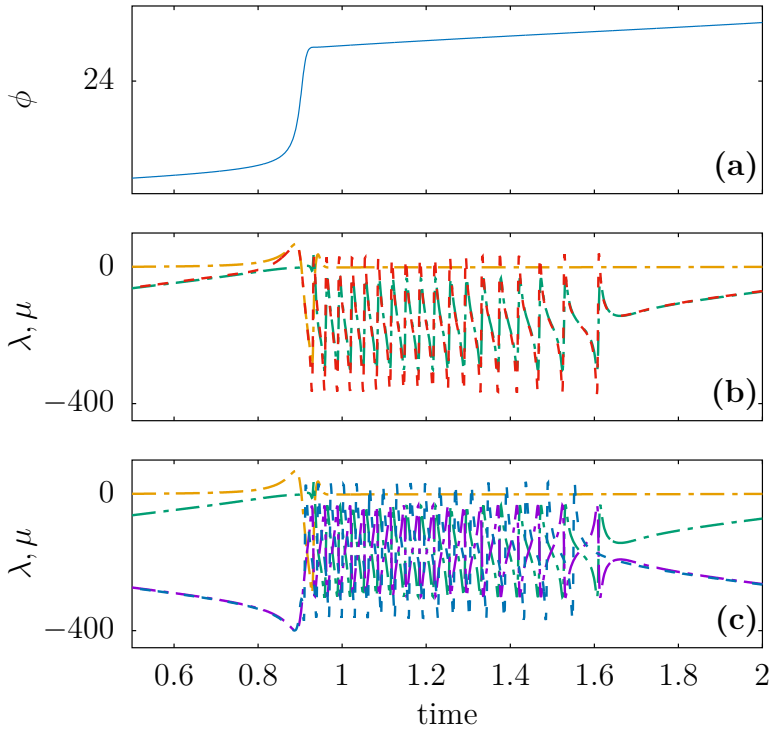

Figure 4.19: In a Josephson junction with $\beta = 0.3$, the finite-time growth rate of the second covariant vector (red line) is similar to the second finite-time Lyapunov exponent (green line). It converges to the first finite-time Lyapunov exponent (orange line) prior to the transition. Although the finite-time growth rate of the third covariant vector (blue line) is similar to the third finite-time Lyapunov exponent (purple line), before the transition the two diverge and afterwards it oscillates between the second and the third finite-time exponent due to frequent intersections of the two. The covariant vectors are computed using Ginelli et al.'s method. (a) Time series of the fast variable, ϕ. (b) Time series of the first two finite-time Lyapunov exponents and the finite-time growth rate of the second covariant Lyapunov vector. (c) Time series of the three finite-time Lyapunov exponents and the finite-time growth rate of the third covariant Lyapunov vector.

the third finite-time Lyapunov exponent has dramatically increased. It can also be seen that during their oscillations they are of the same order of magnitude and therefore frequently intersect. As the result of this frequent alternations in the stability of the second and the third orthogonal directions the second and the third covariant Lyapunov vector frequently merge after each critical transition. Therefore the merging of the second and the third covariant Lyapunov vector can not be an effective indicator of the transition.

The first and the second covariant Lyapunov vector merge during transitions. The rapid rise in the first Lyapunov exponent followed by a sharp decrease beyond the second and then the third finite-time Lyapunov exponent, will cause merging of the vectors. The first and the second vector merge prior to and during the critical transition. The tangency between the first and the third covariant Lyapunov vector however, happens towards the end of the transition.

The finite-time growth rates of the covariant vectors and the finite-time Lyapunov exponents are shown in fig. 4.19. The second covariant Lyapunov vector is a linear combination of the first and the second backward vector. Therefore it's finite-time growth rate is only affected by the alternations in the stability of the first and the second backward vectors. The finite-time growth rate of the second covariant vector is therefore similar to the second finite-time Lyapunov exponent, apart from during the transition that it converges to the first finite-time Lyapunov exponent (see fig. 4.19(b)).

The third covariant vector, however, is a linear combination of all the three backward Lyapunov vectors and it's growth rate is affected by the frequent alternations of the stability between the second and the third backward Lyapunov vector. As a result of this frequent alternations the finite-time growth rate of the third covariant Lyapunov vector is a combination of the second and the third finite-time Lyapunov exponent (see fig. 4.19(c)). Note that merely for the sake of clarity the junction demonstrated in fig. 4.18 and fig. 4.19 are without noise. We then computed the covariant Lyapunov vectors for the Josephson junctions with bigger β. As β grows, the oscillations of the finite-time Lyapunov exponents and the second and the third covariant Lyapunov vector's rotations intensify. Upon further increase of β, the first covariant Lyapunov vector starts to oscillate as well. As a result, during the

critical transition and before landing on the nullcline, the trajectory spirals around the nullcline. The spiraling effect is more enhanced for larger values of β. Figure 4.20 demonstrates three dimensional phase space portraits along with the two dimensional presentation of the absolute value of the cosine of the angle between the covariant Lyapunov vectors of a Josephson junction on the $\phi - \psi$ plane with different values of β. Increasing β also causes a dramatic increase in the second and third Lyapunov exponent. The weakening of the contracting directions eventually leads to the system not having a fast-slow dynamics.

Nonetheless, note that regardless of the spirals, the covariant Lyapunov vectors align during the transitions and diverge once they land on the nullcline fig. 4.20.

In order to evaluate predictive powers of the covariant Lyapunov vectors we also need to compute the vectors with the repetitive iteration method. Figure 4.21 and fig. 4.22 show the results for the repetitive iteration method for $\beta = 0.1$. The results are qualitatively in agreement with the results from the Ginelli et al.. Nonetheless fig. 4.22 shows that the convergence of the growth rate of the second covariant vector to the first finite-time Lyapunov exponent, happens later than in the Ginelli et al.'s method. The reason is due to the fact that iterating back from the far future the covariant vectors of Ginelli take time to react to the local changes in the dynamics and have a delay while the iterative method through repetition of the same interval in the present reacts faster to the local changes.

4.5 Hindmarsh and Rose model

The Hindmarsh-Rose model is a common model to describe neural activity [103] consisting of three coupled first order differential equations. It is a more realistic model for neural activity than the FitzHugh-Nagumo since in the FitzHugh-Nagumo model the duration of the inter-spike interval is almost as big as the duration of one spike, a.k.a action potential. But in the model introduced by Hindmarsh and Rose, first as a two dimensional model [104, 105] and later modified to a three dimensional model [103], each spike is separated from the others by a long inter-spike interval

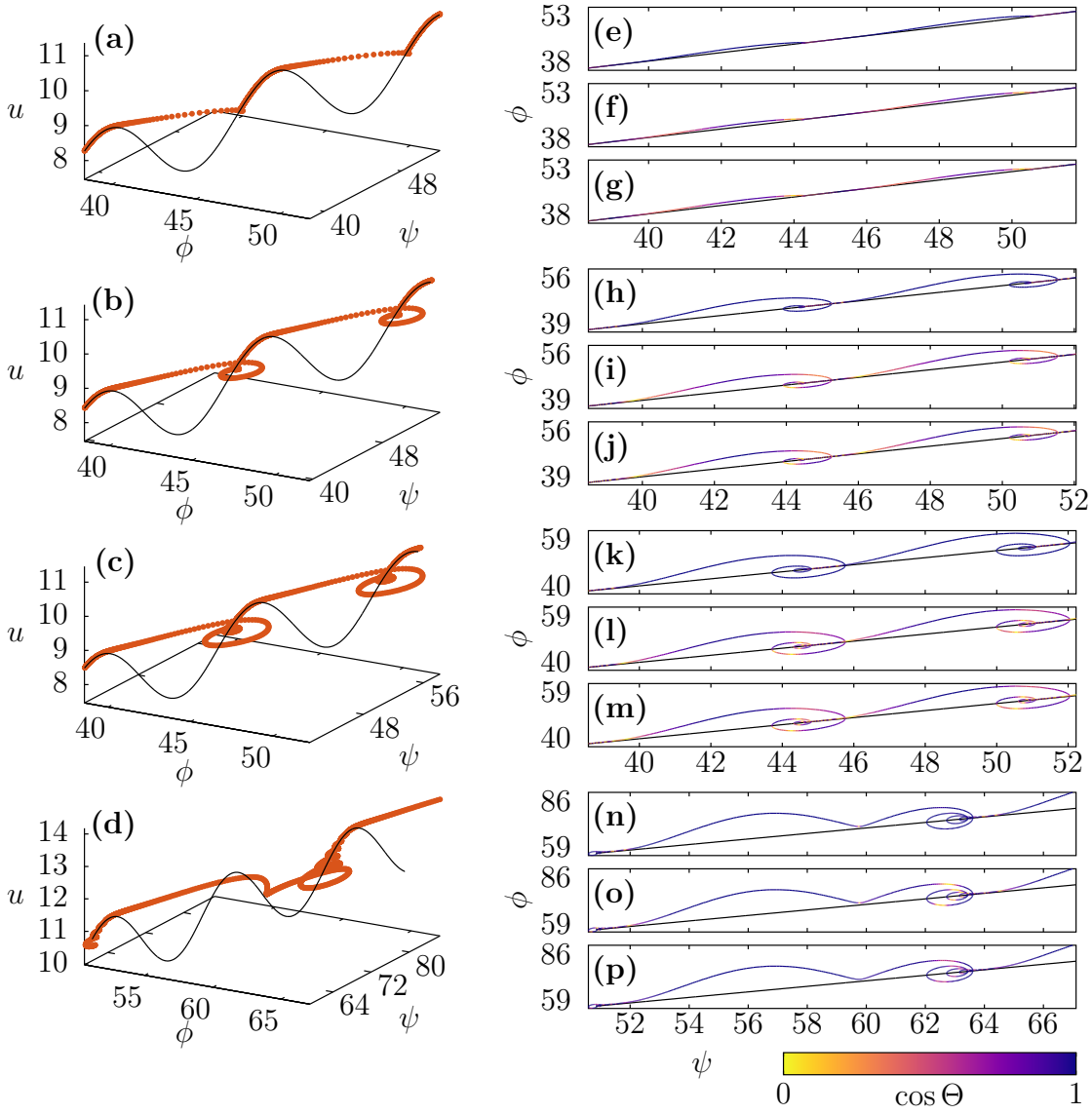

Figure 4.20: Increasing the value of β intensifies the spiraling of the trajectory around the nullcline prior to landing on it. Nonetheless, tangencies between the vectors are significant during all transitions. The left column consists of the nullcline (black line) and the trajectory (red line) and the right column consists of the projection of the nullcline (black line) and the trajectory on the ϕ-ψ plane showing the cosine of the angle between the covariant vectors, (palette). (a,e,f,g)$\beta = 0.5$, (b,h,i,j) $\beta = 3$, (c,k,l,m) $\beta = 6$, (d,n,o,p) $\beta = 18$.

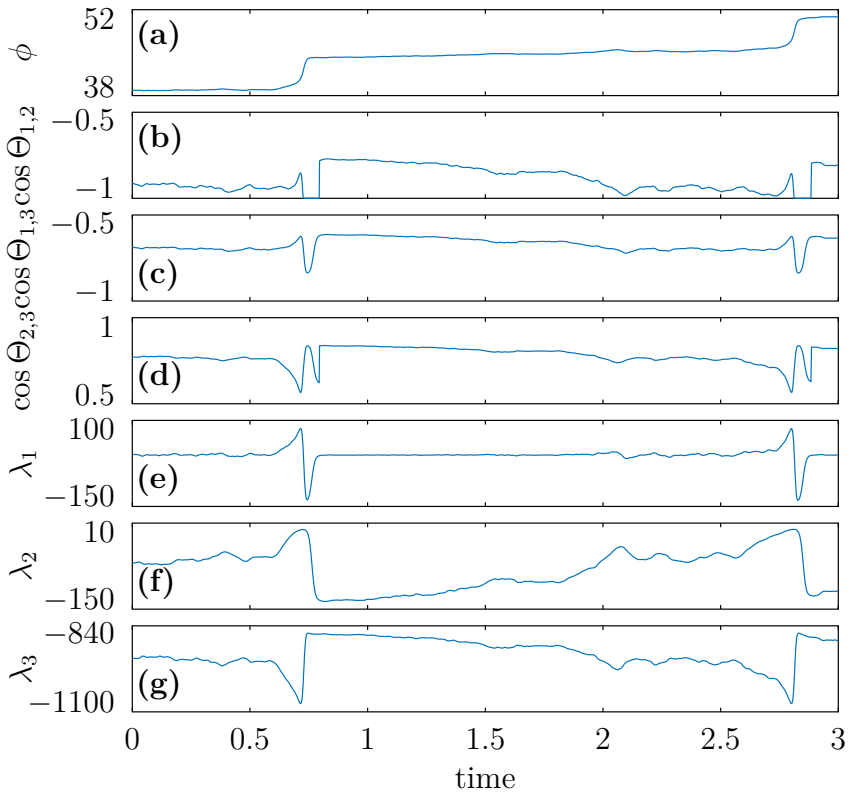

Figure 4.21: The results of estimates of the covariant Lyapunov vectors of the Josephson junction with the repetitive iteration method are in agreement with the results from the Ginelli et al.'s method. $\beta = 0.1, D = 0.2, \hat{\alpha}^{-1} = 0.2$. (a) A typical trajectory of the fast variable ϕ. (b) Time series of the cosine of the angle between the first and the second covariant Lyapunov vector. The first and the second covariant Lyapunov vector are tangent during the transition. (c) Time series of the cosine of the angle between the first and the third covariant Lyapunov vector. Although the transition is announced in the change of the angle between the first and the second vector, they are not tangent during the transition. (d) Time series of the cosine of the angle between the second and the third covariant Lyapunov vector. The angle between the second and the third vector changes prior to the transition. However, they do not align. (e) Time series of the first finite-time Lyapunov exponent. (f) Time series of the second finite-time Lyapunov exponent. (g) Time series of the third finite-time Lyapunov exponent.

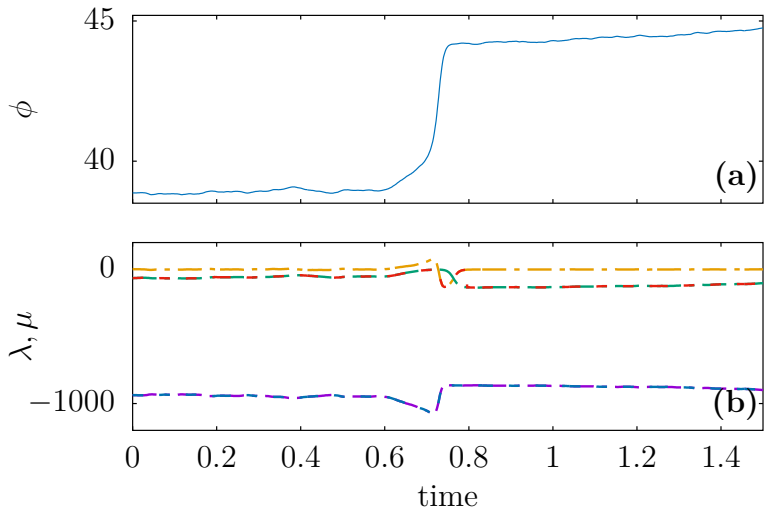

Figure 4.22: The results for the 3-D Josephson junction with the repetitive iteration method show the immediate convergence of the growth rate of the second covariant vector to the first finite-time Lyapunov exponent at the intersection between the first and the second finite-time Lyapunov exponent. $\beta = 0.1, D = 0.2, \hat{\alpha}^{-1} = 0.2$. (a) Time series of the fast variable, ϕ. (b) Time series of the first (orange line), the second (green line) and the third (purple line) finite-time Lyapunov exponent and the finite-time growth rate of the second (red line) and the third (blue line) covariant Lyapunov vector.

that is typical of real neurons. On the other hand it is simpler than the Hodgkin-Huxley model and thus easier to understand. A modified version of this model, containing an additional stochastic term, is given by the following equations,

$$\begin{aligned} \dot{x} &= y - ax^3 + bx^2 - z + J, \\ \dot{y} &= c - dx^2 - y, \\ \dot{z} &= r(s(x - x_0) - z) + \sqrt{2D}\eta(t), \end{aligned} \tag{4.11}$$

where x is a voltage-like variable, y controls the recovery after a spike and z represents an adapting current with slow dynamics. In different parameter ranges this model exhibits bursting as well as regular spiking behavior. We choose a noise strength of $D = 0.05$ and common parameter values, i.e., $r = 0.01, s = 4, x_0 = -1.6, b = 3.5, a = 1, c = 1, J = 2.5$ and $d = 5$. Within this parameter range, the original Hindmarsh-Rose model shows a regular spiking behavior [106]. However, our modification of the model, which consists of adding a stochastic term to the

slow variable, leads to highly irregular spiking.

To understand the dynamics of this system it is easier to look at the nullcline in two dimensions, i.e., in the $x - y$ plane. Figure 4.23(a) illustrates projections of the nullclines of x and y and the trajectory to the x-y-plane. While the trajectory slowly moves close to the nullclines, the drifting of the bifurcation parameter z shifts the x-nullcline and enables an excursion of x and y, called a spike [also see fig. 4.23(b)].

Figure 4.24 shows the time series of the observable x, of all angles between the covariant Lyapunov vectors and of all finite-time Lyapunov exponents computed for the Hindmarsh-Rose model via Ginelli et al.'s method. The first covariant Lyapunov vector, corresponding to the first Lyapunov exponent that is zero [see fig. 4.24(e)], is tangent to the trajectory. However, for the Hindmarsh-Rose model, the second Lyapunov exponent [see fig. 4.24(f)] is also very small (-0.041 for this parameter set), and its finite-time value is also mostly close to zero and very close to the first finite-time exponent, resulting a persistent tangency between the first and the second covariant Lyapunov vector [see fig. 4.24(b)]. The 180 degrees change of the direction of the first and second vector is due to an intersection between the two finite-time exponents, i.e the switching of the stability of the corresponding backward Lyapunov vectors, that can be seen in fig. 4.24(e) and (f). However it is an insignificant change in the stability that does not correspond to the critical transition.

In this system the vector corresponding to the contracting direction is the third covariant Lyapunov vector. The third finite-time Lyapunov exponent is not highly negative either, therefore the third covariant Lyapunov vector has noticeable components along the first and the second covariant vectors. Nonetheless the spikes or the critical transitions are marked by clear tangencies between the first and the third and the second and the third covariant Lyapunov vectors. That is to say, the phenomenon of critical slowing down prior to critical transitions manifests itself in tangencies between the third and the first two covariant Lyapunov vectors [see fig. 4.24(b-d)].

Figure 4.25 shows the finite-time growth rates of the second and the third covariant Lyapunov vectors. As can also be understood from the persistent tangency between the first and the second covariant Lyapunov vector, the finite-time growth rate of the second covariant vector is all the time the same as the finite-time growth

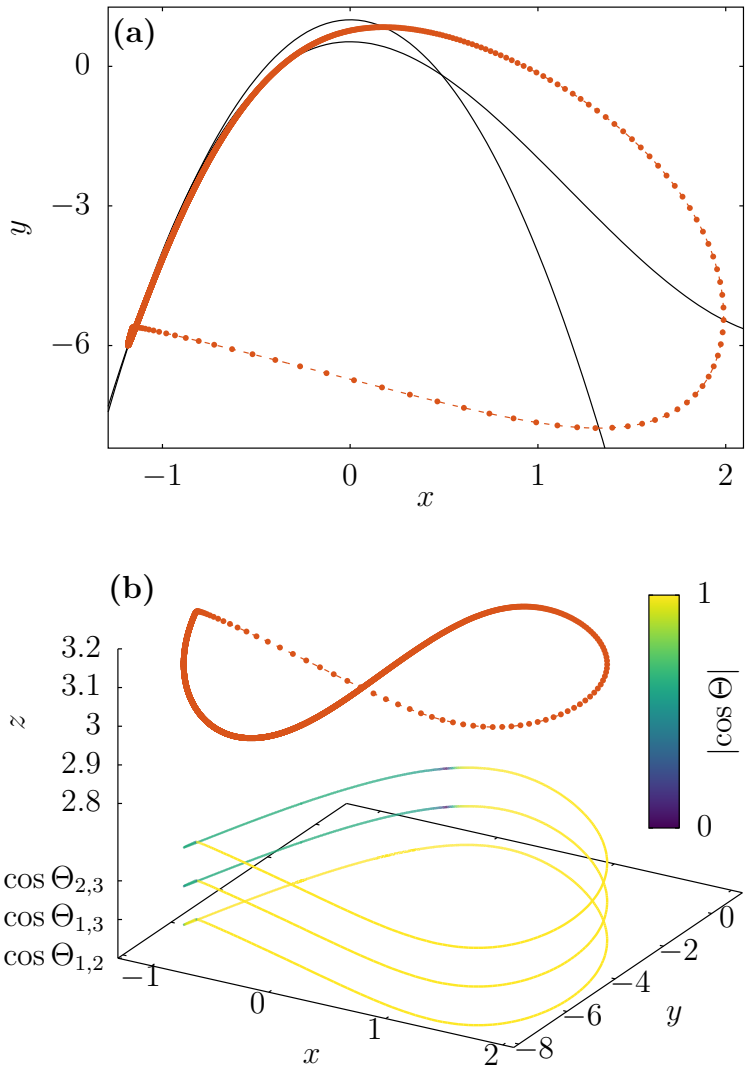

Figure 4.23: Merging of all covariant Lyapunov vectors forecasts spikes in the Hindmarsh-Rose model. (a) Projection of the trajectory of the Hindmarsh-Rose model and the nullclines of x and y variables on the $x - y$ plane. The trajectory (red line) slowly moves up close to the nullclines (black solid lines) before the spike occurs. (b) The three-dimensional phase space portrait of the trajectory shows a slow drift of z as the fast variables go through an excursion. The green-blue lines are the shifted projections of the trajectory on the x-y plane, showing the absolute value of the cosine of the angle between the covariant Lyapunov vectors.

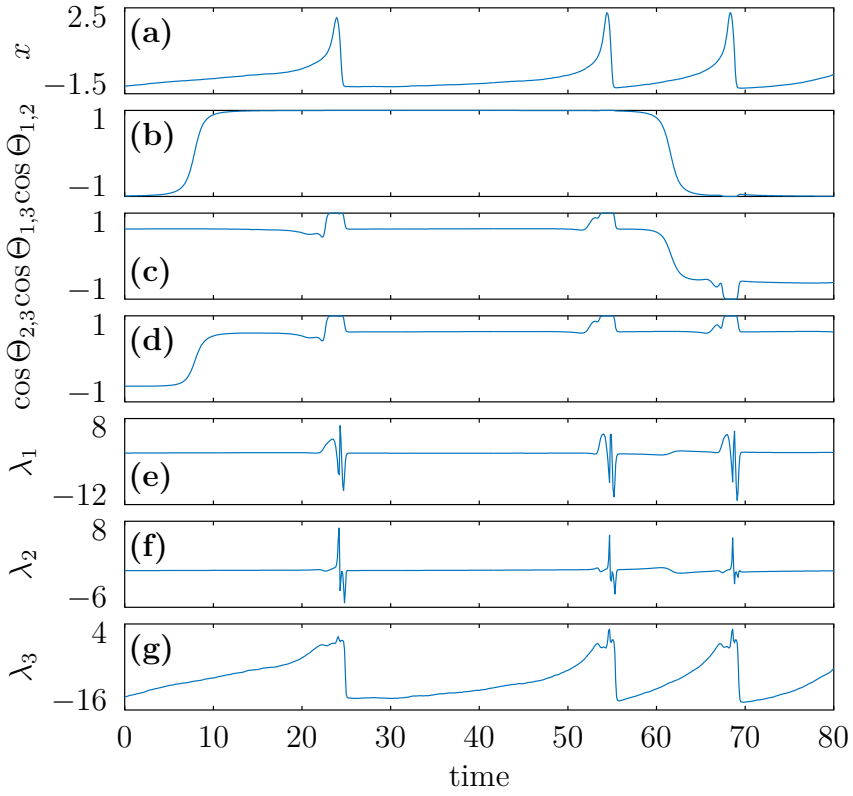

Figure 4.24: The first and the second covariant Lyapunov vector become tangent to the third vector (the most stable direction) during a transition in a Hindmarsh and Rose model with $r = 0.01, s = 4, x_0 = -1.6, b = 3.5, a = 1, c = 1, J = 2.5, d = 5$ and $D = 0$. (a) A typical trajectory of the voltage variable x. (b) Time series of the cosine of the angle between the first and the second covariant Lyapunov vector. (c) Time series of the cosine of the angle between the first and the third covariant Lyapunov vector. Clear alignment of the first and the third covariant vector announces a transition. (d) Time series of the angle between the second and the third covariant Lyapunov vector. The second and the third vector clearly align prior to a transition. (e) Time series of the first finite-time Lyapunov exponent. (f) Time series of the second finite-time Lyapunov exponent. (g) Time series of the third finite-time Lyapunov exponent.

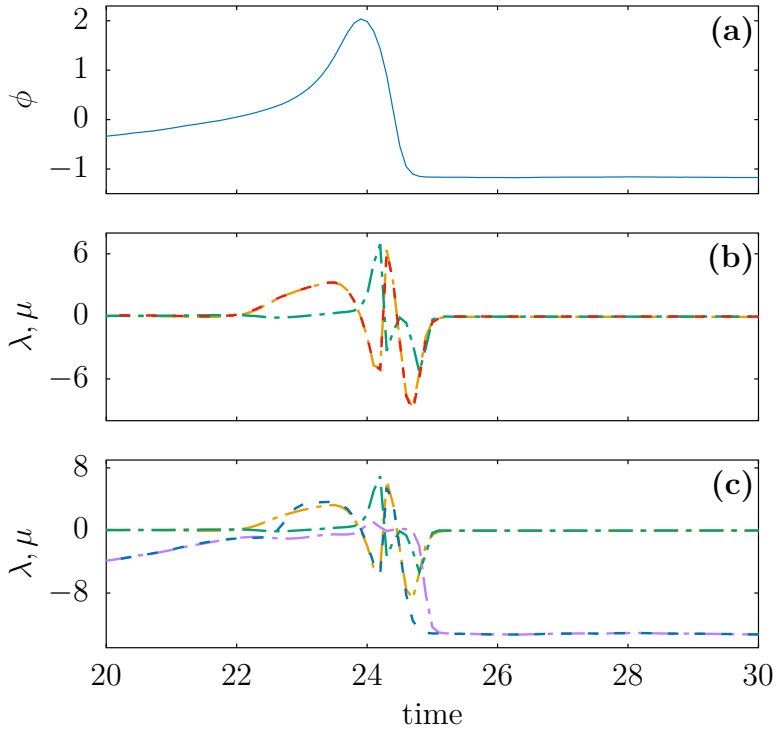

Figure 4.25: Persistent tangency between the first and the second covariant vector manifests itself in the merging of the finite-time growth rate of the second covariant vector (red line) and the first finite-time Lyapunov exponent (orange line). Prior to a transition switching of the stability between the directions of the third and the first finite-time Lyapunov exponent causes the finite-time growth rate of the third covariant vector to converge to the first finite-time Lyapunov exponent. Vectors are compute via Ginelli et al.'s method. (a) Time series of the fast variable, x. (b) Time series of the first (orange line) and the second (green line) finite-time Lyapunov exponent and the finite-time growth rate of the second covariant Lyapunov vector (red line). (c) Time series of the first, second and the third (purple line) finite-time Lyapunov exponent and the finite-time growth rate of the third covariant Lyapunov vector (blue line).

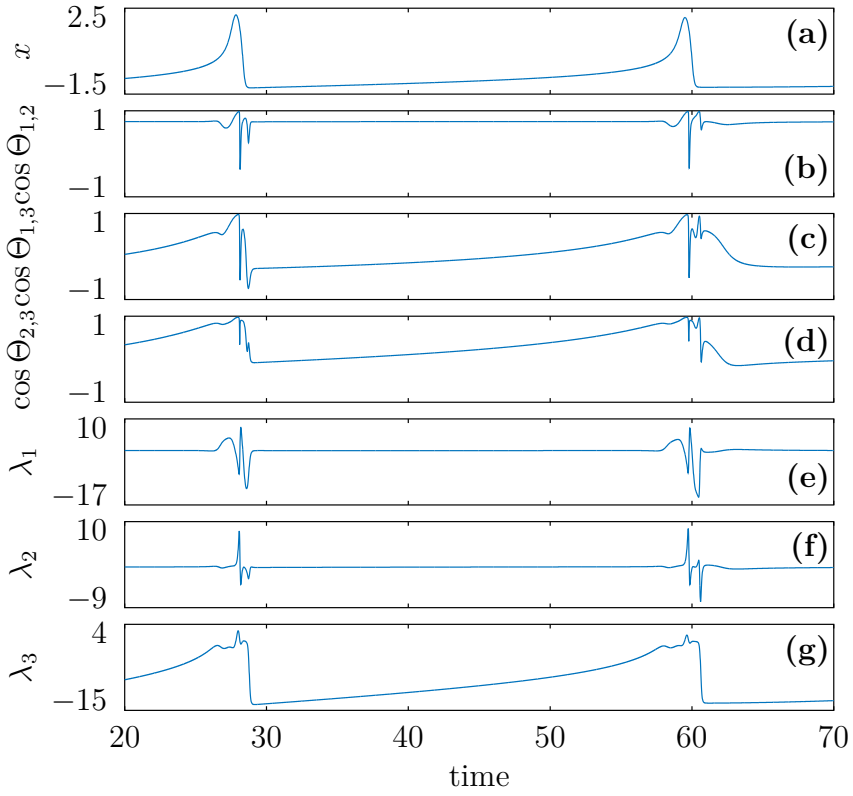

Figure 4.26: In the Hindmarsh-Rose model, all three covariant Lyapunov vectors merge during a critical transition. The vectors obtained with the repetitive iteration method are more sensitive to an upcoming transition than the vectors computed via Ginelli et al.'s method. (a) Time series of the fast variable x. (b-d) Time series of cosine of the angles between the covariant Lyapunov vectors. (e-g) Time series of the finite-time Lyapunov exponents.

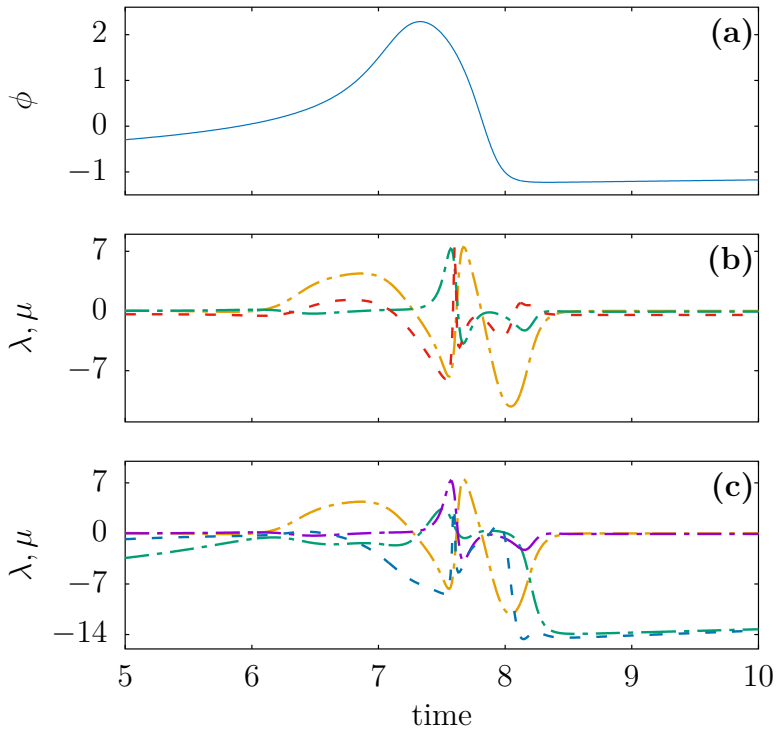

Figure 4.27: The finite-time growth rate of both the second and the third covariant Lyapunov vectors estimated by the repetitive iteration method converge to the first finite-time Lyapunov exponent prior to each transition in the Hindmarsh and Rose model. (a) Time series of the fast variable, ϕ. (b) Time series of the first (orange line) and the second (green line) finite-time Lyapunov exponent and the finite-time growth rate (red line) of the second covariant Lyapunov vector. (c) Time series of the first, second and the third (purple line) finite-time Lyapunov exponent and the finite-time growth rate of the third covariant Lyapunov vector (blue line).

rate of the first covariant vector, i.e., the first finite-time Lyapunov exponent. The growth rate of the third covariant Lyapunov vector, converges to the first finite-time Lyapunov exponent as expected, since the first finite-time Lyapunov exponent falls below both other exponents, temporarily disturbing the order of the stability of the backward Lyapunov vectors directions as discussed previously. Note that the spike like increase in the first and the second finite-time Lyapunov exponents corresponding to the marginal direction during the critical transition, as well as the constant increase in the third finite-time Lyapunov exponent corresponding to the stable direction is in agreement with the models previously studied.

We also used the repetitive iteration method to compute the covariant Lyapunov vector in the Hindmarsh-Rose model. Figure 4.26(b) shows the angle between the first and the second covariant Lyapunov vector computed via repeated iteration method. Interestingly, in contrast to the results of the Ginelli et al.'s method, the angle between the first and the second covariant vector obtained with the iterative method are sensitive to an upcoming transition. Although the angle between the two vectors is always quite small they become tangent only at the beginning of the transition. Moreover towards the end of the transition that the first and the second Lyapunov exponent reach their maximum difference, fig. 4.27(b), thus the increased angle between the first and the second vectors is observed. Figure 4.27(b) shows how, although the first two finite-time Lyapunov exponents are close to each other, prior to the transition the growth rate of the second covariant Lyapunov vector converges to the first finite-time Lyapunov exponent.

The angle between the first and the third covariant Lyapunov vector via the repetitive iteration method is also more sensitive to an upcoming transition than the angle between the first and the third covariant vector from the Ginelli et al.'s method. The angle between the two vectors gradually decreases as the third finite-time Lyapunov exponent increases and it's corresponding direction becomes less and less stable fig. 4.26(g). As the first finite-time Lyapunov exponent decreases beyond the third finite-time Lyapunov exponent fig. 4.27(c) during the transition, the third covariant vector becomes tangent to the first covariant vector. This tangency is interrupted during the transition by the sudden rise of the first Lyapunov exponent that shortly restores the order of the stability of the orthogonal directions. The angle between

the second and the third covariant Lyapunov vector is qualitatively similar to the angle between the first and the third covariant vector as expected.

The covariant vectors obtained with the two different methods show that in dynamical systems such as the Hindmarsh-Rose model with a number of Lyapunov exponents close to each other and frequent violations hyperbolicity, the vectors obtained from the repetitive iteration method are a lot more sensitive to the local changes in the dynamics. While the Ginelli et al.'s method results tangent vectors corresponding to Lyapunov exponents that are close to each other, the repetitive iteration method is able to differentiate between directions that are only slightly different in their stability.

5 Predicting Critical Transitions

In this chapter we test the statistical relevance of the results obtained in chapter 4. We set up prediction experiments in which we use time series of angles between covariant Lyapunov vectors and of finite-time Lyapunov exponents as indicator variables. Further we use finite-time variance as a typical precursor to critical transitions. We then compare the predictive power of the variance and the covariant Lyapunov vectors and finite-time Lyapunov exponents.

5.1 Precursor variables

In order to explore the predictive power of the covariant Lyapunov vectors and the Lyapunov exponents, in this section we use the cosine of the angle between the covariant vectors and the finite-time Lyapunov exponents along with the finite-time variance as precursors to critical transitions.

As previously mentioned, finite-time variance is a typical warning signal for critical transitions. Increase in the variance is a symptom of the phenomenon of critical slowing down that occurs prior to critical transitions. During critical slowing down the system's recovery rate from perturbations decreases, i.e., fluctuations do not die out and therefore the variance of the data increases. The increased variance is usually used as a precursor to critical transitions.

We will now compare the performance of our dynamical precursors to the finite-time variance. As dynamical precursors we will use the angle between the covariant Lyapunov vectors and the finite time Lyapunov exponents. I have also used the difference between the finite-time Lyapunov exponents along with the finite-time

growth rate of the covariant vectors as precursors in fast-slow systems. However, the angles between the vectors proved to be a better precursors and I would not present them here in order to avoid a lengthy thesis. Furthermore, we would not use our precursors for the Hindmarsh-Rose model. Although we demonstrated that the angle between the covariant vectors in the Hindmarsh-Rose model are sensitive to an upcoming transition the same way as the other models, persistent deviations from hyperbolicity makes them unsuitable for our precursor variables.

We will test for the Granger causality [107] of our precursor variables and the critical transitions. That is to say we would like to see if the time series of our precursor variables provides statistically significant information about the lagged values of the time series indicating the critical transitions [108, 109]. There are different tests to determine Granger causality between discrete events and variable of a dynamical system. We apply statistical-inference techniques and analyze the success rate of the inference using Receiver Operating Characteristic curves (ROC-curves) [110], which are common measures for the success of classification algorithms in machine learning and data mining.

5.2 ROC analysis

For each of our models, we first produce a training data set and a test data set. Say our precursor variable is $\rho(t)$ and $\chi(t)$ is the binary tracer variable. $\chi(t)$ is zero if there is a critical transition happening at time t and zero otherwise.Δt is the time lag. That is to say, knowing the value of $\rho(t)$ we want to predict the value of $\chi(t + \Delta t)$.

The first step is to use the training data set to compute the conditional probability distribution $P(\chi(t + \Delta t) = 1|\rho(t)$. In order to do this we first have to bin the indicator variable ρ, go through its time series and compute its marginal probability distribution. Next we go through the time series of the indicator variable ρ and the tracer variable χ and compute the joint probability distribution. That is the distribution of the probability of $\chi(t+\Delta t) = 1$ (a transition happening at time $t+\delta t$) and ρ having a specific value at time t. Dividing the joint probability distribution by

the marginal probability distribution we get the conditional probability distribution. Note that in order to have reliable statistics while binning the indicator variable ρ, enough number of variables should be inside each bin. Very low number in a bin can result unreliable statistics. Since usually ρ is not evenly distributed, typically one ends up with bins of different sizes.

Having estimated the conditional probability distribution using the training data set, we can predict transitions in the test data set. To make predictions, we need a decision variable δ, that lies between zero and the maximum value of the conditional probability, $P(\chi(t+\Delta t) = 1|\rho(t)$. This value is the decision threshold for issuing an alarm. Namely, we go through the indicator time series, $\rho(t)$, of our test data set and if at time t, $P(\chi(t + \Delta t) = 1|\rho(t) > \delta$, we issue an alarm. I.e., we predict a critical transition at time, $t + \Delta t$. Once we are done with the predictions, we can count the fraction of correct predictions out of all observed events (true positive rate), and compare it with the fraction of false alarms out of all non-events (false negative rate). Evidently, the higher the true positive and the lower the false negative rate, the more successful the precursor variable. We then change the decision threshold, δ and repeat the prediction procedure. After computing the true positive and false negative rates for different decision thresholds, we can plot the true positive rates versus the false positive rates in a receiver operating characteristic curve (ROC), see fig. 5.1.

For random predictions, the rate of correct predictions and the rate of false alarms will be approximately the same resulting a diagonal (black-line in fig. 5.1). The more effective and non-random the predictions are, the closer the ROC will get to the upper left corner. A measure that summarizes each ROC-curve and allows for comparison of several indicator variables is the area under the curve (AUC). AUCs range from 0.5 (random predictions) to unity (optimal ROC in the upper left corner.)

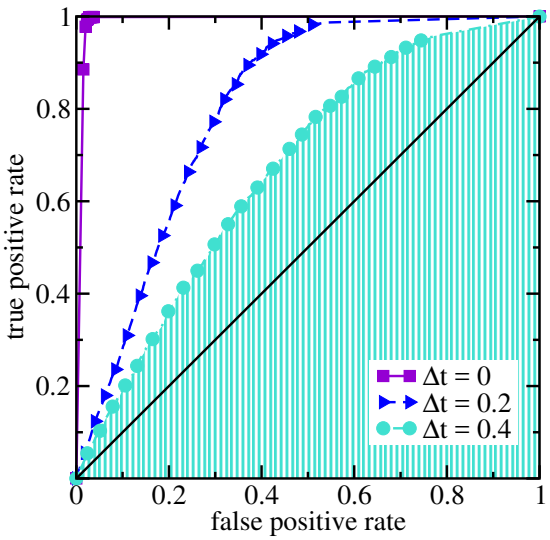

Figure 5.1: The area under the curve (AUC) is a measure of the effectiveness of predictions. Increasing the time lag Δt decreases the success of predictions. Different ROC curves for FitzHugh-Nagumo oscillator D = 0.3.

5.3 Comparing the precursors

In the following we present the results from predicting critical transitions in different models of fast-slow systems using the angle between the covariant Lyapunov vectors, the finite time Lyapunov exponents and finite-time variance.

In order to predict critical transitions we use the vectors computed with Ginelli et al.'s method and our repetitive iteration method. While the repetitive iteration method does not use the information from the future, using the method of Ginelli et al., one has to iterate the system back from the far future. Therefore it is not a practical method for prediction purposes. However, for the sake of completeness we will also use the covariant vectors computed with the Ginelli et al.,'s method for prediction of critical transitions.

Figure 5.2 and fig. 5.3, demonstrate the AUCs for FitzHugh-Nagumo Oscillator in the noise-induced transition regime and the regular spiking regime. The training data set as well as the test data set each consist of 500000 events and 27562 critical transitions. The integration step 0.0001 and the orthogonalization step, $\Delta = 0.001$, is used. The predictions are made with the noise strength, D, of 0, 0.3 and 0.6 and

the time lag of 0.2 and 0.4 time unit. Note that panel for $D = 0$ is absent in fig. 5.2 since the transitions for this system can only be induced by noise.

Figure 5.4, shows the AUC results for the highly dissipative, i.e., 2-D Josephson junction. The training and the test data set each consist of 500000 events, 15100 of which are data points associated with critical transitions. The integration interval used is 0.001 and the orthogonalization interval, $\Delta = 0.01$. The number of repetitions, N for the repetitive iteration method is 10. The predictions are made with the noise strength, D, of 0, 0.4 and 0.8 and the time lag of 0.2 and 0.4 time unit.

Figure 5.5 and fig. 5.6, show the AUC results for the 3D Josephson junction with $\beta = 0.1$ and $\beta = 0.3$. The training and the test data set each consist of 500000 events 14750 of which are associated critical transitions. Integration interval is 0.001 and the orthogonalization interval, $\Delta = 0.01$. The number of repetitions, N for the repetitive iteration method is 5. The predictions are made with the noise strength, D, of 0, 0.4 and 0.8 and the time lag of 0.2 and 0.4 time unit.

Figure 5.7 shows the AUC results for the Van der Pol oscillator. The training and the test data set each consist of 1000000 events and 10120 transitions. Integration interval used is 0.0005 and the orthogonalization interval, $\Delta = 0.005$. The number of repetitions, N for the repetitive iteration method is 100. The predictions are made with the noise strength, D, of 0, 0.1 and 0.2 and the time lag of 0.25 and 0.5 time unit.

The results show that for all the precursors for all the models the predictions with different lead times are far better than random predictions. First and foremost, this implies existence of a Granger causal link between the dynamics of the angles between covariant Lyapunov vectors (i.e., the occurrence of tangencies) and the occurrence of critical transitions.

As expected, for different lead times, without noise ($D = 0$), the predictions by almost all precursors are nearly optimal, AUC ≈ 1. The exception is the variance that is quite unsuccessful in predicting transitions in the further future (larger lead time), even in the deterministic systems ($D = 0$). Increasing the lead time and the noise strength decreases the prediction's success. For larger lead times and

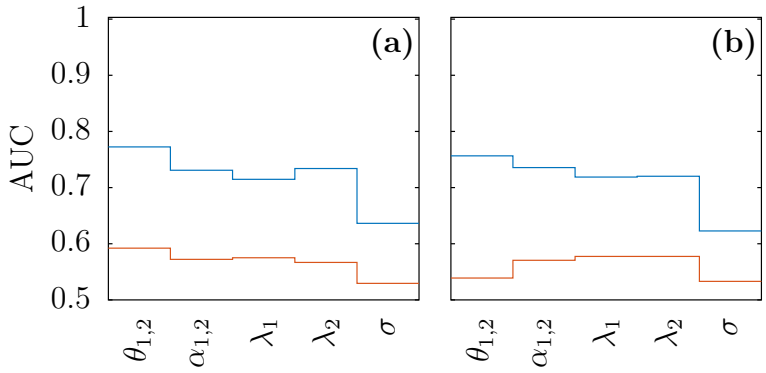

Figure 5.2: Predictions made for a single FitzHugh-Nagumo oscillator in the noise induced transition regime i.e., $a = 1, b = 0.3$, show that the angle between the covariant vectors and the finite-time Lyapunov exponents are more effective precursors than the finite-time variance. AUCs of the angle between the covariant Lyapunov vectors estimated without iterating to the future, $\alpha_{i,j}$, with Ginelli et al.'s method, $\theta_{i,j}$, finite-time Lyapunov exponents, λ_i and finite-time variance, σ, for different noise strengths, D, the lead time of 0.2 (blue line) and 0.4 (redline) are shown. The lead time is the time lag between the prediction and the event. (a) $D = 0.3$ and (b) $D = 0.6$.

increased noise strength angles between covariant Lyapunov vectors, their approximations and finite time Lyapunov exponents lead to better predictions than using the sliding window estimate of the variance. This is actually surprising since the variance is typically considered to be a very robust indicator of critical transitions. It indicates the potential of the angle between the covariant vectors estimated by the repetitive iteration method, as well as the finite-time Lyapunov exponents as indicator variables.

Although the angle between the covariant vectors computed via Ginelli et al.'s method has the unfair advantage of being iterated back from the future, in some cases the repetitive iteration method leads to better results (see fig. 5.6). The reason may be the higher sensitivity of the repetitive iteration method to the changes in the local dynamics as discussed in chapter 4.

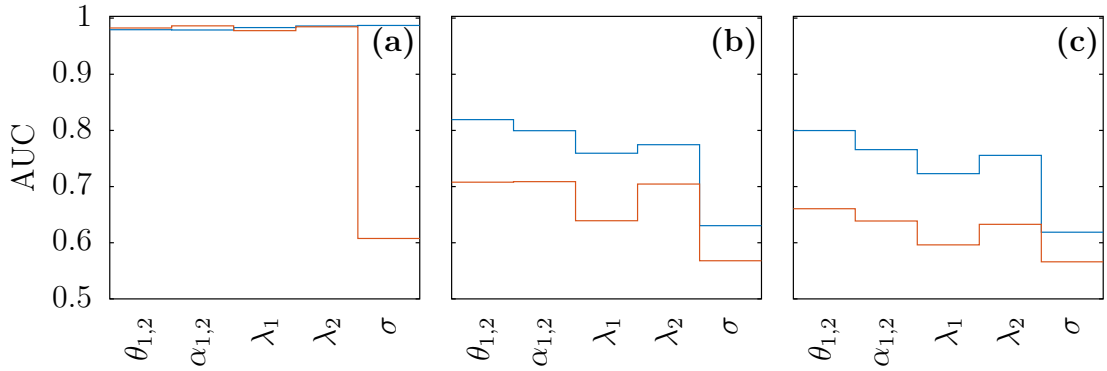

Figure 5.3: Predictions made for a single FitzHugh-Nagumo oscillator with $a = 0.3, b = 0.3$, show that the angle between the covariant vectors along with the second finite-time Lyapunov exponent are more effective precursors than the finite-time variance. AUCs of the angle between the covariant Lyapunov vectors estimated without iterating to the future, $\alpha_{i,j}$, with Ginelli et al.'s method, $\theta_{i,j}$, finite-time Lyapunov exponents, λ_i and the variance, σ, for different noise strengths, D, the lead time of 0.2 (blue line) and 0.4 (redline) are shown. (a) $D = 0$ and (b) $D = 0.3$ (c) $D = 0.6$.

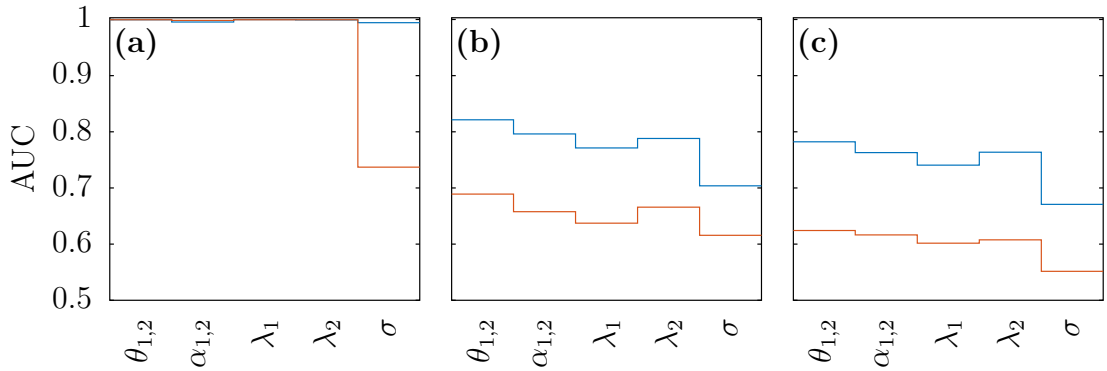

Figure 5.4: Predictions made for a 2-D Josephson junction in the highly dissipative regime show that the angle between the covariant vectors along with the finite-time Lyapunov exponents are more effective precursors than the finite-time variance. AUCs of the angle between the covariant Lyapunov vectors estimated without iterating to the future, $\alpha_{i,j}$, with Ginelli et al.'s method, $\theta_{i,j}$, finite-time Lyapunov exponents, λ_i and the variance, σ, for different noise strengths, D, the lead time of 0.2 (blue line) and 0.4 (redline) are shown. (a) $D = 0$ and (b) $D = 0.4$ (c) $D = 0.8$.

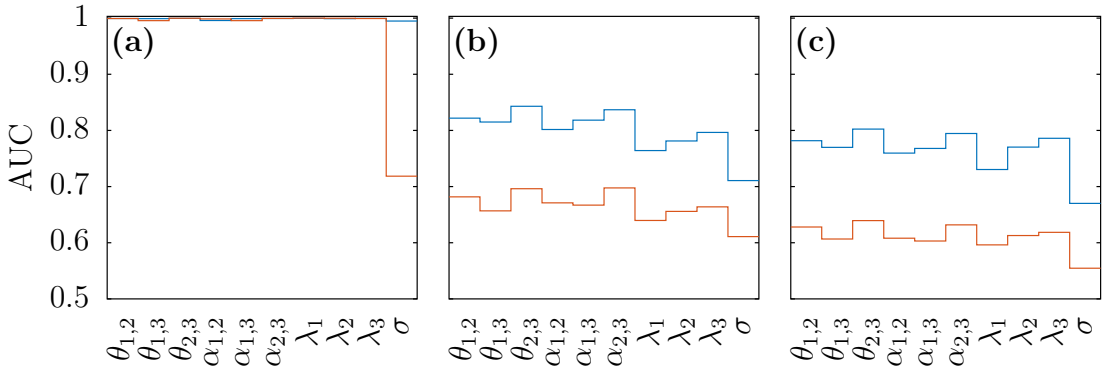

Figure 5.5: Predictions made for a 3-D Josephson junction with $\beta = 0.1$ show that the angle between the covariant vectors along with the finite-time Lyapunov exponents are more effective precursors than the finite-time variance. AUCs of the angle between the covariant Lyapunov vectors estimated without iterating to the future, $\alpha_{i,j}$, with Ginelli et al.'s method, $\theta_{i,j}$, finite-time Lyapunov exponents, λ_i and the variance, σ, for different noise strengths, D, the lead time of 0.2 (blue line) and 0.4 (redline) are shown.(a) $D = 0$ and (b) $D = 0.4$ (c) $D = 0.8$.

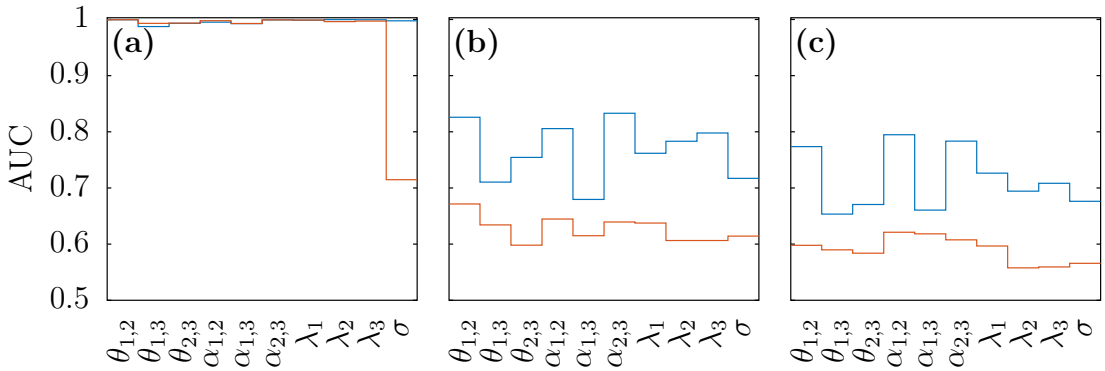

Figure 5.6: Predictions made for a 3-D Josephson junction with $\beta = 0.3$ show that the angle between the covariant vectors along with the finite-time Lyapunov exponents are more effective precursors than the finite-time variance. AUCs of the angle between the covariant Lyapunov vectors estimated without iterating to the future,$\alpha_{i,j}$, with Ginelli et al.'s method, $\theta_{i,j}$, finite-time Lyapunov exponents, λ_i and the variance, σ, for different noise strengths, D the lead time of 0.2 (blue line) and 0.4 (redline) are shown. (a) $D = 0$ and (b) $D = 0.4$ (c) $D = 0.8$.

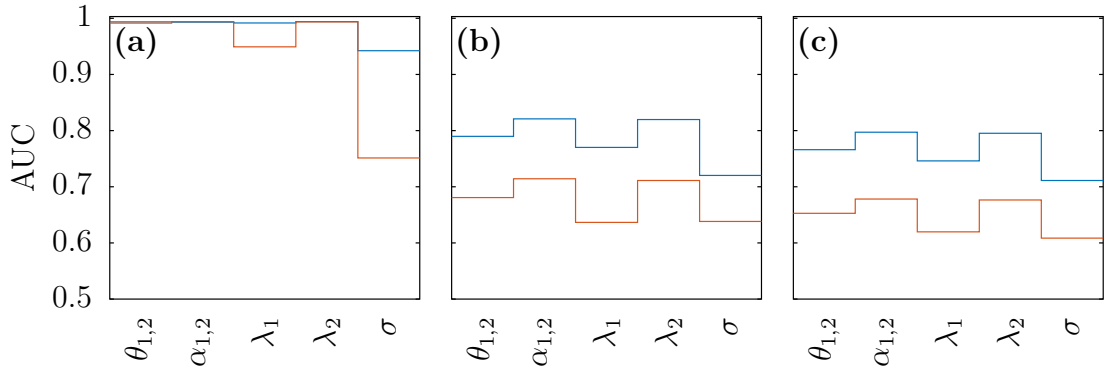

Figure 5.7: AUCs of the angle between the covariant Lyapunov vectors estimated without iterating to the future, α_{ij} and with Ginelli et al.'s method, θ_{ij}, finite-time Lyapunov exponents, λ and the variance, σ, for different noise strengths, D and different lead times, Δt, for the Van der Pol Oscillator. Predictors based on covariant Lyapunov vectors can predict transitions better than conventional indicator variables, such as σ_1^2. The blue line sorrespond to the lead time of 0.25 and the red line corresponds to the lead time of 0.5. The noise strengths are (a) $D = 0$, (b) $D = 0.1$ and (c) $D = 0.2$.

6 Ext reme events: Black Swan or Dragon King? Suppression of the Extreme Events

This chapter is devoted to extreme events in chaotic high-dimensional systems. We look for extreme events in a Lorenz 96 model and in a network of coupled chaotic electronic circuits. We find the Dragon Kings and the Black Swans of the chaotic systems and identify their precursors. We will clarify which types of extreme events have finger prints in the dynamical structure of a system and which type of extreme events do not leave visible traces. Furthermore we suppress the Dragon Kings using occasional feed back.

6.1 Bubbling transitions of chaotic electronic circuits

Spatially extended, coupled oscillators are widely used to model different complex dynamical systems. Examples include dislocation modes in earthquake fault models [111], collective phase synchronization in brain activity [112] and models for stock market fluctuations [113]. The invariant manifold of many coupled chaotic oscillators contain regions with chaotic orbits. Existence of these "hot spots" in the invariant manifold leads to intermittent excursions away from the attractor, a phenomenon referred to as attractor bubbling.

Similar to critical transitions, bubbling transitions occur when one of the directions transverse to the invariant manifold looses it's stability. That is to say, attractor bubbling is preceded by rising of the finite-time Lyapunov exponents corresponding

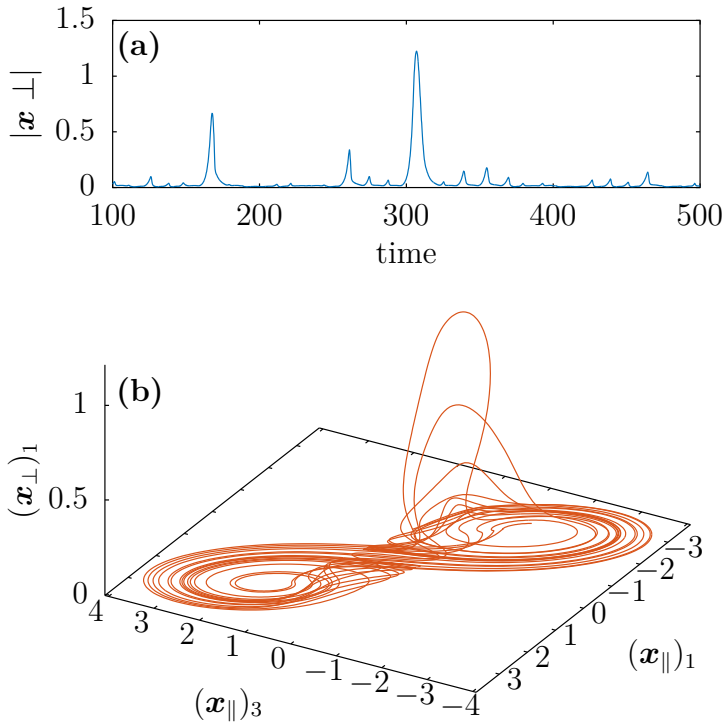

Figure 6.1: This figure is the numerical reproduction of the experimental results in [114]. Two coupled chaotic oscillators exhibiting bubbling transition induced by noise. (a) The time series of the difference between the master and the slave oscillator exhibits bubbling transitions. (b) A 3-D projection of the 6-D phase space of two synchronized oscillators shows extreme events in the form of brief excursions away from the invariant manifold. The subscript i on each axis label indicates the i-th component of the corresponding vector.

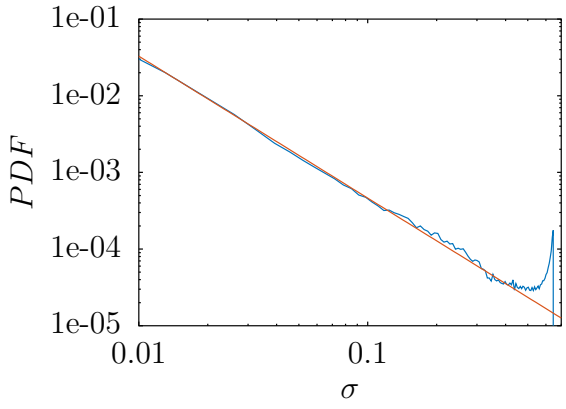

Figure 6.2: Probability distribution function of the events sizes of two coupled chaotic oscillators shows bubbling transitions in the form of Dragon Kings.

to the stable directions transverse to the manifold. Temporary loss of the stability of the stable transverse directions leads to excursions of the trajectory away from the invariant manifold [66, 115, 116]. Bubbling transitions are associated with locally riddled basins. For identical chaotic coupled oscillators, for instance, a bubbling transition happens due to a noise induced jump into a region in which the trajectory is locally repelled from the invariant manifold [117]. Bubbling transitions are of a Dragon King-type and are associated with a wide range of spatially extended dynamical systems.

Here we explore the desynchronization of coupled chaotic electronic circuits as a model exhibiting attractor bubbling. The model was originally used by Gauthier and Bienfang [118] and was in turn a variation of the model used in [119, 120]. Gauthier and Bienfang [118] used it to demonstrate intermittent loss of synchronization in chaotic attractors and suggested new criteria for high-quality synchronization [121–123]. The model consists of two nearly identical chaotic electronic circuits in a master and slave configuration.

Later Sornette, Ott and Gauthier [114] used this model (with two coupled circuits) as an example of a dynamical system, that exhibits extreme events. They showed that, long periods of synchronization of the two circuits is interrupted by irregular desynchronization periods. This phenomenon is an example of attractor bubbling. The blowout bifurcation in the coupled chaotic electric circuit models the type of extreme events that Sornette et al. [114] referred to as Dragon kings [124]. [56, 125, 126].

The differential equations of the system of the two coupled chaotic circuits have the general form,

$$\begin{aligned} \dot{\boldsymbol{X}}_M &= \boldsymbol{F}[\boldsymbol{X}_M], \\ \dot{\boldsymbol{X}}_S &= \boldsymbol{F}[\boldsymbol{X}_S] + c\boldsymbol{K}(\boldsymbol{X}_M - \boldsymbol{X}_S), \end{aligned} \tag{6.1}$$

where M, stands for the master and S, stands for the slave. $\boldsymbol{F}$, is the flow function for each system, c, is the coupling strength and $\boldsymbol{K}$, is the coupling matrix. Sornette et al. [114], used two coupled electronic circuits, each with three variables. For suitable parameter values the two circuits can synchronize. In this case, the 6 dimensional

system will reside in the three dimensional invariant manifold of $\boldsymbol{X_M} = \boldsymbol{X_S}$. It is useful to change the variables to $\boldsymbol{X}_{\parallel} = \boldsymbol{X}_S + \boldsymbol{X}_M$ and $\boldsymbol{X}_{\perp} = \boldsymbol{X}_M - \boldsymbol{X}_S$. While the circuits are synchronized the trajectory resides on the invariant manifold $\boldsymbol{X}_{\perp} = 0$. However if the trajectory goes near the so called hot spots where it is repelled from the invariant manifold, a blowout bifurcation leads to an excursion away from the invariant manifold. Sornette et al. [114], observed the bubbling phenomenon in experimental settings of two coupled chaotic oscillators. The two electronic circuits are almost identical with a slight parameter mismatch that acts as thermal noise in the electric components. The 6-D system has an unstable saddle-node fixed point at $\boldsymbol{X}_{\parallel} = 0$ [118, 127]. A bubbling transition is very probable while the trajectory is in the vicinity of this fixed point.

Figure 6.1 is a numerical reproduction of their experimental results. The time series on the top shows the synchronization error between the two oscillators. The phase space diagram in the bottom shows the trajectory on the invariant manifold while it goes through several excursions away from the attractor. Figure 6.2 shows the probability distribution function of the synchronization error of the two coupled circuits. The large peak at the end, standing out of the power law distribution of the rest of the events indicates the bubbling transitions.

Further more Sornette et al. Devised a method for suppressing the Dragon Kings in the case of two coupled oscillator system.

Sornette et al. [114], showed that the lingering of the trajectory in the vicinity of the unstable fixed point, can be used as a precursor to a bubbling transition. They devised a method of suppressing the extreme events in their system of two coupled chaotic oscillators using occasional feedback of tiny perturbations to the slave whenever the value of the master decreased below a certain threshold. The coupling strength was increased whenever the system was close to the unstable fixed point.

Although Sornette et al. managed to suppress the bubbling transitions in the specific case of the two coupled circuits with a fixed point at the origin, they did not provided a general precursor for this type of extreme events, when the structure of the phase space is not known.

6.1.1 Desynchronization of a Network of Chaotic Coupled Oscillators

Here we modify their model to have a network of coupled chaotic oscillators consisting of N coupled circuits. The equations governing the evolution of the trajectory are as follows,

$$\begin{aligned} \dot{V}_{1j} &= \frac{V_{1j}}{R_1} - g[V_{1j} - V_{2j}], \\ \dot{V}_{2j} &= g[V_{1j} - V_{2j}] - I_j + \sum_{i=1}^{N} cK_{i,j}(V_{2i} - V_{2j}), \\ \dot{I}_j &= V_{2j} - R_4 I_j, \end{aligned} \tag{6.2}$$

where,

$$g(V) = \frac{V}{R_2} + I_r[\exp(\alpha_f V) - \exp(-\alpha_r V)]. \tag{6.3}$$

The parameter values for all the nodes are slight variations of the following values: $R1 = 1.298\Omega, R2 = 3.44\Omega, R4 = 0.193\Omega, Ir = 22.4\mu A, \alpha_f = 11.5$ and $\alpha_r = 11.71$. We computed the covariant Lyapunov vectors for different coupling matrices and different coupling strengths c and different number of oscillators, N.

In a high dimensional system of N oscillators and $3N$ degrees of freedom, examining the angle between the $\frac{3N(3N-1)}{2}$ pairs of vectors is not useful. Therefore we are going to employ principal component analysis (PCA), one of the most popular techniques of multivariate analysis [128, 129], on our covariant vectors. PCA, helps us to reduce the dimensionality of the data set and to identify the directions in which the data set has most variation. The data is transformed into a new set of variables. The new variables are ordered according to their variance. Hence the first principal component indicates the main direction of alignment. An increase in its variance implies higher degree of alignment between the vectors and stronger localization at the same location.

Figure 6.3: The variance of the first principal component increases well before the desynchronization of the oscillators starts in a ring of 40 oscillators with coupling strength, $c = 10.$(a) Time series of V_1j, $j = 1 \dots 40$ (b) Synchronization error (c) Variance of the first principal component. Spectrum of the covariant vectors along with the first principal component in (d) the synchronized state long before the transition, (e) synchronized state closer to the transition and (f) desynchronized state

The dynamical system consisting of a large number of coupled chaotic oscillators, similar to the case of two coupled oscillators goes through long episodes of synchronization interrupted by temporary desynchronization episodes, which are excursions away from the synchronized manifold. However these self-propagating shifts away from the completely synchronized state may also lead to transitions to another region of the phase space where two clusters of synchronized oscillators coexist.

Principal component analysis of the covariant vectors shows an increase in the variance of the first principal component prior to desynchronization events. That is to say, similar to critical transitions in our fast-slow systems, prior to excursions away from the attractors the covariant vectors tend to align.

As previously discussed attractor bubbling occurs once the system's state enters the hot spots of the phase space. The regions in which, the directions transverse to the invariant manifold loose their stability and therefore, a slight perturbation will lead to repelling of the trajectory from the invariant manifold. In other words the finite-time Lyapunov exponents corresponding to previously stable directions increase dramatically. This deviation from hyperbolicity, as mentioned in chapter 4 manifests itself in the reduction of the angle between the covariant vectors. As the trajectory is going through an excursion away from the invariant manifold the direction along the trajectory previously corresponding to the neutral direction turns into the contracting direction, ergo, the interchange between the stability of the transverse directions leads to tangencies between the covariant vectors. The increase in the variance of the first principal component precedes both bubbling transitions as well as critical transitions to the synchronized clusters.

Figure 6.3 demonstrates a desynchronization event of 40 coupled oscillators, i.e., a 120 dimensional system. Figure 6.3(a) shows the time series of the first variables, $V_1 j$, of all circuits. Figure 6.3(b) demonstrates the variance of the first variables, $V_1 j$, of all the circuits, i.e., the synchronization error. The variance is zero in the synchronized state, it increases as the oscillators desynchronize further. The variance of the first principal component is shown in fig. 6.3(c). The covariant vectors are computed using Gienllie et al.'s method. Increasing of the variance of the first principal component starts well before the start of the desynchronization. That is to say, higher degree of alignment between the vectors announces the system entering a

"danger zone" in which any perturbation leads to repelling of the trajectory from the invariant manifold. This observation is similar to our results from critical transitions in fast-slow systems.

Figure 6.3(d-f) show the spectrum of the covariant vectors as well as the first principal component at three different instances. As evident from fig. 6.3(d-f) the first principal component shows increased localization on several of the oscillators prior to desynchronization. Perturbations of the variables of these oscillators rapidly escalate and lead to desynchronization.

Once the system has transitioned to the state of two clusters of synchronized oscillators, transitions of single oscillators from one cluster to another happen irregularly. The first PCA variance increases prior to each transition. Prior to a transition, the covariant vectors and hence the first principal component highly localize at the transitioning unit. In other words the localization of the covariant vectors warns an oscillator entering a spot of transverse instability that can shoot the oscillator to another cluster.

6.1.2 Prediction and Suppression

The next step is to check for the statistical relevance of our observations. Furthermore we use our results to suppress the Dragon Kings. We use the synchronization error (the variance of the variables of the oscillators) and the PCA variance to predict desynchronization events. In order to determine the onset of the extreme event, we used the threshold of 0.4 on the synchronization error. Namely an extreme event has occurred once the synchronization error reaches 0.4.

Figure 6.4(a) shows that for small lead times the synchronization error predicts the transition better than the PCA variance. Yet for larger lead times, the PCA variance is a far better precursor than the synchronization error.

While predicting extreme events is very useful another important question is the possibility of suppressing them.

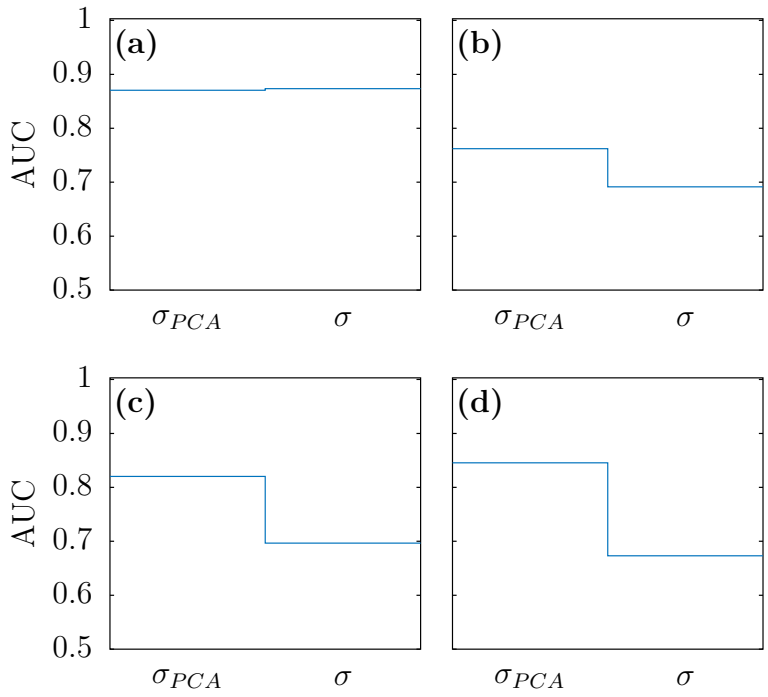

Figure 6.4: For large lead times the PCA variance, σ_{PCA} predicts a desynchronization event far better than the variance of the oscillators, σ. The predictions are made for 40 circularly coupled circuits, i.e, dimension of the system was 120, the coupling strength $c = 100$. (a) AUC for lead time, $\Delta t = 10$ (b) AUC for lead time, $\Delta t = 100$ (c) AUC for lead time, $\Delta t = 200$ (d) AUC for $\Delta t = 300$

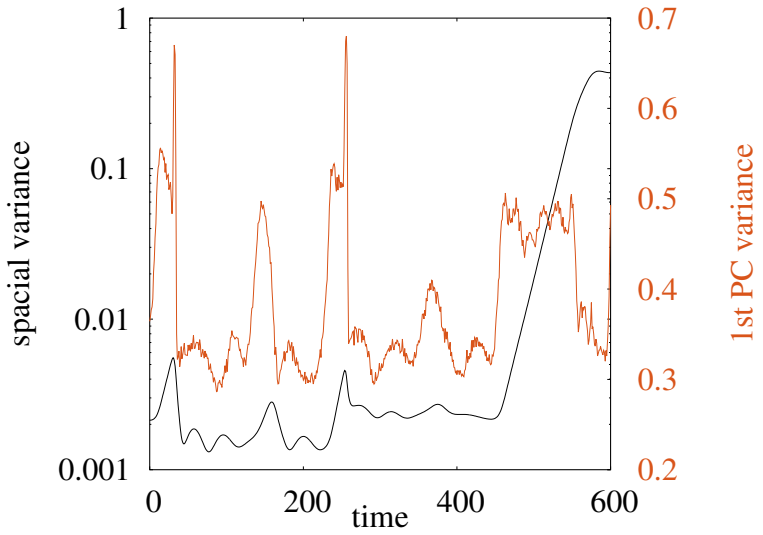

Figure 6.5: The variance of the first principal component of the covariant vectors computed via repetitive iteration method is snesitive to upcoming desynchronization episodes of different sizes for 20 circularly coupled circuits

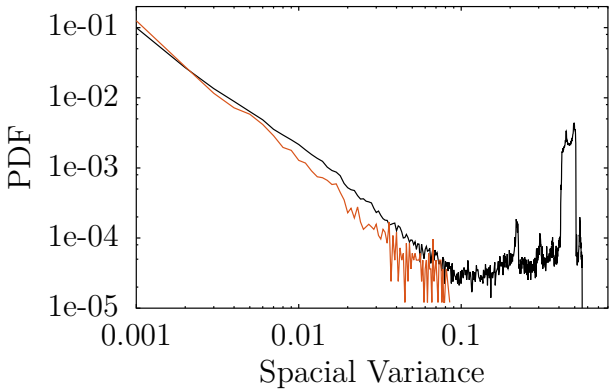

Figure 6.6: Occasional perturbations in the form of increased coupling strength whenever the variance of the first principal component stays above the threshold of 0.31 more than 1 time unit can suppress the extreme events. The distribution function of the uncontrolled and the controlled system are compared, for a network of 20 oscillators. The covariant vectors are computed with the repetitive iteration method.

Suppressing the events is only possible if vectors are computed with the repetitive iteration method. The reason is that each time we suppress an event the trajectory of the system changes, therefore, it is not possible to iterate the system back from the far future. Computing the covariant vectors with the repetitive iteration method, however, gives quite accurate results. However as mentioned in chapter chapter 4, the estimates of the covariant vectors with the repetitive iteration method are far more sensitive to the changes of the local dynamics. While the covariant vectors computed via Ginelli et al.'s method are results of iterating from the far future, the repetitive iteration method iterates the vectors backwards from the immediate future repeatedly. Therefore it is largely influenced by the local dynamical changes. As a result the vectors computed with the repetitive iteration method are much more sensitive to slight desynchronization events than the vectors from Ginelli et al.'s method. Figure 6.5 shows the variance of the first principal component of the covariant vectors estimated via the repetitive iteration method. All the peaks of the PCA variance correspond to a slight desynchronization, i.e., a bump in the synchronization error. As opposed to the covariant vectors computed with Ginelli et al.'s method that only detected more persistent desynchronization episodes. These vectors are sensitive to any deviation from the synchronized state. Nonetheless, while the peaks corresponding to a slight desynchronization are quite sharp, the increase in the first PCA variance that is followed by a big desynchronization episode is very persistent. Therefore the big and the small desynchronization episodes are distinguishable with the PCA variance. Just for the sake of demonstrating how small perturbations can suppress the extreme events, assume that it is costly to keep the coupling strength high all the time and this perturbation to the system can only be briefly activated. If we only increase the coupling strength for a short period of time when the PCA variance is staying above a threshold value we can effectively suppress the extreme events. Figure 6.6 shows the probability distribution of the synchronization error in the absence and presence of the control mechanism. By purely activating the strong coupling briefly when the first PCA variance of the covariant vectors, estimated from the repetitive iteration method, stays for some time above a certain threshold we could suppress the giant desynchronization episodes while ignoring the small ones.

Although the suppression mechanism used here is not a general tool applicable to

all systems it can be used in different networks of coupled oscillators.

6.2 Lorenz 96

In this brief section we take a look at the arrangement of the covariant Lyapunov vectors prior to occurrence of an event on the tail of the event-size distribution.

In 1996 Edward Lorenz one of the key figures of chaos theory introduced a new atmospheric model [130, 131]. This model, usually referred to as "Lorenz 96" was initially developed to tackle problems of predictability in weather forecasting. In spite of its simplifications, it has remained one of the most prominent models in atmospheric sciences. It has been extensively studied as a continuous in time and discrete in space model for spatially extended chaotic systems (see [132–137] as several examples. The model contains K variables,

$$\dot{X}_i = -X_{i-2}X_{i-1} + X_{i-1}X_{i+1} - X_i + F, \tag{6.4}$$

Where $X_{i-K} = X_{i+K} = X_K$. The variables represent an atmospheric quantity, say temperature, in K sectors of a latitude circle [130]. The constant F represents external forcing, the linear term stands for internal dissipation while, the quadratic terms replicating advection, conserve the total energy. The variables are rescaled and the time unit is 5 days. For very small F, the system converges to the steady state of $X_1 = \cdots = X_K = F$. For relatively larger values of F, solutions become periodic and for yet larger values of F, chaos emerges.

Lorenz 96 model is frequently used in ensemble forecasting. The approach of ensemble forecasting as a form of Monte Carlo analysis, instead of a single prediction gives a number of forecasts. The simulation runs multiple times each with slightly different initial conditions. Evidently, the growth of perturbations and the directions of perturbation growth are of great importance in the domain of ensemble forecasting. Consequently the Lyapunov exponents and the Lyapunov vectors of the Lorenz 96 model have been studied before [24, 133, 138, 139].

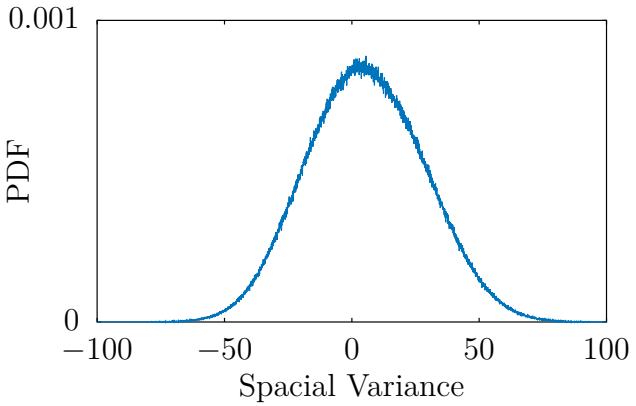

Figure 6.7: The probability distribution function of the event sizes of Lorenz 96. The 0.0001% of the events on the tail are our extreme events.

We test our method for predicting extreme events in a Lorenz 96 model with 128 variables. Figure 6.7, shows the distribution of the values of the nodes. We can assume the 0.001% largest values lying on the tail of the distribution to be the extreme events. Figure 6.8 shows the spectrum of the covariant Lyapunov vectors as one of the nodes exhibits an extreme value. As opposed to our other examples of extreme events, no change in the structure of the covariant Lyapunov vectors is visible.

The tails of event distributions, although extreme, are generated due to the same mechanisms as other events and hence, do not leave traces in the dynamical structure.

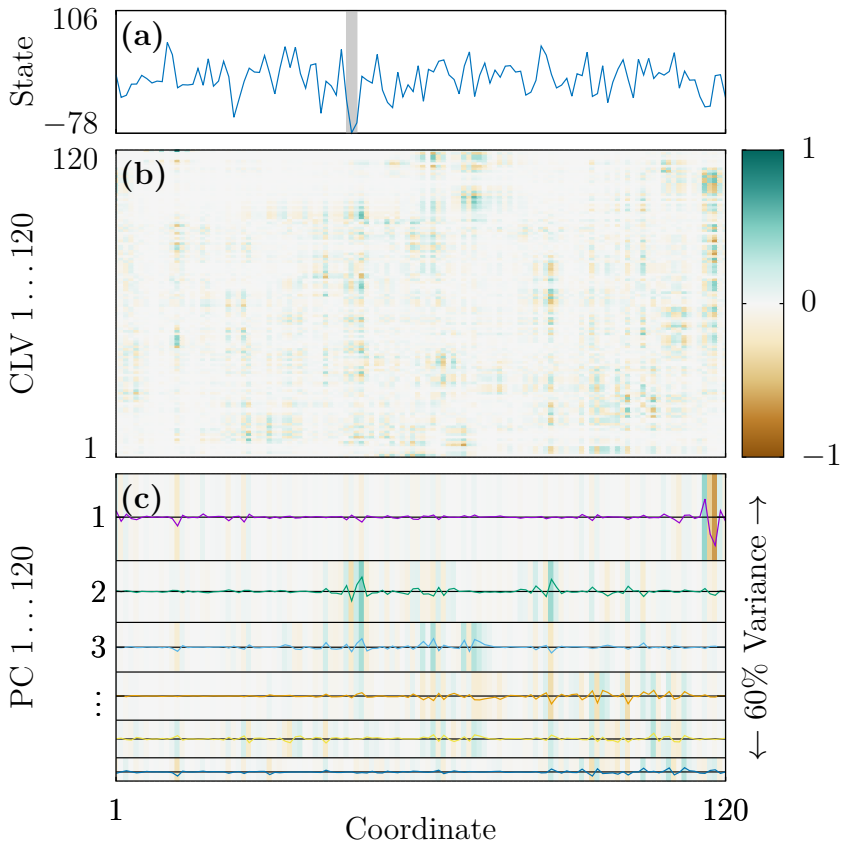

Figure 6.8: The localization of the covariant vectors in the Lorenz 96 model does not predict the Black Swan type events of this system. (a) The values of the 120 nodes. (b) The spectrum of the covariant vectors computed via Ginelli et al.'s method. (c) 60% of the variances of the principal components.

7 Discussion

This thesis was an effort to contribute to the growing field of prediction of critical transitions and extreme events.

Extreme events and critical transitions have been subject of study from the dynamical systems perspective in the past [12, 140–145]. In this thesis, using tools from dynamical systems theory we aimed to show that a dynamical view towards the prediction of extreme events, not only helps understanding the roots of such events, but also provides us with more efficient tools for predicting them. Using dynamics of the covariant Lyapunov vectors as directions of perturbation growth, we presented a unifying approach towards prediction of extreme events. In different models, we explored the dynamical changes that lead to catastrophic events. We demonstrated the tangencies between the vectors and the changes in their localization announce the system's state entering "danger zones" in which the trajectory is repelled from the invariant manifold. Employing principal component analysis, we used alignment between the covariant vectors to predict extreme events. Furthermore, we showed that the covariant Lyapunov vectors as well as the finite-time Lyapunov exponents can predict critical transitions far better than typical predictors of critical transitions such as finite-time variance.

Estimating the Covariant Lyapunov Vectors at the Present. In recent years after almost simultaneous introduction of multiple computational methods, the covariant Lyapunov vectors have become an effective tool for characterizing dynamical systems. Available methods for computing the vectors depend on asymptotic behavior of the system iterated forward from the far past and backwards from the far future. The method of Samelson and Wolfe [22], views the covariant vectors as intersections of the Oseledec subspaces and determines them as linear combinations

of both forward and backward Lyapunov vectors. Kuptsov and Parlitz [25], used LU factorization to compute the covariant vectors. Both mentioned methods require computation of backward and forward Lyapunov vectors, i.e., iteration of the system forward from the far past and backwards from the far future. The method of Ginelli et al. [146], that is used in this thesis as well, uses the asymptotic properties of the covariant vectors by iterating them backwards from the far future while confining them to their respective Oseledec subspaces.

We used the method introduced by Ginelli et al. [23] to compute the covariant Lyapunov vectors and probe the dynamical structure of systems exhibiting extreme events. An important part of this project, however, was not only to characterize dynamical changes that lead to extreme events, but also to use those changes to predict the extreme events. Therefore, we had to develop a method to estimate the covariant vectors without iterating the system to the far future. This method uses the linearized dynamics of the immediate future as an estimate of the near future by repeatedly iterating the vectors backwards from the immediate future to the present. Furthermore it uses the covariance property of the vectors to improve the estimates. I.e., it uses the forward iteration of the vectors computed in the past as starting points for repeated backwards iterations. Namely using the information from the past the vectors gradually converge to the set of covariant vectors with out going to the far future.

We then used this method to compute the covariant Lyapunov vectors in our models in order to predict extreme events using the changes in the different features of the vectors.

Critical Transitions. While it is not possible to effectively predict the tails of event distributions, a large group of extreme events lying outside the distribution of their peers are in fact, predictable. These events, referred to as Dragon Kings, rise from unique origins and are mechanistically and statistically different from their smaller peers. Positive feedback mechanisms present in certain regions of the phase space of a dynamical system lead to these events becoming much larger than others.

Critical transitions represent a wide class of the Dragon Kings. Many complex systems have critical thresholds or tipping points, where they exhibit transitions from one stable state to another. Once the trajectory approaches the critical point any

perturbation or change in the bifurcation parameter can lead to a self propagating shift to another stable state. As intrinsic directions of perturbation growth it is natural to expect the dynamics of the covariant Lyapunov vectors to indicate when the trajectory is entering a region in which perturbations lead to catastrophes.

Using the mathematical framework of fast-slow systems we modeled critical transitions. We explained how interchange of stability between the orthogonal directions, leads to tangencies between the covariant Lyapunov vectors. We pointed out that the interchange of stability between the transverse directions although not exclusive to critical transitions, is a generic sign of this type of threshold crossing. Consequently in our different models we observed a reduction of the angle between the covariant vectors corresponding to the marginal and the stable manifold prior to critical transitions, followed by tangencies between the vectors during transitions.

Merging of covariant Lyapunov vectors indicates homoclinic tangencies between the stable and unstable manifolds which can occur in dynamical structures called *wild hyperbolic sets* [147]. Newhouse [148–150] proved the existence of hyperbolic invariant sets in which stable and unstable manifolds can have persistent homoclinic tangencies that are robust against perturbations. Tangencies between the covariant vectors can also be understood as a mechanism contributing to the phenomenon of critical slowing down. Critical slowing down describes a system's loss of resilience towards external perturbations, approaching a bifurcation point. We showed that it is not only the increase in the growth rates of perturbations, but also constraints on possible growth directions, that cause critical slowing down. Tangencies between the covariant Lyapunov vectors represent a temporal reduction of the dimension of the tangent space. During and close to the transitions in our fast-slow models, the tangent space is effectively one-dimensional, allowing only perturbation growth in the direction of the trajectory, i.e., in the direction of the transition. In other words, shortly before the transition, while the vectors tend to align, any perturbation in any direction will grow such that it triggers the transition. During the transition any perturbation will grow such that it contributes to the transition. In other words, the alignment of both possible directions of perturbation growth, prior to and during a critical transition, indicates that the dimension of the tangent space is reduced during a transition, allowing only one possible change of the trajectory: towards the next (meta) stable state.

Towards higher dimensions: Dragon King or Black Swan? Using two different models of high dimensional chaotic systems we further clarified what types of extreme events are foreseeable by the geometrical structure of the tangent space and what type of events, the structure of the tangent space does not account for.

Inspired by the work of Sornette et al. [114], we explored systems of coupled chaotic electronic circuits. In our model of a large number of coupled nearly identical chaotic oscillators, with appropriate coupling strength, we showed that the system goes through long episodes of synchronization interrupted by brief desynchronization intervals, (i.e. bubbling transitions), until it finally transitions to a desynchronized state in which several clusters of synchronized oscillators coexist.

We used principle component analysis to identify the directions of alignment in the tangent space. We showed that the variance of the first principal component increases prior to attractor bubblings. Bubbling transition happens when the trajectory enters a region of the invariant manifold where the transverse stability is lost. As previously discussed, loss of transverse stability manifests itself in tangencies between the covariant Lyapunov vectors. Therefore, higher degree of alignment between the vectors indicates the system's state entering one of the hot spots of the phase space in which loss of transverse stability leads to repelling of the trajectory from the invariant manifold. We showed that well before the transition of the system to a state with several synchronized clusters, the variance of the first principal component dramatically increases. Similar to our models of fast-slow systems higher alignment between the covariant vectors indicates reduced dimensionality of the tangent space. The reduced dimensionality, by constraining the perturbation growth pushes the system's state towards a transition.

Moreover, after the transition to several synchronized clusters, an increase in the PCA variance and the localization of the covariant vectors on a single oscillator indicate the proximity of the oscillator transitioning from one cluster another. That is to say, a high degree of localization of the vectors on an oscillator indicates that oscillator entering a region in the phase space in which perturbations to its state rapidly escalate forcing it to go another cluster.

Sornette et al. [114] used this model to show the Dragon King type of events in a pair of coupled electronic circuits. They identified a saddle type fixed point in the

system of two coupled oscillators and showed that the bubbling transition happens when ever the system's state lingers close to the unstable fixed point. We introduced a more general prediction scheme, using the variance of the PCA of the covariant vectors, in high-dimensions where the geometry of the phase space is not known.

Our last model, was a high-dimensional chaotic atmospheric model introduced by Edward Lorenz in 1966 [130]. We merely displayed this model to show a type of extreme event that does not leave clear fingerprints on the dynamical structure and hence can not be predicted by the covariant Lyapunov vectors. We identified extreme events of this model in the tail of event size distribution. We showed that these Black Swan type of events are not reflected in the geometrical structure of the tangent space and therefore, can not be predicted by our dynamical precursors.

Prediction. We used our dynamical precursors to predict extreme events and compared their predictive powers to other precursors of extreme events. In our models of critical transitions, we established existence of a Granger causal link between the alignment of the covariant vectors, the finite-time Lyapunov exponents and critical transitions. That is to say, we verified the statistical relevance of the time series of our dynamical variables to future critical transitions. Verification was done by carrying out a set of prediction experiments which consist of identifying indicatory behavior of time series derived from covariant Lyapunov vectors in training data sets, predicting critical transitions occurring in test data sets and evaluating the prediction success using common measures of forecast verification. Testing was necessary, since in systems with increased noise strength, some transitions can potentially occur without previous alignment or some alignments might occur without a following critical transition. In order to verify the existence of a Granger causal link, it is sufficient to verify that the predictions based on the alignment are better than random predictions. For all prediction experiments we found that the angle between covariant Lyapunov vectors was able to predict the occurrence of critical transitions significantly better than chance. That is, we found a Granger causal link between the alignment of covariant Lyapunov vectors prior to and during critical transitions and the occurrence of critical transitions. Additionally we found another Granger causal link between the specific dynamics in the time series of finite-time Lyapunov exponents prior and during critical transitions and the occurrence of critical transitions. For systems with increased noise strength and predictions with

longer lead time the angle between covariant Lyapunov vectors predicted critical transitions significantly better than common indicator variables for critical slowing down, such as the sliding-window estimate of the variance.

In the case of the network of coupled chaotic oscillators, we showed that the increase in the variance of the first principal component can predict the desynchronization with large lead times. We also used the increase in the synchronization error as a precursor and showed that the PCA variance performs significantly better than the synchronization error. We also used our estimating method to compute the covariant vectors in the network of coupled oscillators. We then used the increase in the variance of the first principal component of the resulting covariant vectors to not only predict but also suppress the Dragon Kings by brief occasional perturbations.

Outlook. We presented a unifying approach towards the prediction of Dragon Kings: Reduction of the dimension of the tangent space precedes Dragon Kings. The angle between the vectors and in the case of high-dimensional systems the increase in the variance of the first principal component, can be used as precursors of this type of extreme events.

However, although the first principal component of the covariant Lyapunov vectors indicates the main direction of alignment in the tangent space, information about partial alignment of the vectors in different subspaces of the tangent space is encoded in the other principal components. We predicted big episodes of desynchronization using the increase in the first variance. However we did not explore the role of the changes in the variance of the higher order principal components. Investigating PCA variances of higher orders will reveal information about the alignment of the vectors in subspaces of tangent space. For instance, in the discussed model of coupled chaotic oscillators, using this information we may be able to differentiate between the desynchronization episodes that are merely excursions away from the synchronized state, i.e., bubbling of the attractor and the ones that are permanent transitions to the clustered state. Furthermore, investigating not only the variance but also the localization and changes in the directions of the principal components of the covariant vectors, will offer more insight into the underlying mechanisms of extreme events.

Bibliography

[1] J. Venegas et al. “Self-organized patchiness in asthma as a prelude to catastrophic shifts”. In: *Nature* 434 (2005), pp. 777–782.

[2] P. McSharry, L. Smith, and L. Tarassenko. “Prediction of epileptic seizures”. In: *Nature Med.* 9 (2003), pp. 241–242.

[3] R. May, S. Levin, and G. Sugihara. “Ecology for bankers”. In: *Nature* 451 (2008), pp. 893–895.

[4] T. Lenton et al. “Tipping elements in the Earth’s climate system”. In: *Proc. Natl. Acad. Sci. USA* 105.6 (2008), pp. 1786–1793.

[5] R. B. Alley et al. “Abrupt climate change”. In: *science* 299.5615 (2003), pp. 2005–2010.

[6] M. Scheffer et al. “Early-warning signals for critical transitions”. In: *Nature* 461 (2009), p. 08227.

[7] J. Suárez-Lledó. “The black swan: the impact of the highly improbable.” In: *The Academy of Management Perspectives* 25.2 (2011), pp. 87–90.

[8] M. Ghil et al. “Extreme events: dynamics, statistics and prediction”. In: *Nonlinear Processes in Geophysics* 18.3 (2011), pp. 295–350.

[9] R. W. Katz, M. B. Parlange, and P. Naveau. “Statistics of extremes in hydrology”. In: *Advances in water resources* 25.8 (2002), pp. 1287–1304.

[10] R. L. Smith. “Statistics of extremes, with applications in environment, insurance and finance”. In: *Extreme values in finance, telecommunications and the environment* (2003), pp. 1–78.

[11] D. Sornette. *Critical phenomena in natural sciences: chaos, fractals, selforganization and disorder: concepts and tools*. Springer Science & Business Media, 2006.

[12] S. Albeverio, V. Jentsch, and H. Kantz. *Extreme events in nature and society*. Springer Science & Business Media, 2006.

[13] M. Scheffer et al. "Catastrophic shifts in ecosystems". In: *Nature* 413.6856 (2001), p. 591.

[14] M. Scheffer. *Critical transitions in nature and society*. Princeton University Press, 2009.

[15] S. Hallerberg et al. "Precursors of extreme increments". In: *Physical Review E* 75.1 (2007), p. 016706.

[16] D. R. Easterling et al. "Observed variability and trends in extreme climate events: a brief review". In: *Bulletin of the American Meteorological Society* 81.3 (2000), pp. 417–425.

[17] K. E. Trenberth, J. T. Fasullo, and T. G. Shepherd. "Attribution of climate extreme events". In: *Nature Climate Change* 5.8 (2015), pp. 725–730.

[18] A. B. Davis and D. Sornette. "Celebrating the physics in geophysics". In: *Eos, Transactions American Geophysical Union* 86.46 (2005), pp. 461–467.

[19] D. Sornette. "Predictability of catastrophic events: Material rupture, earthquakes, turbulence, financial crashes, and human birth". In: *Proceedings of the National Academy of Sciences* 99.suppl 1 (2002), pp. 2522–2529.

[20] V. Dakos and J. Bascompte. "Critical slowing down as early warning for the onset of collapse in mutualistic communities". In: *Proceedings of the National Academy of Sciences* 111.49 (2014), pp. 17546–17551.

[21] M. Scheffer et al. "Generic indicators of ecological resilience: Inferring the chance of a critical transition". In: *Annual Review of Ecology, Evolution, and Systematics* 46 (2015), pp. 145–167.

[22] C. L. Wolfe and R. M. Samelson. "An efficient method for recovering Lyapunov vectors from singular vectors". In: *Tellus A* 59.3 (2007), pp. 355–366.

[23] F. Ginelli et al. "Characterizing dynamics with covariant Lyapunov vectors". In: *Physical review letters* 99.13 (2007), p. 130601.

[24] D. Pazó et al. “Structure of characteristic Lyapunov vectors in spatiotemporal chaos”. In: *Physical Review E* 78.1 (2008), p. 016209.

[25] P. V. Kuptsov and U. Parlitz. “Theory and computation of covariant Lyapunov vectors”. In: *Journal of nonlinear science* 22.5 (2012), pp. 727–762.

[26] A. Pikovsky and A. Politi. *Lyapunov exponents: a tool to explore complex dynamics*. Cambridge University Press, 2016.

[27] M. Tabar et al. “Dynamics of the Markov time scale of seismic activity may provide a short-term alert for earthquakes”. In: *arXiv preprint physics/0510043* (2005).

[28] E. J. Gumbel. *Statistics of extremes*. Courier Corporation, 2012.

[29] R. A. Fisher and L. H. C. Tippett. “Limiting forms of the frequency distribution of the largest or smallest member of a sample”. In: *Mathematical Proceedings of the Cambridge Philosophical Society*. Vol. 24. 2. Cambridge University Press. 1928, pp. 180–190.

[30] S. Coles et al. *An introduction to statistical modeling of extreme values*. Vol. 208. Springer, 2001.

[31] R. J. Adler. *The geometry of random fields*. SIAM, 2010.

[32] J.-D. Deuschel and D. W. Stroock. *Large deviations*. Vol. 137. Academic press Boston, 1989.

[33] M. I. Freidlin and A. D. Wentzell. “Random Perturbations”. In: *Random Perturbations of Dynamical Systems*. Springer, 1998, pp. 15–43.

[34] M. I. Freidlin and A. D. Wentzell. *Random perturbations of Hamiltonian systems*. Vol. 523. American Mathematical Soc., 1994.

[35] A. Dembo and O. Zeitouni. *Large deviations techniques and applications, volume 38 of Stochastic Modelling and Applied Probability*. 2010.

[36] R. Ellis. *Entropy, large deviations, and statistical mechanics*. Springer, 2007.

[37] U. Frisch and D. Sornette. “Extreme deviations and applications”. In: *Journal de Physique I* 7.9 (1997), pp. 1155–1171.

[38] J.-Y. Fortin and M. Clusel. “Applications of extreme value statistics in physics”. In: *Journal of Physics A: Mathematical and Theoretical* 48.18 (2015), p. 183001.

[39] V. Balakrishnan, C. Nicolis, and G. Nicolis. "Extreme value distributions in chaotic dynamics". In: *Journal of Statistical Physics* 80.1-2 (1995), pp. 307–336.

[40] D. Ruelle. *Chance and chaos*. Princeton University Press, 1993.

[41] A. Berger. *Chaos and chance: an introduction to stochastic aspects of dynamics*. Walter de Gruyter, 2001.

[42] V. I. Arnol'd. *Catastrophe theory*. Springer Science & Business Media, 2003.

[43] T. Poston and I. Stewart. *Catastrophe theory and its applications*. Courier Corporation, 2014.

[44] V. I. Arnol'd et al. *Dynamical systems V: bifurcation theory and catastrophe theory*. Vol. 5. Springer Science & Business Media, 2013.

[45] P. Bak, C. Tang, and K. Wiesenfeld. "Self-organized criticality: An explanation of the 1/f noise". In: *Physical review letters* 59.4 (1987), p. 381.

[46] P. Bak, C. Tang, and K. Wiesenfeld. "Self-organized criticality". In: *Physical review A* 38.1 (1988), p. 364.

[47] P. Bak and K. Chen. "Self-organized criticality". In: *Scientific American* 264.1 (1991), pp. 46–53.

[48] A. Sornette and D. Sornette. "Self-organized criticality and earthquakes". In: *EPL (Europhysics Letters)* 9.3 (1989), p. 197.

[49] P. Bak. *How nature works: the science of self-organized criticality*. Springer Science & Business Media, 2013.

[50] A. Deluca, N. R. Moloney, and Á. Corral. "Data-driven prediction of thresholded time series of rainfall and self-organized criticality models". In: *Physical review E* 91.5 (2015), p. 052808.

[51] H. J. Jensen. *Self-organized criticality: emergent complex behavior in physical and biological systems*. Vol. 10. Cambridge university press, 1998.

[52] P. Bak and M. Paczuski. "Complexity, contingency, and criticality". In: *Proceedings of the National Academy of Sciences* 92.15 (1995), pp. 6689–6696.

[53] H. Kantz and T. Schreiber. *Nonlinear time series analysis*. Vol. 7. Cambridge university press, 2004.

[54] M. W. Denny et al. “On the prediction of extreme ecological events”. In: *Ecological Monographs* 79.3 (2009), pp. 397–421.

[55] C. Domb. *Phase transitions and critical phenomena*. Vol. 19. Academic press, 2000.

[56] D. Sornette. “Dragon-kings, black swans and the prediction of crises”. In: (2009).

[57] J.-P. Eckmann and D. Ruelle. “Ergodic theory of chaos and strange attractors”. In: *Reviews of modern physics* 57.3 (1985), p. 617.

[58] D. Ruelle. *Thermodynamic formalism: the mathematical structure of equilibrium statistical mechanics*. Cambridge University Press, 2004.

[59] R. Livi, A. Politi, and S. Ruffo. “Distribution of characteristic exponents in the thermodynamic limit”. In: *Journal of Physics A: Mathematical and General* 19.11 (1986), p. 2033.

[60] P. Grassberger. “Information content and predictability of lumped and distributed dynamical systems”. In: *Physica Scripta* 40.3 (1989), p. 346.

[61] J.-P. Eckmann et al. “Lyapunov modes in hard-disk systems”. In: *Journal of statistical physics* 118.5 (2005), pp. 813–847.

[62] I. Shimada and T. Nagashima. “A numerical approach to ergodic problem of dissipative dynamical systems”. In: *Progress of Theoretical Physics* 61.6 (1979), pp. 1605–1616.

[63] G. Benettin et al. “All Lyapunov characteristic numbers are effectively computable.” In: *Academie des Sciences Paris Comptes Rendus Serie B Sciences Physiques* 286 (1978), pp. 431–433.

[64] G. Benettin et al. “Lyapunov characteristic exponents for smooth dynamical systems and for Hamiltonian systems; a method for computing all of them. Part 1: Theory”. In: *Meccanica* 15.1 (1980), pp. 9–20.

[65] V. I. Oseledets. “A multiplicative ergodic theorem. Characteristic Ljapunov, exponents of dynamical systems”. In: *Trudy Moskovskogo Matematicheskogo Obshchestva* 19 (1968), pp. 179–210.

[66] P. Ashwin, J. Buescu, and I. Stewart. "Bubbling of attractors and synchronisation of chaotic oscillators". In: *Physics Letters A* 193.2 (1994), pp. 126–139.

[67] B. Legras and R. Vautard. "A guide to Liapunov vectors". In: *Proceedings 1995 ECMWF Seminar on Predictability*. Vol. 1. Citeseer. 1996, pp. 143–156.

[68] V. I. Oseledec. "A multiplicative ergodic theorem. Lyapunov characteristic numbers for dynamical systems". In: *Trans. Moscow Math. Soc* 19.2 (1968), pp. 197–231.

[69] N. R. Council et al. *New directions for understanding systemic risk: a report on a conference cosponsored by the Federal Reserve Bank of New York and the National Academy of Sciences*. National Academies Press, 2007.

[70] R. M. May, S. A. Levin, and G. Sugihara. "Complex systems: Ecology for bankers". In: *Nature* 451.7181 (2008), pp. 893–895.

[71] R. Leemans and R. de Groot. *Millennium Ecosystem Assessment: Ecosystems and human well-being: a framework for assessment*. Island Press, 2003.

[72] T. M. Lenton et al. "Tipping elements in the Earth's climate system". In: *Proceedings of the national Academy of Sciences* 105.6 (2008), pp. 1786–1793.

[73] R. M. May. "Thresholds and breakpoints in ecosystems with a multiplicity of stable states". In: *Nature* 269.5628 (1977), pp. 471–477.

[74] J. G. Venegas et al. "Self-organized patchiness in asthma as a prelude to catastrophic shifts". In: *Nature* 434.7034 (2005), p. 777.

[75] B. Litt et al. "Epileptic seizures may begin hours in advance of clinical onset: a report of five patients". In: *Neuron* 30.1 (2001), pp. 51–64.

[76] P. E. McSharry, L. A. Smith, and L. Tarassenko. "Prediction of epileptic seizures: are nonlinear methods relevant?" In: *Nature medicine* 9.3 (2003), pp. 241–242.

[77] M. R. Schroeder. *Fractals, chaos, power laws: Minutes from an infinite paradise*. Courier Corporation, 2012.

[78] C. Wissel. "A universal law of the characteristic return time near thresholds". In: *Oecologia* 65.1 (1984), pp. 101–107.

[79] O. Ovaskainen and I. Hanski. "Transient dynamics in metapopulation response to perturbation". In: *Theoretical population biology* 61.3 (2002), pp. 285–295.

[80] E. H. Van Nes and M. Scheffer. "Slow recovery from perturbations as a generic indicator of a nearby catastrophic shift". In: *The American Naturalist* 169.6 (2007), pp. 738–747.

[81] N. Berglund and B. Gentz. "Metastability in simple climate models: pathwise analysis of slowly driven Langevin equations". In: *Stochastics and Dynamics* 2.03 (2002), pp. 327–356.

[82] S. Carpenter and W. Brock. "Rising variance: a leading indicator of ecological transition". In: *Ecology letters* 9.3 (2006), pp. 311–318.

[83] R. Biggs, S. R. Carpenter, and W. A. Brock. "Turning back from the brink: detecting an impending regime shift in time to avert it". In: *Proceedings of the National academy of Sciences* 106.3 (2009), pp. 826–831.

[84] A. R. Ives. "Measuring resilience in stochastic systems". In: *Ecological Monographs* 65.2 (1995), pp. 217–233.

[85] H. Held and T. Kleinen. "Detection of climate system bifurcations by degenerate fingerprinting". In: *Geophysical Research Letters* 31.23 (2004).

[86] V. Dakos et al. "Slowing down as an early warning signal for abrupt climate change". In: *Proceedings of the National Academy of Sciences* 105.38 (2008), pp. 14308–14312.

[87] V. Guttal and C. Jayaprakash. "Changing skewness: an early warning signal of regime shifts in ecosystems". In: *Ecology letters* 11.5 (2008), pp. 450–460.

[88] W. Horsthemke and R. Lefever. "Markovian Dichotomous Noise: An Exactly Soluble Colored-Noise Case". In: *Noise-Induced Transitions: Theory and Applications in Physics, Chemistry, and Biology* (1984), pp. 258–292.

[89] S. Carpenter et al. "Leading indicators of trophic cascades". In: *Ecology letters* 11.2 (2008), pp. 128–138.

[90] R. FitzHugh. "Mathematical models of threshold phenomena in the nerve membrane". In: *The bulletin of mathematical biophysics* 17.4 (1955), pp. 257–278.

[91] R. Fitzhugh. "Motion picture of nerve impulse propagation using computer animation." In: *Journal of applied physiology* 25.5 (1968), pp. 628–630.

[92] R. FitzHugh. "Impulses and physiological states in theoretical models of nerve membrane". In: *Biophysical journal* 1.6 (1961), p. 445.

[93] J. Nagumo, S. Arimoto, and S. Yoshizawa. "An active pulse transmission line simulating nerve axon". In: *Proceedings of the IRE* 50.10 (1962), pp. 2061–2070.

[94] W. E. Sherwood. "Fitzhugh–Nagumo Model". In: *Encyclopedia of Computational Neuroscience* (2015), pp. 1202–1211.

[95] J. Buescu et al. *Bifurcation, symmetry and patterns*. Birkhäuser, 2012.

[96] B. Van der Pol. "The nonlinear theory of electric oscillations". In: *Proceedings of the Institute of Radio Engineers* 22.9 (1934), pp. 1051–1086.

[97] B. Van der Pol. "LXXXVIII. On "relaxation-oscillations"". In: *The London, Edinburgh, and Dublin Philosophical Magazine and Journal of Science* 2.11 (1926), pp. 978–992.

[98] C. Kuehn. "A mathematical framework for critical transitions: normal forms, variance and applications". In: *Journal of nonlinear science* 23.3 (2013), pp. 457–510.

[99] B. D. Josephson. "Possible new effects in superconductive tunnelling". In: *Physics letters* 1.7 (1962), pp. 251–253.

[100] B. D. Josephson. "The discovery of tunnelling supercurrents". In: *Reviews of Modern Physics* 46.2 (1974), p. 251.

[101] N. Berglund and B. Gentz. *Noise-induced phenomena in slow-fast dynamical systems: a sample-paths approach*. Springer Science & Business Media, 2006.

[102] E. Neumann and A. Pikovsky. "Slow-fast dynamics in Josephson junctions". In: *The European Physical Journal B-Condensed Matter and Complex Systems* 34.3 (2003), pp. 293–303.

[103] J. Hindmarsh and R. Rose. "A model of neuronal bursting using three coupled first order differential equations". In: *Proceedings of the Royal Society of London B: Biological Sciences* 221.1222 (1984), pp. 87–102.

[104] J. Hindmarsh and R. Rose. "A model of the nerve impulse using two first-order differential equations". In: *Nature* 296.5853 (1982), pp. 162–164.

[105] J. Hindmarsh and R. Rose. "BVP models of nerve membrane (reply)". In: *Nature* 299.5881 (1982), pp. 375–375.

[106] M. Storace, D. Linaro, and E. de Lange. "The Hindmarsh–Rose neuron model: bifurcation analysis and piecewise-linear approximations". In: *Chaos: An Interdisciplinary Journal of Nonlinear Science* 18.3 (2008), p. 033128.

[107] C. W. Granger. "Some recent development in a concept of causality". In: *Journal of econometrics* 39.1 (1988), pp. 199–211.

[108] S. Kim et al. "A Granger Causality Measure for Point Process Models of Ensemble Neural Spiking Activity". In: *PLOS Computational Biology* 7.3 (2011), pp. 1–13.

[109] S. Hallerberg and A. S. de Wijn. "Understanding and controlling regime switching in molecular diffusion". In: *Phys. Rev. E* 90 (2014), p. 062901.

[110] J. P. Egan. *Signal Detection Theory and ROC Analysis*. Academic Press, 1975.

[111] J. Schmittbuhl, J.-P. Vilotte, and S. Roux. "Propagative macrodislocation modes in an earthquake fault model". In: *EPL (Europhysics Letters)* 21.3 (1993), p. 375.

[112] P. Gong, A. R. Nikolaev, and C. van Leeuwen. "Intermittent dynamics underlying the intrinsic fluctuations of the collective synchronization patterns in electrocortical activity". In: *Physical Review E* 76.1 (2007), p. 011904.

[113] H. Takayasu et al. "Statistical properties of deterministic threshold elements—the case of market price". In: *Physica A: Statistical Mechanics and its Applications* 184.1 (1992), pp. 127–134.

[114] H. L. d. S. Cavalcante et al. "Predictability and suppression of extreme events in a chaotic system". In: *Physical review letters* 111.19 (2013), p. 198701.

[115] P. Ashwin, J. Buescu, and I. Stewart. "From attractor to chaotic saddle: a tale of transverse instability". In: *Nonlinearity* 9.3 (1996), p. 703.

[116] S. C. Venkataramani, B. R. Hunt, and E. Ott. "Bubbling transition". In: *Physical Review E* 54.2 (1996), p. 1346.

[117] Y. Maistrenko, T. Kapitaniak, and P. Szuminski. "Locally and globally riddled basins in two coupled piecewise-linear maps". In: *Physical Review E* 56.6 (1997), p. 6393.

[118] D. J. Gauthier and J. C. Bienfang. "Intermittent loss of synchronization in coupled chaotic oscillators: Toward a new criterion for high-quality synchronization". In: *Physical Review Letters* 77.9 (1996), p. 1751.

[119] A. Kittel, K. Pyragas, and R. Richter. "Prerecorded history of a system as an experimental tool to control chaos". In: *Physical Review E* 50.1 (1994), p. 262.

[120] H. Dedieu, M. P. Kennedy, and M. Hasler. "Chaos shift keying: Modulation and demodulation of a chaotic carrier using self-synchronizing Chua's circuits". In: *IEEE Transactions on Circuits and Systems II: Analog and Digital Signal Processing* 40.10 (1993), pp. 634–642.

[121] S. H. Strogatz. *Nonlinear dynamics and chaos: with applications to physics, biology, chemistry, and engineering*. Westview press, 2014.

[122] A. S. Pikovsky and P. Grassberger. "Symmetry breaking bifurcation for coupled chaotic attractors". In: *Journal of Physics A: Mathematical and General* 24.19 (1991), p. 4587.

[123] T. Kapitaniak, J. Wojewoda, and J. Brindley. "Synchronization and desynchronization in quasi-hyperbolic chaotic systems". In: *Physics Letters A* 210.4-5 (1996), pp. 283–289.

[124] J. Laherrere and D. Sornette. "Stretched exponential distributions in nature and economy:"fat tails" with characteristic scales". In: *The European Physical Journal B-Condensed Matter and Complex Systems* 2.4 (1998), pp. 525–539.

[125] D. Sornette and G. Ouillon. "Dragon-kings: mechanisms, statistical methods and empirical evidence". In: *The European Physical Journal-Special Topics* 205.1 (2012), pp. 1–26.

[126] V. Pisarenko and D. Sornette. "Robust statistical tests of Dragon-Kings beyond power law distributions". In: *The European Physical Journal-Special Topics* 205.1 (2012), pp. 95–115.

[127] S. C. Venkataramani et al. “Transitions to bubbling of chaotic systems”. In: *Physical review letters* 77.27 (1996), p. 5361.

[128] H. Abdi and L. J. Williams. “Principal component analysis”. In: *Wiley interdisciplinary reviews: computational statistics* 2.4 (2010), pp. 433–459.

[129] S. Wold, K. Esbensen, and P. Geladi. “Principal component analysis”. In: *Chemometrics and intelligent laboratory systems* 2.1-3 (1987), pp. 37–52.

[130] E. N. Lorenz. “Predictability: A problem partly solved”. In: *Proc. Seminar on predictability*. Vol. 1. 1. 1996.

[131] E. N. Lorenz and K. A. Emanuel. “Optimal sites for supplementary weather observations: Simulation with a small model”. In: *Journal of the Atmospheric Sciences* 55.3 (1998), pp. 399–414.

[132] S. Herrera et al. “The role of large-scale spatial patterns in the chaotic amplification of perturbations in a Lorenz’96 model”. In: *Tellus A* 63.5 (2011), pp. 978–990.

[133] A. Trevisan and F. Pancotti. “Periodic orbits, Lyapunov vectors, and singular vectors in the Lorenz system”. In: *Journal of the atmospheric sciences* 55.3 (1998), pp. 390–398.

[134] D. Orrell. “Model error and predictability over different timescales in the Lorenz’96 systems”. In: *Journal of the atmospheric sciences* 60.17 (2003), pp. 2219–2228.

[135] J. L. Anderson. “Spatially and temporally varying adaptive covariance inflation for ensemble filters”. In: *Tellus A* 61.1 (2009), pp. 72–83.

[136] J. L. Kaplan and J. A. Yorke. “Preturbulence: a regime observed in a fluid flow model of Lorenz”. In: *Communications in Mathematical Physics* 67.2 (1979), pp. 93–108.

[137] D. S. Wilks. “Effects of stochastic parametrizations in the Lorenz’96 system”. In: *Quarterly Journal of the Royal Meteorological Society* 131.606 (2005), pp. 389–407.

[138] A. Karimi and M. R. Paul. “Extensive chaos in the Lorenz-96 model”. In: *Chaos: An Interdisciplinary Journal of Nonlinear Science* 20.4 (2010), p. 043105.

[139] G. A. Gottwald and I. Melbourne. "Testing for chaos in deterministic systems with noise". In: *Physica D: Nonlinear Phenomena* 212.1 (2005), pp. 100–110.

[140] H. Aytaç, J. Freitas, and S. Vaienti. "Laws of rare events for deterministic and random dynamical systems". In: *Transactions of the American Mathematical Society* 367.11 (2015), pp. 8229–8278.

[141] V. Lucarini et al. "Towards a general theory of extremes for observables of chaotic dynamical systems". In: *Journal of statistical physics* 154.3 (2014), pp. 723–750.

[142] G. Lapeyre. "Characterization of finite-time Lyapunov exponents and vectors in two-dimensional turbulence". In: *Chaos: An Interdisciplinary Journal of Nonlinear Science* 12.3 (2002), pp. 688–698.

[143] M. W. Beims and J. A. Gallas. "Alignment of Lyapunov Vectors: A Quantitative Criterion to Predict Catastrophes?" In: *Scientific Reports* 6 (2016), p. 37102.

[144] D. Pazó and J. M. López. "Characteristic Lyapunov vectors in chaotic time-delayed systems". In: *Physical Review E* 82.5 (2010), p. 056201.

[145] M. Cencini and F. Ginelli. "Lyapunov analysis: from dynamical systems theory to applications". In: *Journal of Physics A: Mathematical and Theoretical* 46.25 (2013), p. 250301.

[146] F. Ginelli et al. "Covariant lyapunov vectors". In: *Journal of Physics A: Mathematical and Theoretical* 46.25 (2013), p. 254005.

[147] H. Guckenheimer. *Nonlinear oscillations, dynamical systems, and bifurcations of vector fields*. Springer Science & Business Media, 20013.

[148] S. E. Newhouse. "The abundance of wild hyperbolic sets and non-smooth stable sets for diffeomorphisms". In: *Publications Mathématiques de l'IHÉS* 50 (1979), pp. 101–151.

[149] S. Gonchenko, L. Shilnikov, and O. Stenkin. "On Newhouse regions with infinitely many stable and unstable invariant tori". In: *Proceedings of the Int. Conf."Progress in Nonlinear Scienc", dedicated to*. Citeseer. 2002, pp. 2–6.

[150] J. Yang. “Newhouse phenomenon and homoclinic classes”. In: *Ergodic Theory and Dynamical Systems* 31.05 (2011), pp. 1537–1562.

Acknowledgment

Foremost, I would like to express my gratitude towards my supervisor Marc Timme, for giving me the opportunity to be a part of the Network Dynamics group. I would like to thank him for the freedom he gave me to explore, for his kindness and his support. I would like to thank Sarah Hallerberg for initiating this project and for her supervision and support. I would like to express my appreciation to Sarah for replacing me at Dynamics days on short notice. I am very grateful to Prof. Parlitz for his kindness and valuable feedback, especially during the last days of writing. Thank you for your inspiring and comprehensive paper on the computational methods of the covariant Lyapunov vectors, from which that I learned a lot. I thank Prof. Kree for his valuable input and for his time. I am thankful to all the members of my examination board for agreeing to review my work.

I thank the members of the Network Dynamics group for creating a relaxed and friendly working environment. I thank Dimitra and Florencia, the companions of the long nights for being there. I am grateful to Gunter, Lea and Lotta for their patience, understanding and emotional support during the last long months. I thank my family for their unconditional love and support.